SANDIA REPORT SAND84—0254 • Unlimited Release • UC—66c
Printed March 1984

Development of a Borehole Directional Antenna at VHF

Hsi-Tien Chang, Larry Scott

Prepared by
Sandia National Laboratories
Albuquerque, New Mexico 87185 and Livermore, California 94550
for the United States Department of Energy
under Contract DE-AC04-76DP00789

DISCLAIMER

DO NOT MICROFILM COVER

Issued by Sandia National Laboratories, operated for the United States Department of Energy by Sandia Corporation.

Printed in the United States of America
Available from
National Technical Information Service
U.S. Department of Commerce
5285 Port Royal Road
Springfield, VA 22161

NTIS price codes
Printed copy: A06
Microfiche copy: A01

SAND84-0254
Unlimited Release

DEVELOPMENT OF A BOREHOLE DIRECTIONAL ANTENNA AT VHF

Hsi-Tien Chang
Geothermal Technology Development Division, 6241
Sandia National Laboratory
Albuquerque, New Mexico 87185

Larry Scott
Mission Research Corporation
Albuquerque, New Mexico 87106

SAND--84-0254

DE84 010746

ABSTRACT

This report investigates the feasibility of constructing a directional VHF (30 MH_z to 300 MH_z) antenna to physically fit into a small borehole. The study was carried out in a test chamber containing a 15 cm diameter borehole surrounded by sand which can be moistened with water or brine to adjust the dielectric constant and electrical conductivity. Electric field measurements were made for an eccentrically positioned monopole, a corner reflector and a two-element array for a number of possible configurations. Using an eccentric monopole, the best beamwidth obtained was 78° and the front-to-back ratio was 3.5 db. The front-to-back ratio was increased to 8.5 db when two element arrays were arranged in such a way as to provide the optimum radiation pattern. However, the best results were achieved using a corner reflector: 60° beamwidth and 13 db front-to-back ratio. It is concluded that a directional VHF antenna can be designed for downhole application.

CONTENTS

Section		Page
1	INTRODUCTION	7
2	EXPERIMENTAL DESIGN	9
	2.1 Electrical Considerations	9
	2.1.1 Test Chamber	9
	2.1.2 Ground Screen	11
	2.1.3 Monopole Characteristics	12
	2.1.4 Field Pattern Accuracy	12
	2.1.5 Corner Reflector	13
	2.1.6 Pulse Generator Feed Line	13
	2.1.7 Reference Signal for Timing	13
	2.1.8 Oscilloscope Bandwidth	14
	2.1.9 Two-element Drive Lines	14
	2.1.10 Media Electrical Properties Measurement	17
	2.2 Mechanical Considerations	17
	2.2.1 Test Chamber and Simulated Borehole	17
	2.2.2 Transmitting Antenna Mounting Hardware	20
	2.2.3 Receiving Probe Mounting Hardware	20
	2.2.4 Antenna Feed Assembly	28
	2.2.5 Corner Reflector Assembly	28
3	TEST PROCEDURE	32
	3.1 Calibrations	32
	3.1.1 Oscilloscope Specifications	32
	3.1.2 Vector Voltmeter Specifications	33
	3.1.3 Pulser Specifications	33
	3.1.4 V-I Probe Specifications	34
	3.2 Data Collection and Processing	34
	3.2.1 Raw Data	34
	3.2.2 Digitized Data	34
	3.2.3 Fourier Transforms	35
	3.3 Measurement Procedures	35
	3.3.1 Standard Precautions	35
	3.3.2 Leakage Tests	37
	3.3.3 Maximum Bandwidth	37
	3.3.4 Identifying Chamber Wall Reflections	37

CONTENTS (Continued)

Section		Page
4	RESULTS	39
	4.1 Monopole in Simulated Borehole	39
	4.1.1 Excitation	39
	4.1.2 Field Patterns	42
	4.1.3 Tabulated Results	
	4.2 Corner Reflector Antenna	42
	4.2.1 Excitation	51
	4.2.2 Field Patterns	51
	4.2.3 Tabulated Results	60
	4.3 Synthesized Two-element Array	60
	4.3.1 Excitation	63
	4.3.2 Filed Patterns	64
	4.3.3 Tabulated Results	64
	4.4 Measured Two-element Array	64
	4.4.1 Excitation	67
	4.4.2 Field Patterns	67
	4.4.3 Tabulated Results	68
	4.5 Media Electrical Properties	68
	4.5.1 Dry Sand	71
	4.5.2 Wet Sand	73
5	DISCUSSIONS	74
	5.1 Utility of Three Designs	75
	5.1.1 Eccentric Monopole	75
	5.1.2 Corner Reflector	77
	5.1.3 Two Element Array	80
	5.2 Fourier Transforms	85
	5.2.1 Eccentric Monopole	85
	5.2.2 Corner Reflector	88
	5.2.3 Two Element Array	93
	5.2.4 Driving Pulse	93
	5.3 Transfer Functions	98
	5.3.1 Eccentric Monopole	98
	5.3.2 Corner Reflector	98
	5.3.3 Two-Element Array	98
	5.4 Path Loss Calculations	98

CONTENTS (Continued)

Section		Page
6	CONCLUSIONS	106
	REFERENCES	107
	DISTRIBUTION	108

LIST OF ILLUSTRATIONS

Figure		Page
2.1	Test chamber for borehole simulation.	10
2.2	Transmitter pulse.	11
2.3	Electric field measurement setup.	15
2.4	Test setup for two-element array measurements.	16
2.5	Test setup for measuring media electrical properties.	18
2.6	Test container for borehole simulation.	19
2.7	Cross sectional view of plastic watertight vessel.	21
2.8	Collar (fits on top of plastic cylinder) (1 each).	22
2.9	Basic rotating antenna carriage (2 each).	23
2.10	Hole pattern for rotating antenna carriage (monopole)(1 each).	24
2.11	Hole pattern for rotating antenna carriage (2-element) (1 each).	25
2.12	Field probe plate (1 each).	26
2.13	Antenna hole plugs.	27
2.14	Details of antenna assembly.	29
2.15	Antenna probe collar (5 each).	30
2.16	Corner reflector assembly.	31
3.1	Typical field waveform with time reference.	36
3.2	Wall reflection identification.	38
4.1	Pulser output used to drive antennas (scale = 1 ns/div).	40
4.2	Field pattern for the eccentric monopole place at 3.19 cm off center.	41
4.3a	Field pattern using first pulse for monopole. (radius = 2.37 cm)	43
4.3b	Field pattern using second pulse for monopole. (radius = 2.38 cm)	44
4.4a	Field pattern using first pulse for monopole. (radius = 3.19 cm)	45
4.4b	Field pattern using second pulse for monopole. (radius = 3.19 cm)	46
4.5a	Field pattern using first pulse for monopole. (radius = 4.85 cm)	47
4.5b	Field pattern using second pulse for monopole. (radius = 4.85 cm)	48
4.6a	Field pattern using first pulse for corner reflector. (monopole at radius = 0.00 cm)	52
4.6b	Field pattern using second pulse for corner reflector. (monopole at radius = 0.00 cm)	53
4.7a	Field pattern using first pulse for corner reflector. (monopole at radius = 2.37 cm)	54

LIST OF ILLUSTRATIONS (Concluded)

Figure		Page
4.7b	Field pattern using second pulse for corner reflector. (monopole at radius = 2.37 cm)	55
4.8a	Field pattern using first pulse for corner reflector. (monopole at radius = 3.19 cm)	56
4.8b	Field pattern using second pulse for corner reflector. (monopole at radius = 3.19 cm)	57
4.9a	Field pattern using first pulse for corner reflector. (monopole at radius = 4.85 cm)	58
4.9b	Field pattern using second pulse for corner reflector. (monopole at radius = 4.85 cm)	59
4.10a	Field pattern using first pulse for synthesized two-element array. (elements at radius = 3.19 cm)	65
4.10b	Field pattern using second pulse for synthesized two-element array. (elements at radius = 3.19 cm)	66
4.11a	Field pattern using first pulse for measured two-element array. (elements at radius = 3.19 cm)	69
4.11b	Field pattern using second pulse for measured two-element array. (elements at radius = 3.19 cm)	70
5.1a	Field pattern for the eccentric monopole. (First pulse with radius = 3.19 cm)	78
5.1b	Field pattern for the eccentric monopole. (Second pulse with radius = 3.19 cm)	79
5.2a	Field pattern for the corner reflector antenna. (First pulse with radius = 3.19 cm)	81
5.2b	Field pattern for the corner reflector antenna. (Second pulse with radius = 3.19 cm)	82
5.3a	Field patterns for synthesized and measured two-element array. (First pulse with radius = 3.19 cm)	83
5.3b	Field patterns for synthesized and measured two-element array. (Second pulse with radius = 3.19 cm)	84
5.4	Eccentric monopole response (2 ns/div).	86
5.5	Driving pulse (1 ns/div).	86
5.6	Digitized monopole response.	87
5.7	Fourier transform of monopole response.	89
5.8	Corner reflector response.	90
5.9	Digitized corner reflector response.	91
5.10	Fourier transform of corner reflector antenna response.	92
5.11	Two-element array antenna response.	94
5.12	Digitized two-element array response.	95
5.13	Fourier transform of two-element array antenna response.	96
5.14	Fourier transform of driving pulse.	97
5.15	Fourier transform for eccentrically positioned monopole.	99
5.16	Fourier transform for corner reflector antenna.	100
5.17	Fourier transform for two-element array.	101

LIST OF TABLES

Table		Page
3.1	PULSE CALIBRATION	33
4.1	MONOPOLE LOCATIONS BY NUMBER ON BOREHOLE RADIUS	40
4.2	BEAM WIDTHS FOR THE ECCENTRICALLY POSITIONED MONOPOLE	42
4.3	MONOPOLE IN RADIUS #1 (CENTERED)	49
4.4	MONOPOLE IN RADIUS #2 (2.37 cm)	49
4.5	MONOPOLE IN RADIUS #3 (3.19 cm)	49
4.6	MONOPOLE IN RADIUS #4 (4.85 cm)	50
4.7	BEAM WIDTHS FOR THE CORNER REFLECTOR ANTENNA	60
4.8	MONOPOLE IN RADIUS #1 (CENTERED)	61
4.9	MONOPOLE IN RADIUS #2 (2.37 cm)	61
4.10	MONOPOLE IN RADIUS #3 (3.19 cm)	62
4.11	MONOPOLE IN RADIUS #4 (4.85 cm)	62
4.12	SYNTHESIS TABLE FOR TWO-ELEMENT ARRAY PATTERN	63
4.13	SYNTHESIZED TWO-ELEMENT ARRAY (ELEMENTS PLACED AT RADIUS = 3.19 cm)	67
4.14	BEAM WIDTHS FOR THE SYNTHESIZED TWO-ELEMENT ARRAY	68
4.15	MEASURED TWO-ELEMENT ARRAY (ELEMENTS AT RADIUS = 3.19 cm)	71
4.16	DRY MEDIA ELECTRICAL PROPERTIES	72
4.17	WET MEDIA ELECTRICAL PROPERTIES	73
5.1	SUMMARY OF BEAM WIDTHS AND FRONT-TO-BACK RATIOS FOR THE ECCENTRIC MONOPOLE, CORNER REFLECTOR AND TWO-ELEMENT ARRAY	76
5.2	SUMMARY OF OPTIMAL CONFIGURATIONS FOR THREE ANTENNAS	77
5.3	ANTENNA RESPONSE AND PATH LOSS AT ONE METER RANGE	102
5.4	ATTENUATION FOR VARIOUS CONDUCTIVITIES AND RANGES	103
5.5	MEDIA 1: RADAR RETURN SIGNAL LEVELS FOR A 1 kV PULSE DRIVER	104
5.6	MEDIA 2: RADAR RETURN SIGNAL LEVELS FOR A 1 kV PULSE DRIVER	104
5.7	MEDIA 3: RADAR RETURN SIGNAL LEVELS FOR A 1 kV PULSE DRIVER	105

SECTION 1
INTRODUCTION

In geothermal and petroleum exploration, a "non-productive" dry hole constitutes the main frustration in drilling and field development. Since extensive surface electromagnetic (EM) and seismic surveys usually are conducted prior to drilling, operators have reason to believe that a reservoir exists in the general area. However, the inability to pinpoint an existing reservoir fracture system (into which a well can be drilled) is one of the main deficiencies of these surface survey techniques. The low frequencies used in the surface EM and seismic surveys have limited resolution and cannot identify a fine structure such as millimeter thick fractures. In addition, the skin depth effect limits the depth that an EM technique can "see" from the surface.

Downhole instruments conceivably will provide more information on the subsurface structure than the surface techniques. (Such instrumentation could be used in existing wells.) According to preliminary calculations, a VHF radar can penetrate up to 100 meters into the rock from a borehole and also provide high-resolution data. If such a radar system has a directional capability, its return may locate the naturally occurring fracture zones and provide guidance for drilling offset wells that are "productive".

A directional VHF antenna designed for free space application would have dimensions on the order of feet and thus cannot be fitted into a small borehole. The objective of this effort was to conduct laboratory experiments which would gather the necessary time domain data for development of an optimized VHF directional antenna for use in remote detection of fracture zones down a borehole. This is the first known measurement for the eccentrically located dipole or monopole in a high dielectric cylinder, although theoretical predictions have been reported (ref. 1.1).

This experiment accurately modeled a full-scale antenna element operating in a water-filled borehole, together with the surrounding rock modeled by sand having appropriate electrical properties. These properties may be adjusted by

introducing fresh or salt water to vary the dielectric constant and conductivity of the sand.

The antenna element was driven with a fast rise time, short duration pulse and the resulting broad band azimuthal electric field response was recorded for that element located at numerous positions on the radius of the borehole. In a few instances, the antenna system was excited with a fast rise time step function to aid in the understanding of the antenna/borehole system response.

From monopole data, an optimized two-element antenna array pattern was synthesized to illustrate the optimization procedure and feasibility. Finally, this two-element array was constructed and its measured field pattern was compared with that found in the synthesis procedure above. In addition, a corner reflector design was investigated and the resulting field patterns and path losses were recorded.

This report is divided into six major sections. Section 2 covers the experimental design, including special electromagnetic considerations and detailed mechanical design. Section 3 outlines the test procedure and details calibration specifications. Section 4 presents the experimental results for the monopole, the corner reflector and the two-element array. Finally, Section 5 discusses the results and Section 6 draws conclusions.

SECTION 2
EXPERIMENTAL DESIGN

2.1 Electrical Considerations

The electrical design for this experiment was constrained primarily by the minimum borehole size that would be of interest. That size was selected to be 15 cm. Also considered was the fact that we expect to find many boreholes filled with some aqueous solution either fresh water or brine. To minimize the discontinuities seen by the outward traveling waves emitted by the antenna, it was decided to immerse the antenna in distilled water. This, of course, electrically lengthens the antenna by a factor of the square root of the relative dielectric constant or about nine for water. We also wanted to investigate antenna performance for this configuration in the VHF radio band. Thus, the antenna length for the monopole element was selected to be 5.08 cm (2 inches).

2.1.1 Test Chamber

A test chamber similar to that pictured in Figure 2.1 has a borehole of about 15 cm diameter with the surrounding media, sand, simulating the electrical properties of granite. This simulation was accomplished by using kiln dried sand-blasting sand. The test box was designed so that the sand could be moistened with water or brine to adjust the dielectric constant and electrical conductivity. Drain holes were provided in the bottom of the box and plastic was placed on the floor to catch any water percolating through. This arrangement modeled at full scale, the physical properties of a downhole electromagnetic radar probe.

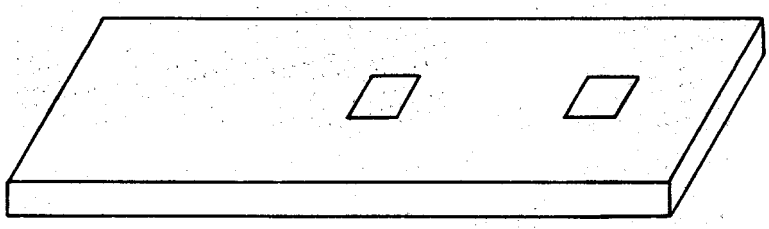

Equipment bridge.

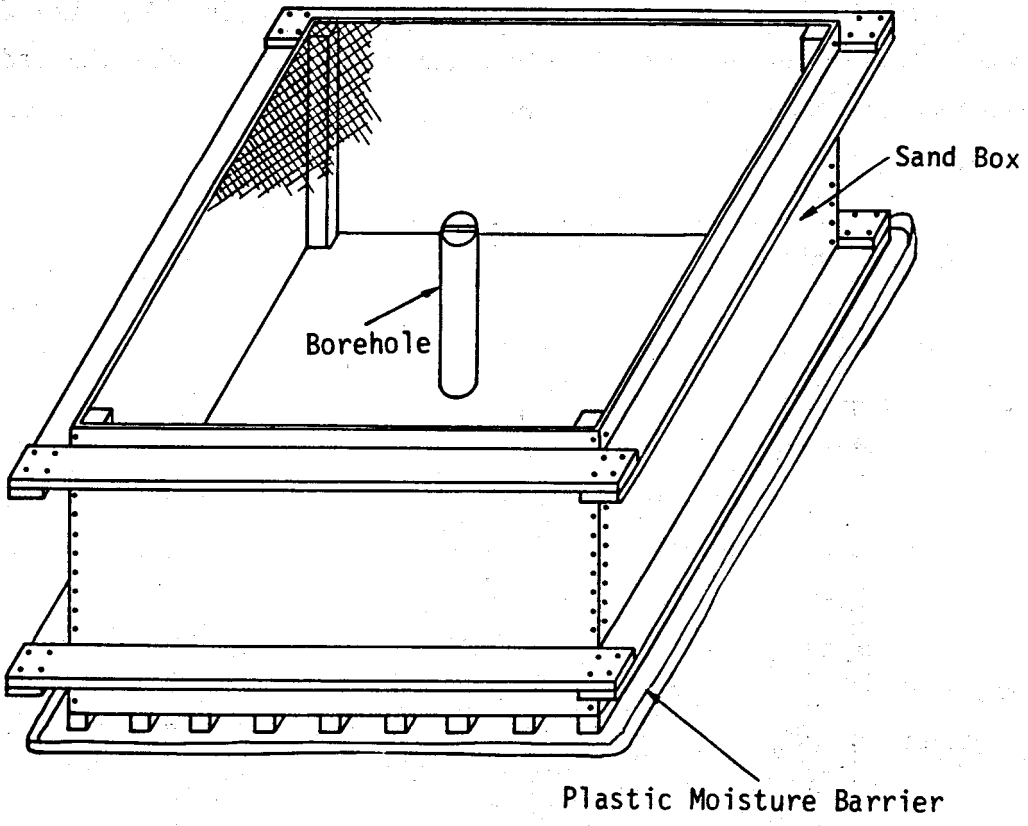

Figure 2.1. Test chamber for borehole simulation.

2.1.2 Ground Screen

The test chamber top surface (sand) was covered with a brass ground screen that forms a surface in which the entire test chamber is imaged. This provides an exact simulation of the downhole situation, yet provides the test operator ready access for repositioning the antenna and test equipment for the various measurements.

2.1.2 Reflection Management

Because of the practical limits of the test chamber size, a low power, fast rise time (0.7 ns), short duration (1.3 ns) pulse (Fig. 2.2) was used to excite the various antenna configurations. This is also a very practical pulse to generate in a downhole environment. Our ability to time window the responses by designing the relative distances between transmitter antenna, receiver antenna and the test chamber walls and floor allowed us to avoid undesired reflections from contaminating the early time data.

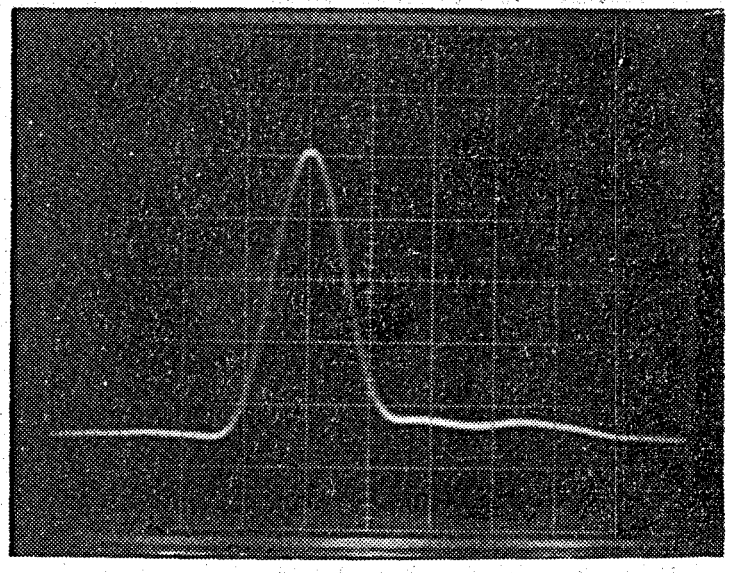

1 ns/div.

Figure 2.2. Transmitter pulse.

2.1.3 Monopole Characteristics

The monopole is 5.08 cm long, 0.15875 cm in radius and immersed in a lossless dielectric with a relative dielectric constant of 78.5.

The travel time is found from the antenna length divided by the velocity of propagation in the media. For the antenna length of 5.08 cm and a velocity of propagation the speed of light in the media or 3.39×10^7 meters/second (relative dielectric constant of 78.5). Then the travel time is 1.498 nanoseconds (ns).

From this calculation you would expect to see a ring down response with a period of about 2.996 ns or a frequency of 334 MH_z which agrees well with that measured.

2.1.4 Field Pattern Measurements

It is our desire to measure the field patterns both in the near zone and the far zone. The far zone, in this instance, starts at a distance of about 7.5 meters from the transmitter. Because of the constraints in the size of the test box, we can only measure the field pattern one meter away from the transmitter. We hope to set up this experiment in a larger area in the future to carry out far field measurements.

2.1.5 Corner Reflector

The corner reflector design was constrained to be the largest practical reflector that could be fit into the borehole. This was, however, consistent with normal design guidelines for corner reflectors (Ref. 2.3). Recommended dimensions are to place the driven element between 0.25 and 0.7 wavelengths from the apex and for the sides of the reflector to be about 0.5 wavelength from apex to front extent with a height of at least 5/16 wavelength for a monopole over a ground plane.

2.1.6 Pulse Generator Feed Line

The pulse generator was connected to the antenna via a long low loss 50 Ohm cable. It was 13.365 meters long and had a velocity of propagation of 0.81 the speed of light. Andrews FSJ4-50 heliax was used for this cable and was fitted with a type "N" connector on one end and a type GR 874 connector on the other end. With this cable length, the antenna reflection due to impedance mismatch was not be seen for about 110 ns. This allowed ample clear time for recording the data of primary interest.

2.1.7 Reference Signal for Timing

A reference signal is needed for data recording to provide a common time from which to measure time of arrival. This is important for the synthesis of multi-element arrays using the measured data from the eccentrically positioned monopole. To provide this reference with the greatest resolution in time we used the "V-I Probe" that was originally designed

for frequency domain impedance measurements (Section 4.5) to pick up a signal near the drive point on the monopole. This signal was proportional to the derivative of the driving pulse and as such provides an excellent reference with a stable zero crossing in the waveform from which to measure time. Figure 2.3 illustrates the overall measurement setup and the relative location of the various devices.

2.1.8 Oscilloscope Bandwidth

Since it was our intent, to investigate the VHF band response of an antenna in the borehole environment, our selection of an oscilloscope was directed to one that had flat response up to 300 MHz. This is reasonable in the sense of modeling a realistic downhole instrumentation package as this frequency bandwidth is achieved readily. This bandwidth limitation does however affect our data in that it will attenuate in a graceful manner, that is with a smooth roll off, all energy above 300 MHz. Specifically at 300 MHz the scope response is down 3 dB and this is why the apparent rise time on the pulser looks like 0.7 ns rather than the 0.25 ns as specified by the manufacturer (Section 3.1.3).

2.1.9 Two-element Drive Lines

The array that was investigated was selected to be a two-element array of monopoles driven with a relative time delay so that the first positive pulse arriving at the target would add constructively when the target was on a line passing through the two elements (i.e., endfire array). This is illustrated in Figure 2.4 where we see the two feed lines are adjusted so that the one feeding the forward element is just a bit longer that the other to provide the appropriate delay to cause the first pulse responses to add at the target. A section of GR 874 trombone air-line was used to "tune" the feed lines while using two matched length sections of low loss 50 Ohm heliax cable.

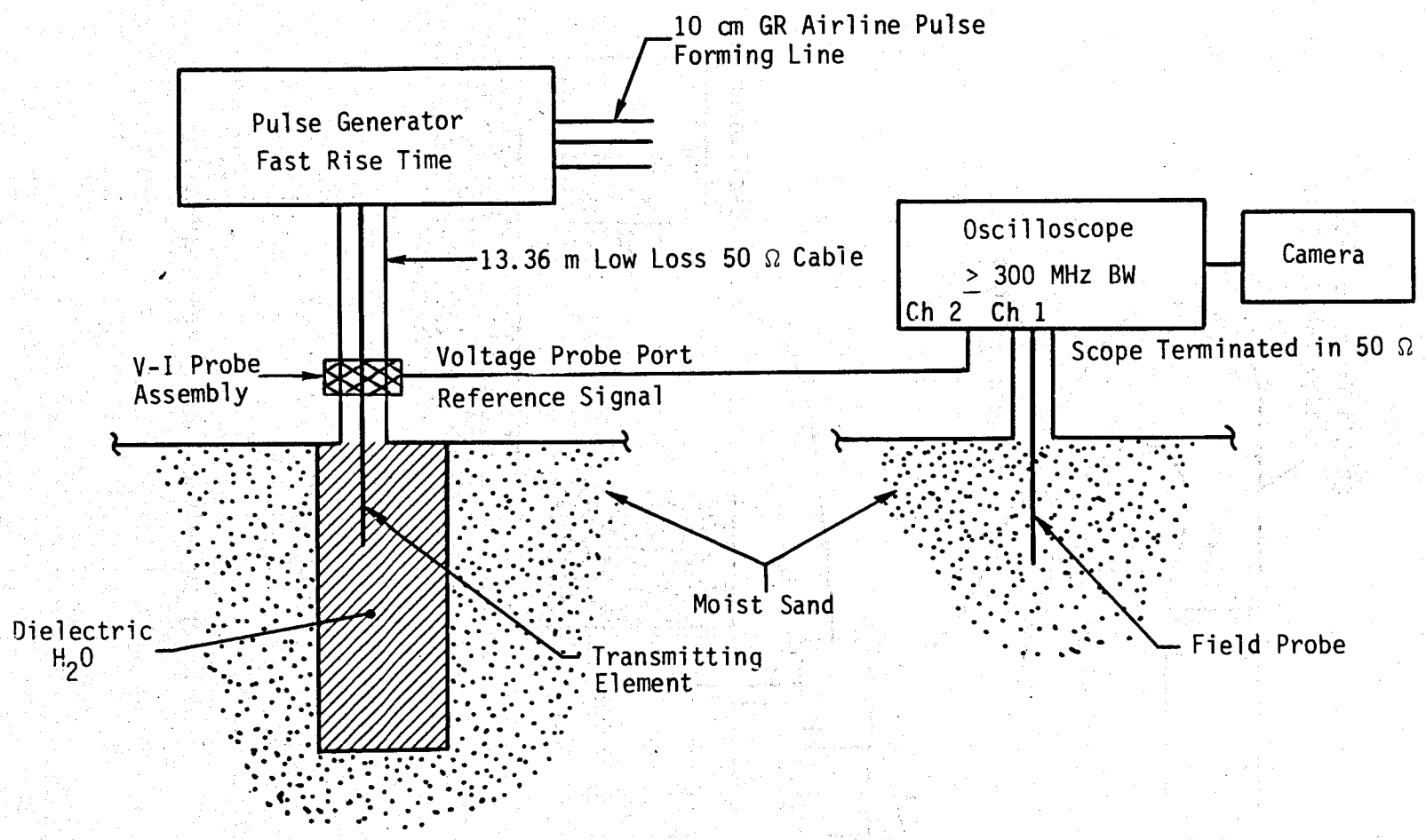

Figure 2.3. Electric field measurement setup.

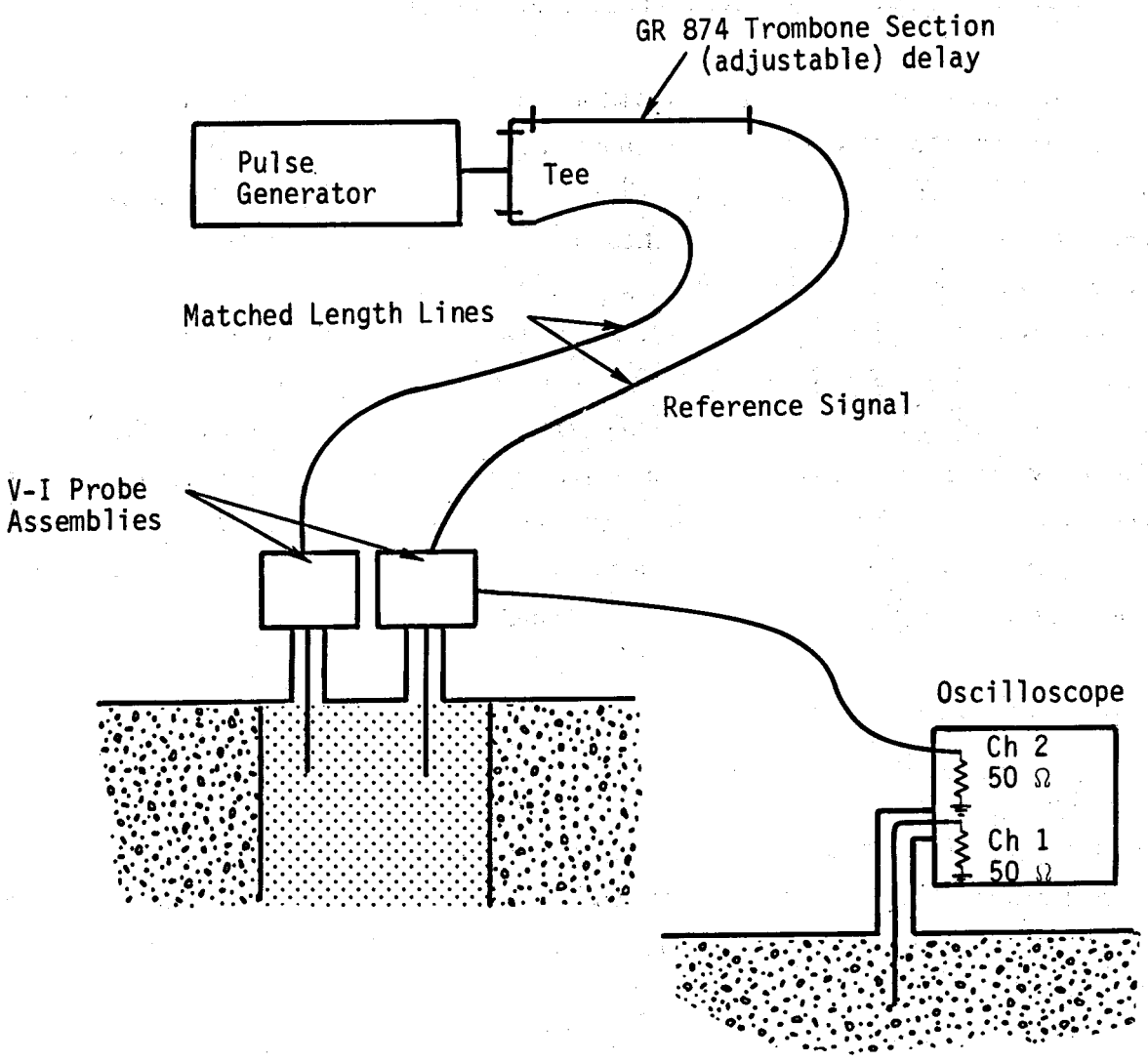

Figure 2.4. Test setup for two-element array measurements.

2.1.10 Media Electrical Properties Measurement

The technique used to determine the electrical properties of the media is that of measuring the input impedance of the receiving monopole in the VHF Band. Figure 2.5 shows the hookup using an oscillator to excite the antenna radiating into the media which couples back to the antenna causing its impedance to be uniquely determined by the electrical properties of the media. This method is described in Reference 2.4 and was developed by Scott (Ref. 2.4). With this setup, the Vector Voltmeter measures voltage and current signals from the V-I Probe which are directly related to the apparent impedance on the transmission line at the probe reference plane. This impedance is translated to the antenna feed point by the classical transmission line equations and the media dielectric constant and conductivity found by solving these equations.

2.2 Mechanical Considerations

The mechanical design for this experiment was constrained by the requirement to have an indoor facility in which to investigate the borehole antenna design. This leads to the maximum size constraint based on floor space and floor loading considerations. The electromagnetic modeling considerations discussed above, lead to the minimum size constraints in considering our experimental ability to resolve undesired echos or reflections from the desired responses to be recorded within the test environment.

2.2.1 Test Chamber and Simulated Borehole

The test chamber consists of a moisture resistant treated box 4 feet high by 8 feet square constructed primarily of 4 feet by 8 feet by 3/4 inch plywood. A platform, also made of plywood and two-by-fours, was constructed to place the test equipment on during measurements. The borehole consisted of a thin walled plastic cylinder placed in the center of the box (see Fig. 2.6).

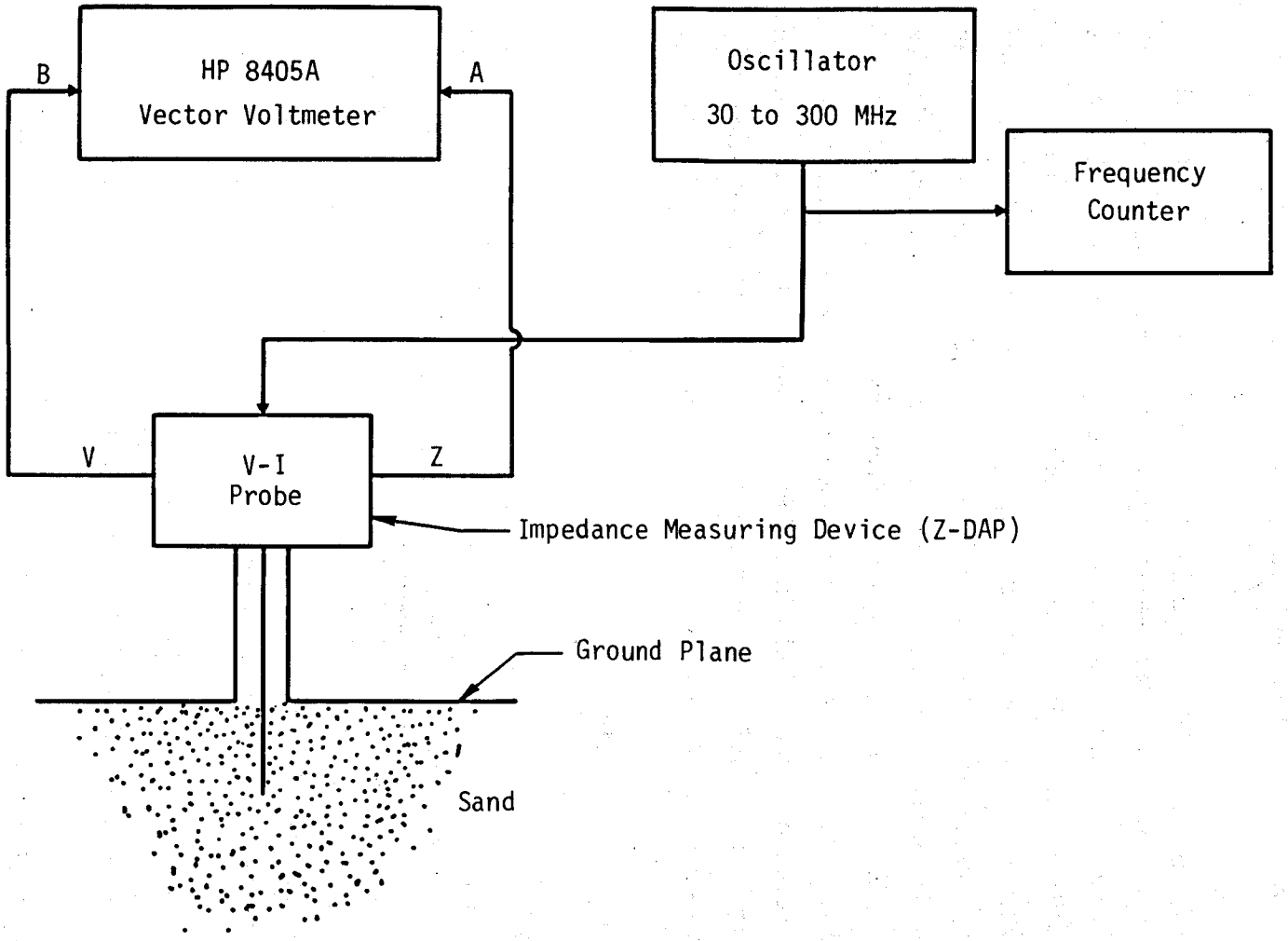

Figure 2.5. Test setup for measuring media electrical properties.

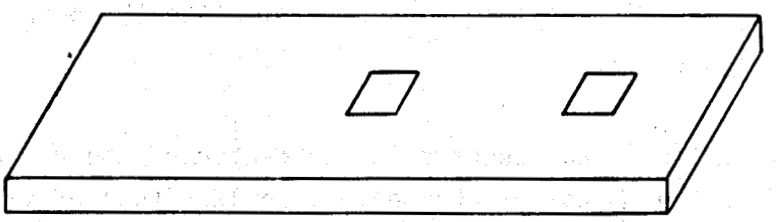

Equipment bridge.

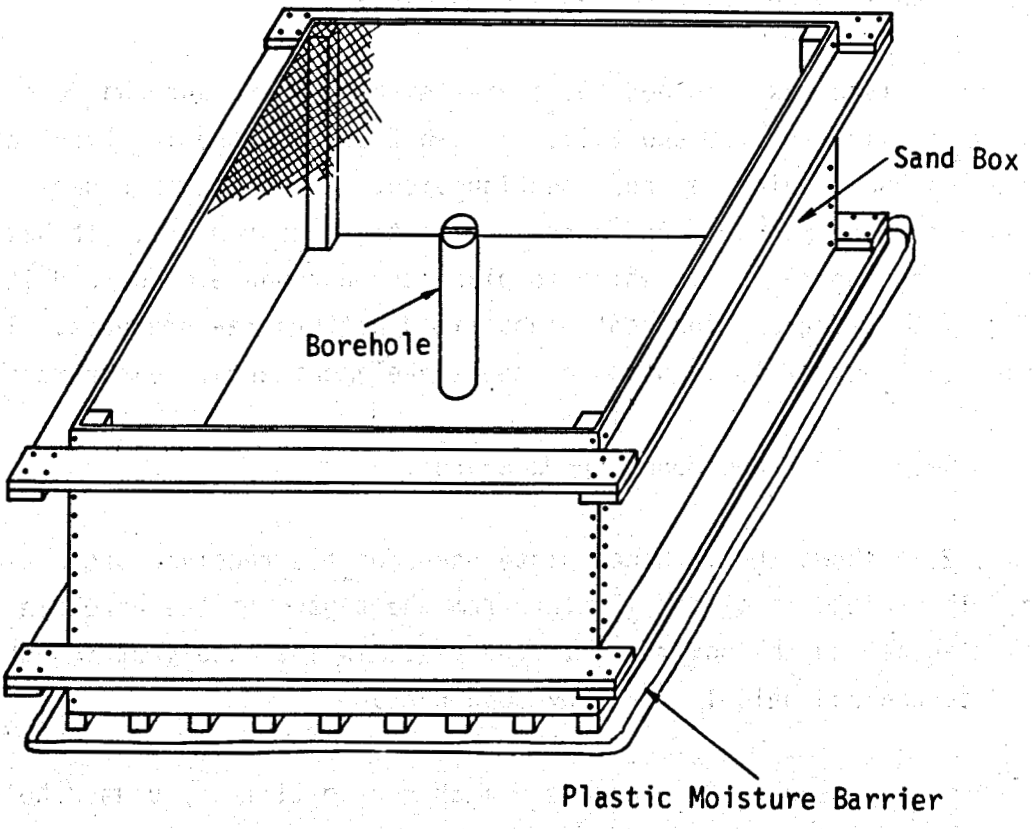

Figure 2.6. Test container for borehole simulation.

Details of the plastic cylinder used to simulate the borehole are illustrated in Figure 2.7.

The plastic cylinder was secured in the center of the box by a plywood collar attached to the bottom of the box. Then 12.5 tons of kiln dried medium grit sand-blasting sand was placed in the box up to within 1/4 inch of the top of the plastic cylinder (i.e., 1 inch of the top of the box). Then a machined brass plate was placed over the open end of the simulated borehole (see Fig. 2.8 for machining details) and the brass ground screen attached. The ground screen covers the entire top surface of the sand and is held in intimate contact with sand bags.

2.2.2 Transmitting Antenna Mounting Hardware

The brass plate was machined to receive either of two antenna mounting plates shown in Figures 2.10 and 2.11. Figure 2.9 gives the location of indexing holes and provides a cross section view. The plate in Figure 2.10 is used for the monopole and corner reflector measurements. It has five holes along the radius in which to place the antenna element and it is indexed every 22.5 degrees for convenient field pattern measurements. The plate shown in Figure 2.11 is used for the two-element array measurements.

2.2.3 Receiving Probe Mounting Hardware

Figure 2.12 shows the machined plate used for the receiver probe mounting. This plate is placed 1 meter from the center of the borehole along the diagonal to the box corner. The plate is intimately attached to the ground screen and held in place by sand bags.

A number of antenna hole plugs were machined to fill any unused hole during measurements if needed. These are shown in Figure 2.13.

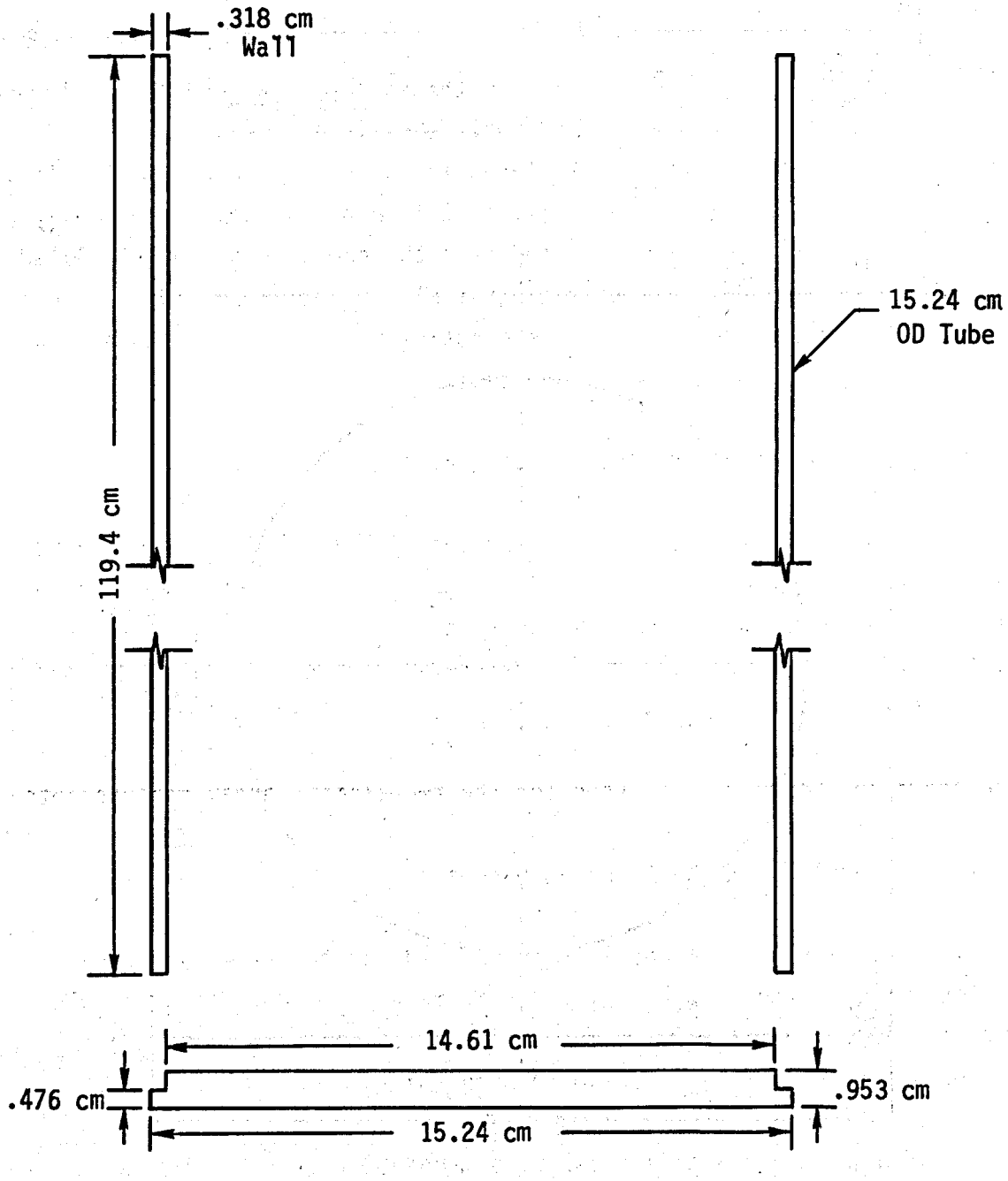

Material: Clear acrylic plastic.

Figure 2.7. Cross sectional view of plastic watertight vessel.

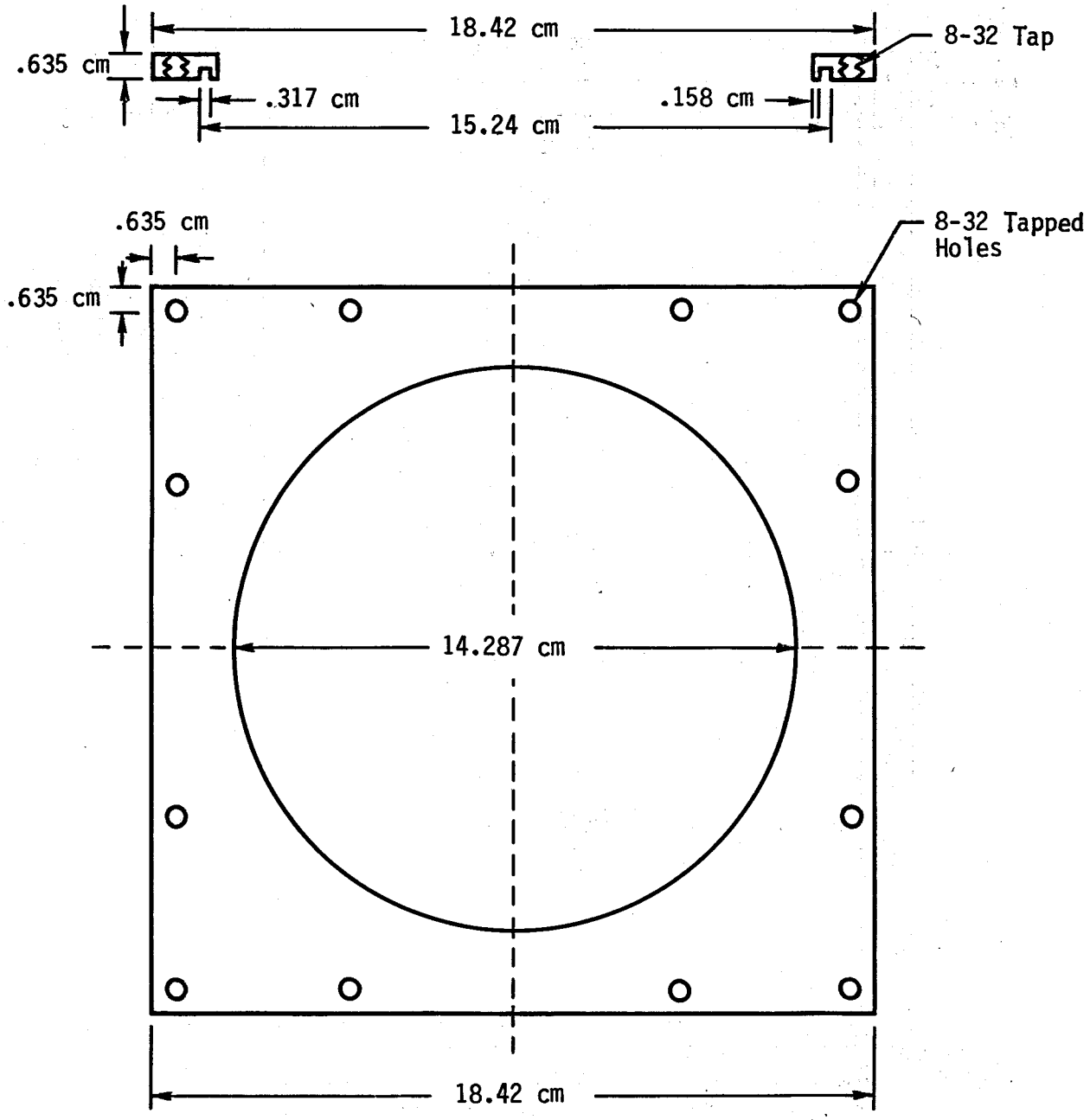

Figure 2.8. Collar (fits on top of plastic cylinder) (1 each).

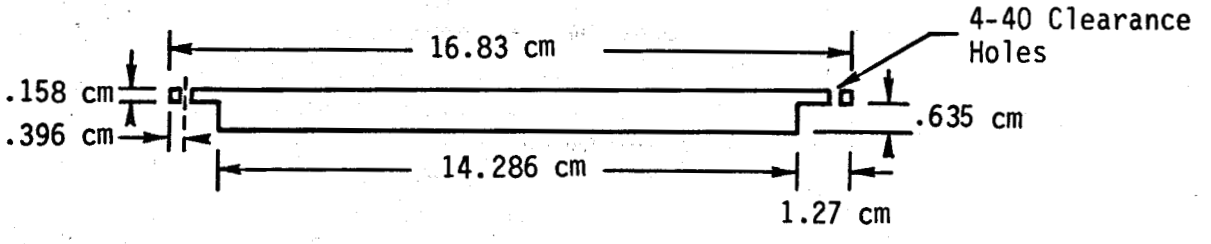

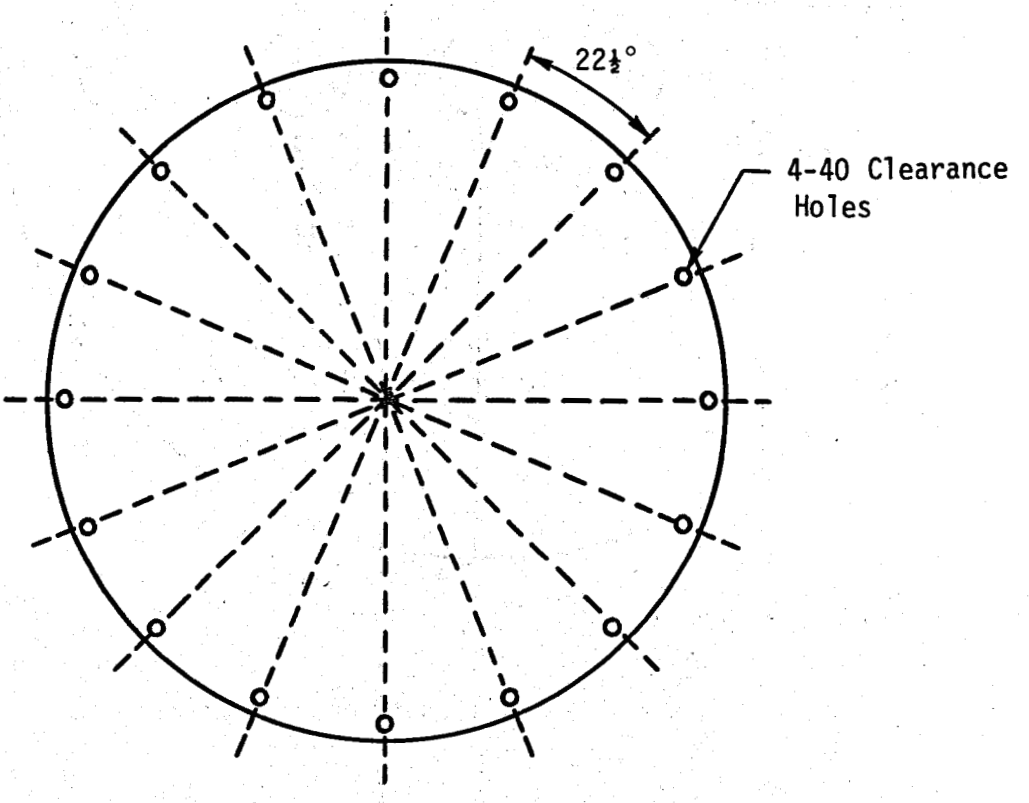

Figure 2.9. Basic rotating antenna carriage (2 each).

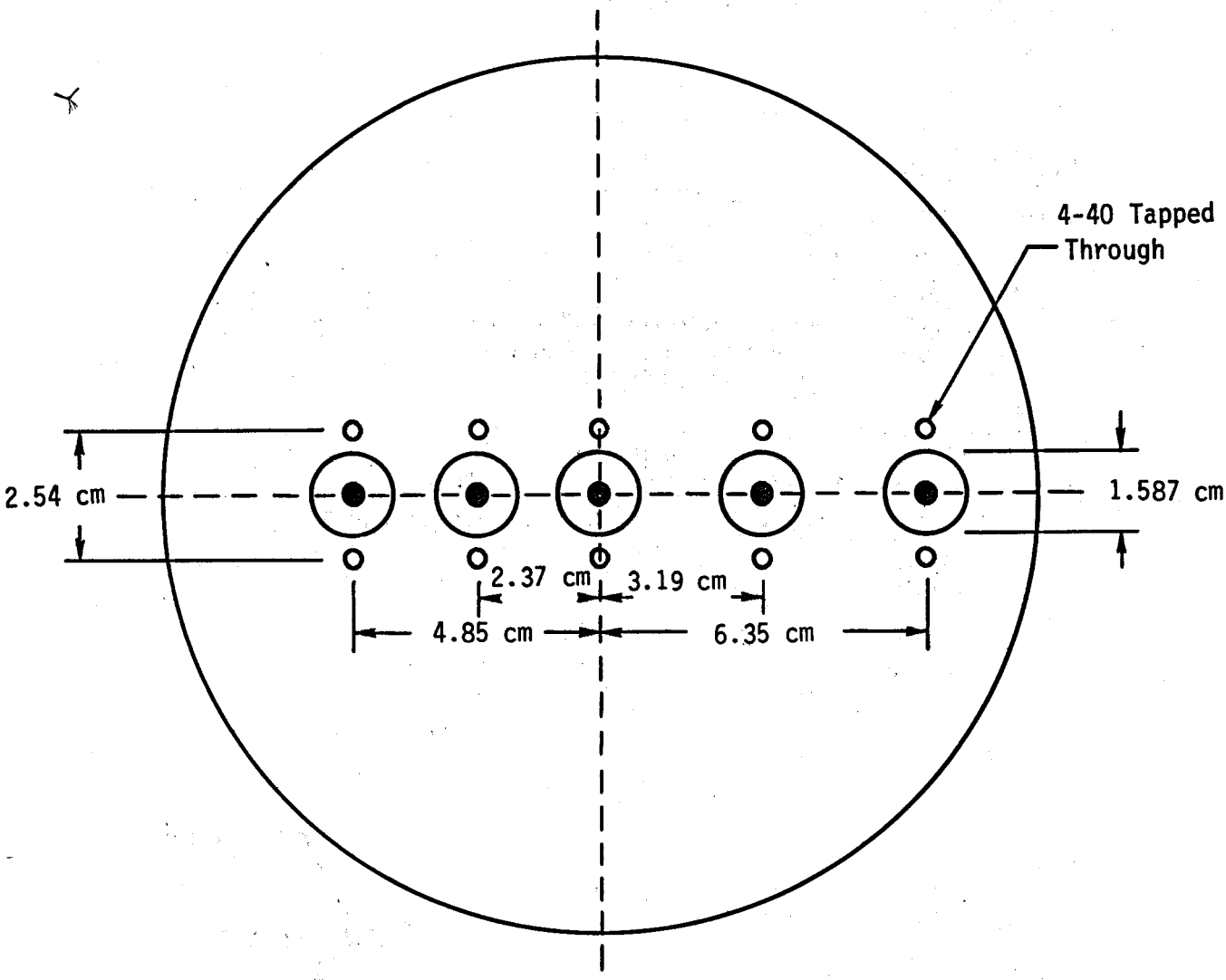

Figure 2.10. Hole pattern for rotating antenna carriage (monopole) (1 each).

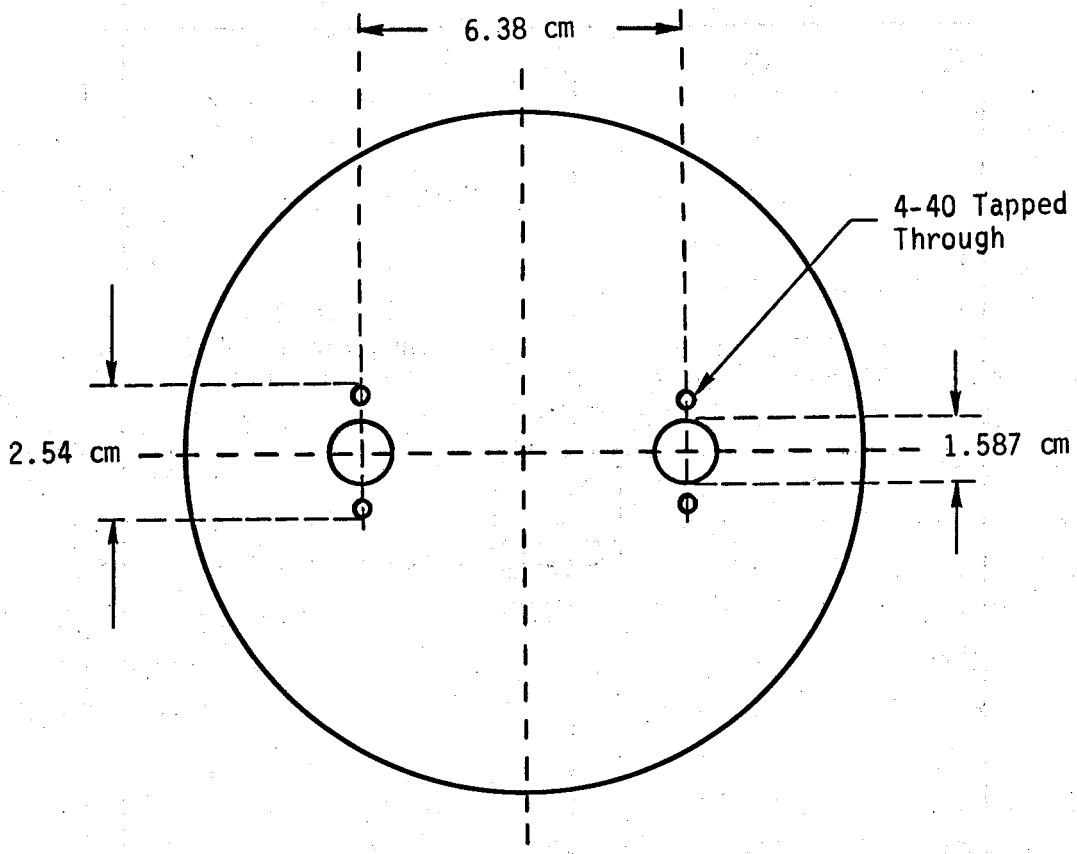

Figure 2.11. Hole pattern for rotating antenna carriage (2-element) (1 each).

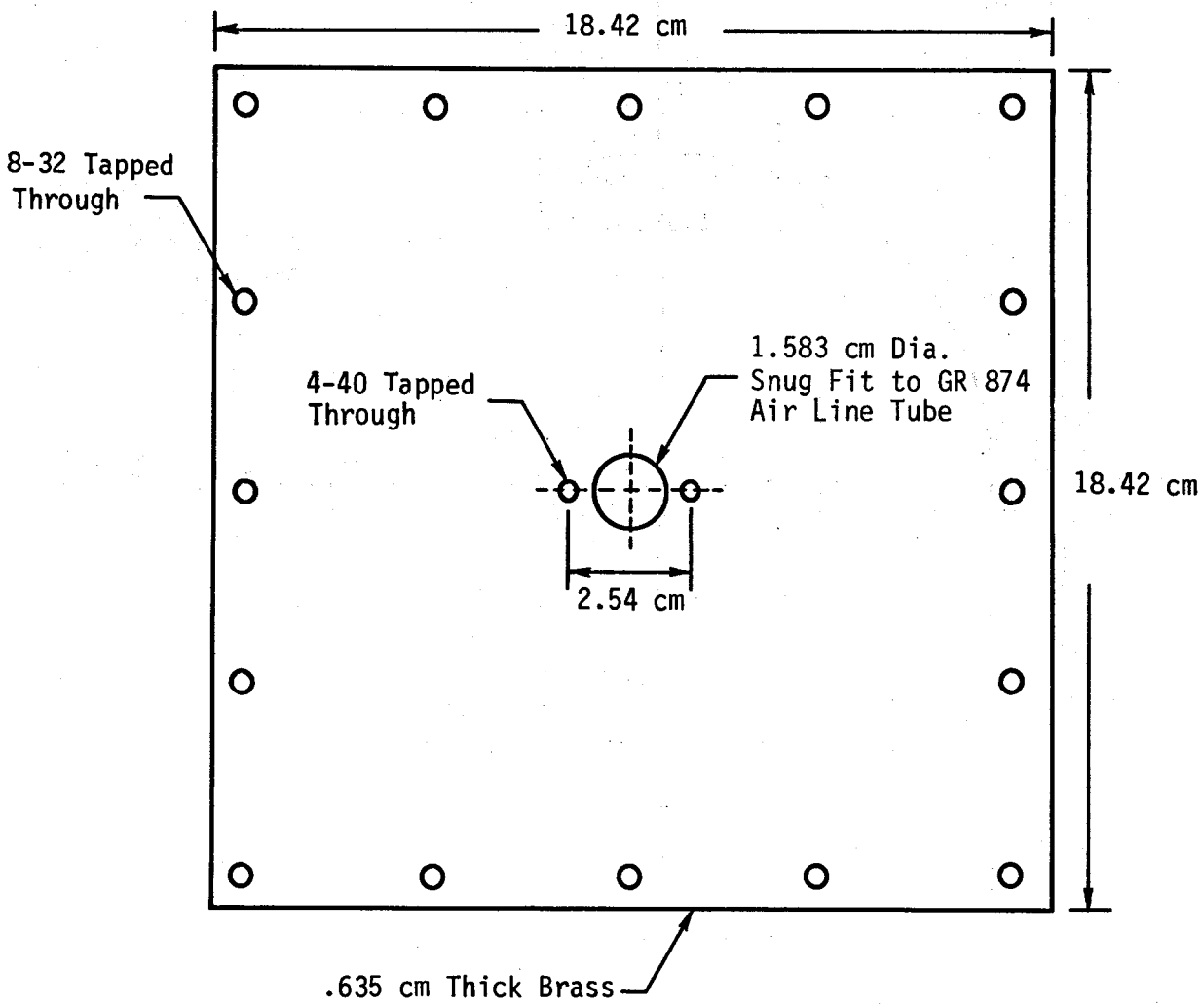

Figure 2.12. Field probe plate (1 each).

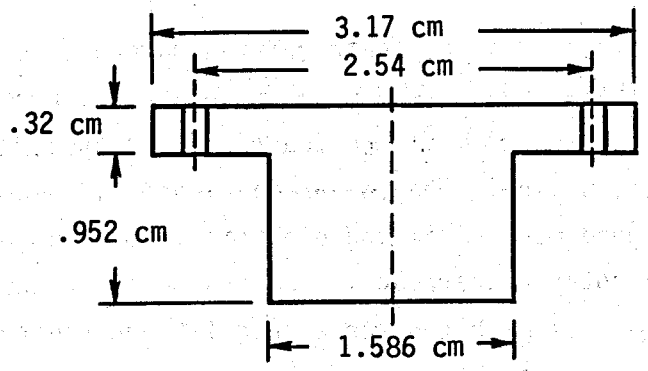

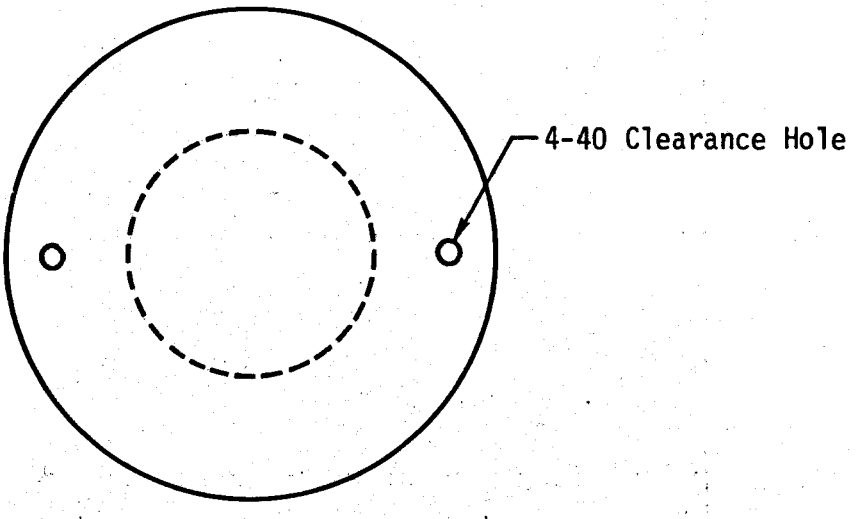

Figure 2.13. Antenna hole plugs.

2.2.4 Antenna Feed Assembly

Finally, the antenna elements and their driving hardware is shown in Figures 2.14 and 2.15. The elements were made of thin brass rods as shown that are screwed into a section of modified General Radio type 874, 50 ohm air dielectric, transmission line. The collar in Figure 2.15 was soldered to the GR line to allow good mechanical and electrical mounting of the antenna element onto the rotating carriage. The insulator at the antenna/ transmission line junction was machined for a snug fit and treated with silicon grease to form a water tight seal.

2.2.5 Corner Reflector Assembly

The last mechanical assembly to be described is the corner reflector. It was formed from sheet brass into a right angle attached with four screws to the rotating antenna mounting plate (Fig. 2.10). Its dimensions are shown in Figure 2.16.

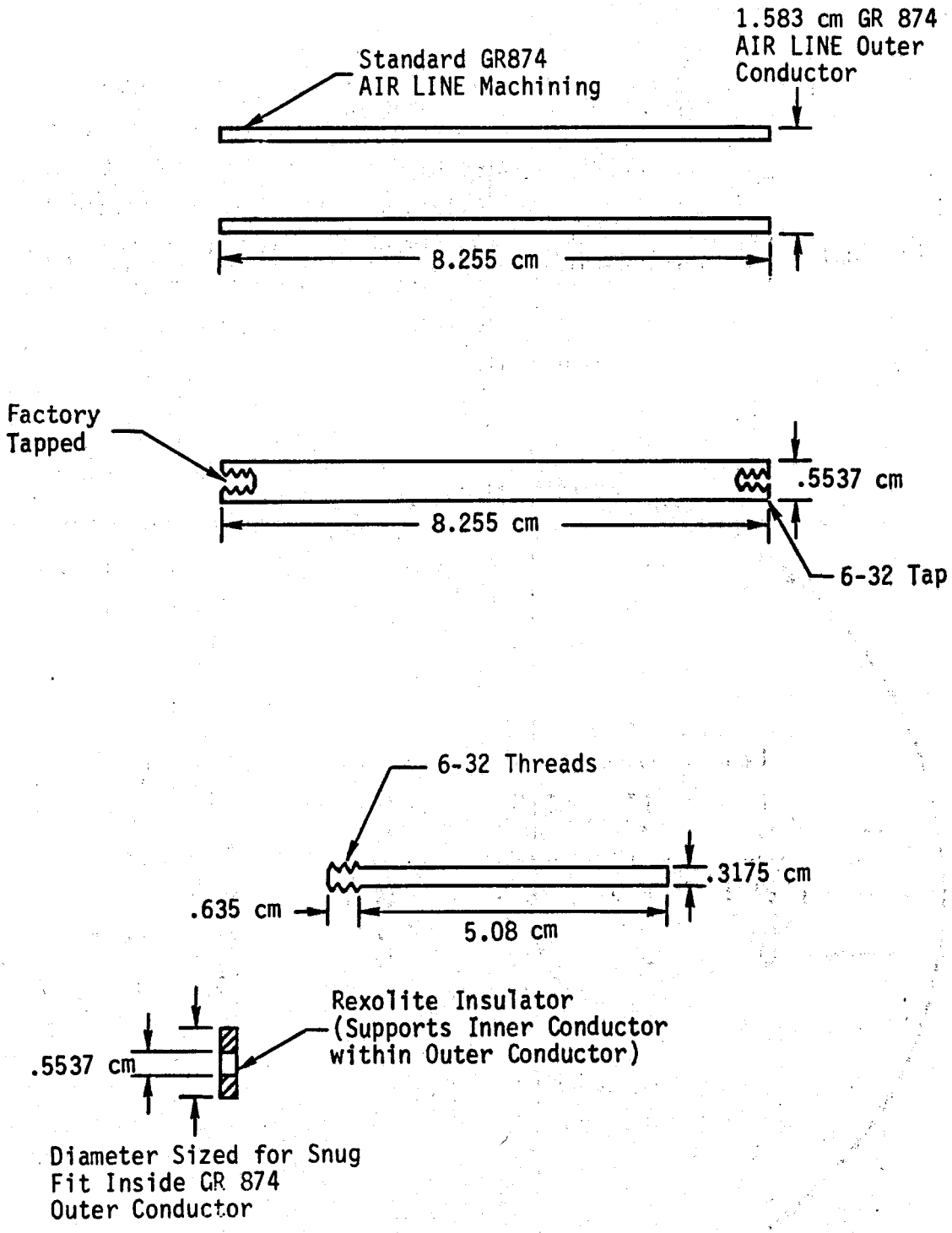

Figure 2.14. Details of antenna assembly.

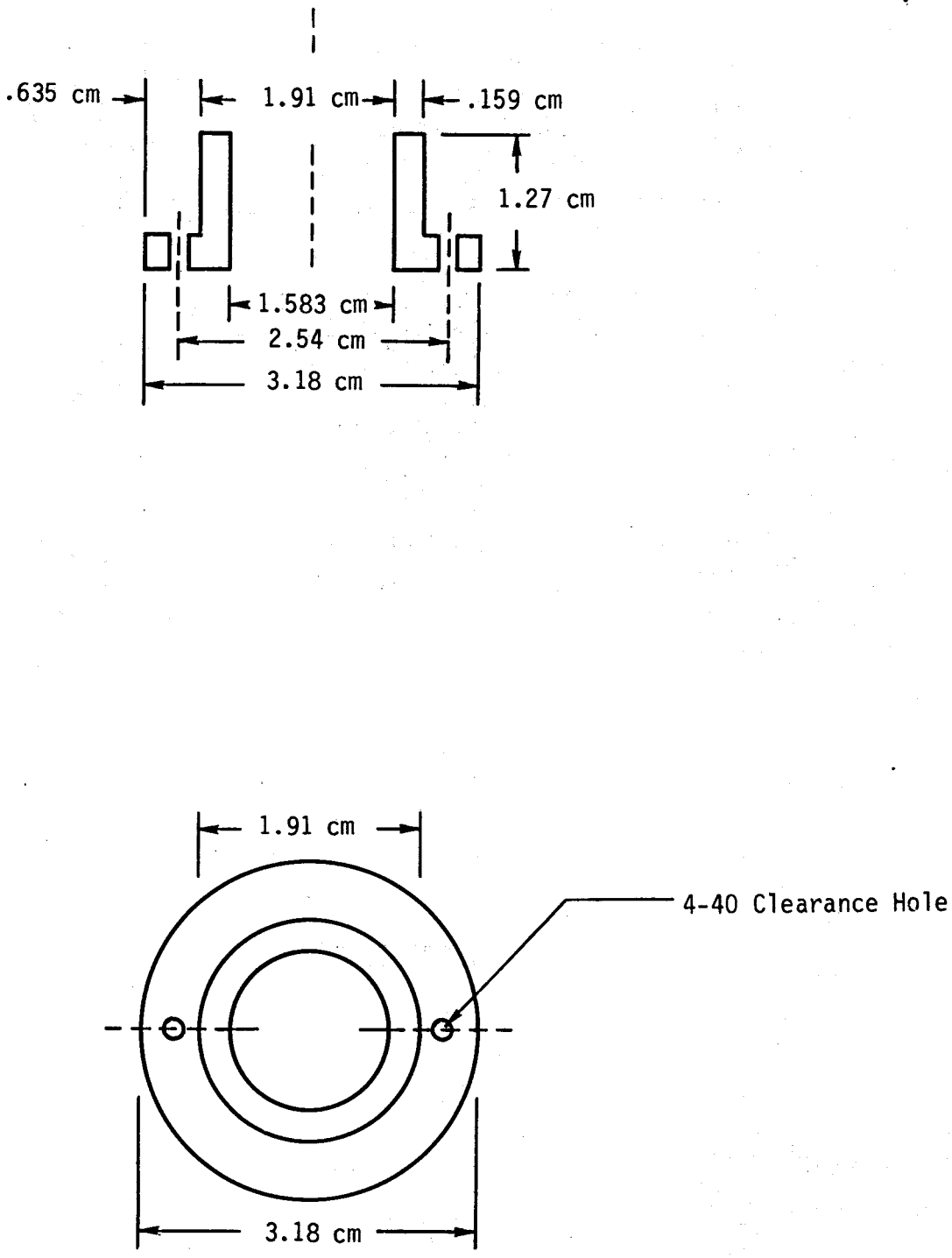

Figure 2.15. Antenna probe collar (5 each).

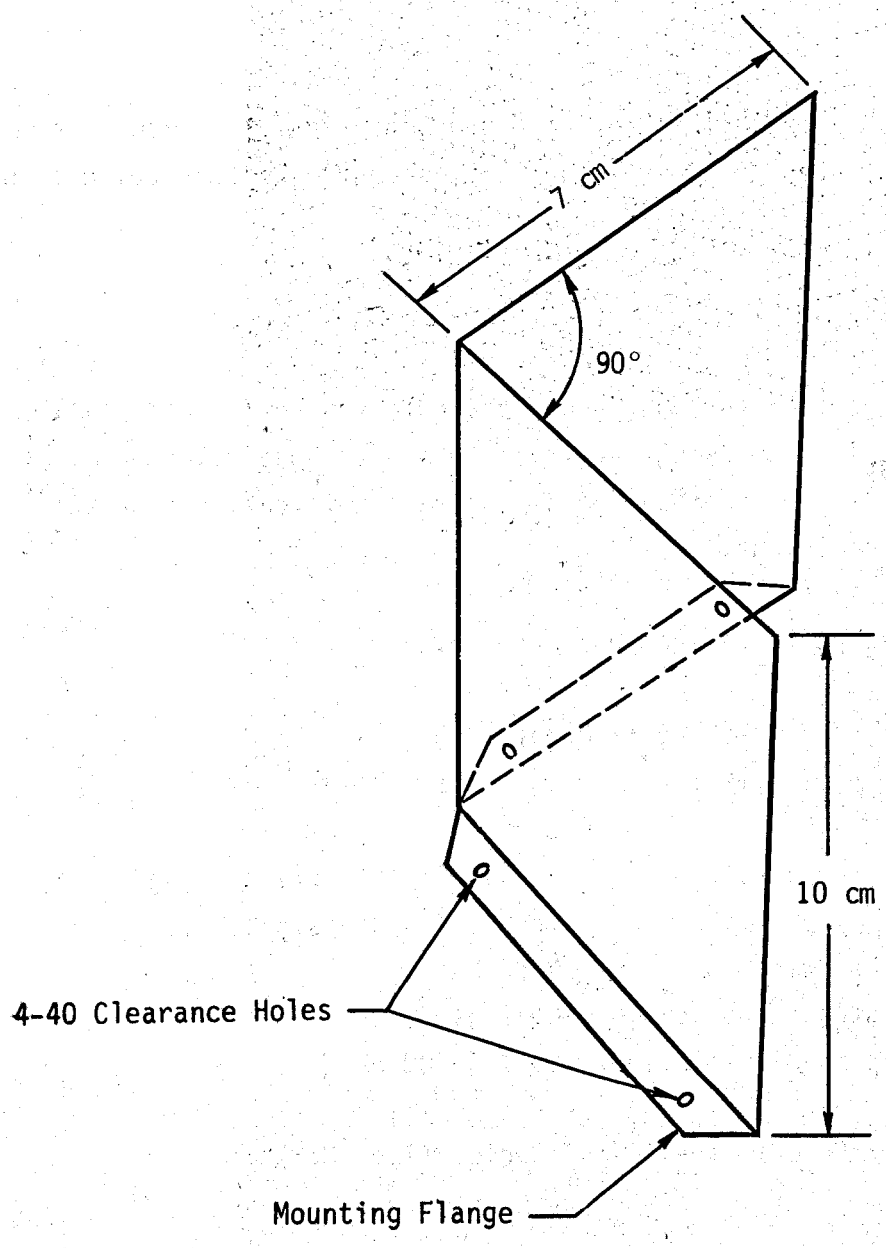

Figure 2.16. Corner reflector assembly.

SECTION 3
TEST PROCEDURE

This section summarizes first the test equipment specifications for all special equipment used for this experiment; second, the data collection and processing and; finally the test procedures.

3.1 Calibrations

All equipment had been through recent periodic inspection and calibration procedures. The following specifications are those relevant to this experiment and are not represented as entire specifications for the particular piece of equipment.

3.1.1 Oscilloscope Specifications (Ref. 3.1)

Tektronix Model 2465

sensitivity:	ch1 5 mv-5 v/div
	ch2 "
accuracy:	+/- 1.25% of V/div setting
	for 4 to 5 division signal
bandwidth:	>300 MHz
step response:	1.17 ns
channel isolation:	50:1 @ 300 MHz

Tektronix Camera Model C-30B Series (Ref. 3.2)

3.1.2 Vector Voltmeter Specifications (Ref. 3.3)

Hewlett Packard Model 8405A

sensitivity:	<20 microvolts
frequency range:	1 to 1000 MHz
accuracy:	2% amplitude
	2 degrees phase

3.1.3 Pulser Specifications (Ref. 3.4)

Tektronix Model 109

rise time:	0.25 nano-seconds
output voltage:	0 to 50 volts with internal power
pulse duration:	determined by length of charge line
	(experiment used 10 cm air line)

TABLE 3.1. PULSER CALIBRATION

	Pulser Dial Setting	Measured Output Peak Value	Photo ID Number
	50 volts	44 volts	445
single cable	40	38	444
50 Ohm load	30	27	442
	12.5	9.2	441
twin cable	20	11.4	440
each 50 Ohm	15	8.4	438

3.1.4 V-I Probe Specifications (Ref. 3.5)

TSC Model Z-DAP	
characteristic Zc:	50 Ohms
impedance range:	1 to 10K Ohms
accuracy:	2% for Zc/8 to 8Zc
	Z/(3Zc)% for >400 Ohms
	(0.3Zc)/Z% for <6 Ohms
electrical length to sensors:	20 cm or 10 cm

3.2 Data Collection and Processing

Data was recorded primarily by oscilloscope photographs along with a log sheet recording the scope settings, pulser level, setup, configuration and other pertinent information. Selected raw data was processed by tabulating, normalizing, plotting, digitizing, Fourier transforming and taking ratios.

3.2.1 Raw Data

Data is collected in raw form by photographing the oscilloscope traces of the time reference signal together with the received field signal. The pulser was operated in a repetitive mode so that medium speed film was adequate for recording the traces. Also, it was possible to view the oscilloscope screen with the unaided eye.

3.2.2 Digitized Data

All data was digitized to some degree. For field patterns, it was necessary only to pick the peak values for the first and second peaks in the waveform. These were positive and negative respectively for the test setup used. These values were tabulated and normalized to produce the field patterns displayed in Section 4.

The whole waveforms for eccentrically mounted monopoles were digitized in their entirety with particular care in starting time at the zero crossover for the time reference signal (see Fig. 3.1).

Also, the overall best configuration for the eccentric monopole, the corner reflector and, the measured two-element antenna array was completely digitized for subsequent Fourier transforming and ratioing with the transformed pulser signal.

3.2.3 Fourier Transforms

In order to better understand the borehole antenna responses and performance, we selected the three cases mentioned above to transform and plot. We also took the ratio of the pulser voltage to received signal to get a look at the system transfer function. Since no rigorous calculations were to be performed with these results, but just to view the data in a different domain, only the magnitude of the Fourier transform was plotted. Since all of the data is archived, the complex transfer function can be calculated at a future time should it be needed.

3.3 Measurement Procedures

In this section we discuss and point out some of the special considerations necessary to execute a successful experimental investigation.

3.3.1 Standard Precautions

The measurement procedures used were straightforward consisting of assuring oneself that all of the equipment was operating within specifications and that all settings were correct and logged accurately. Care was taken to ensure that the borehole was completely filled with distilled

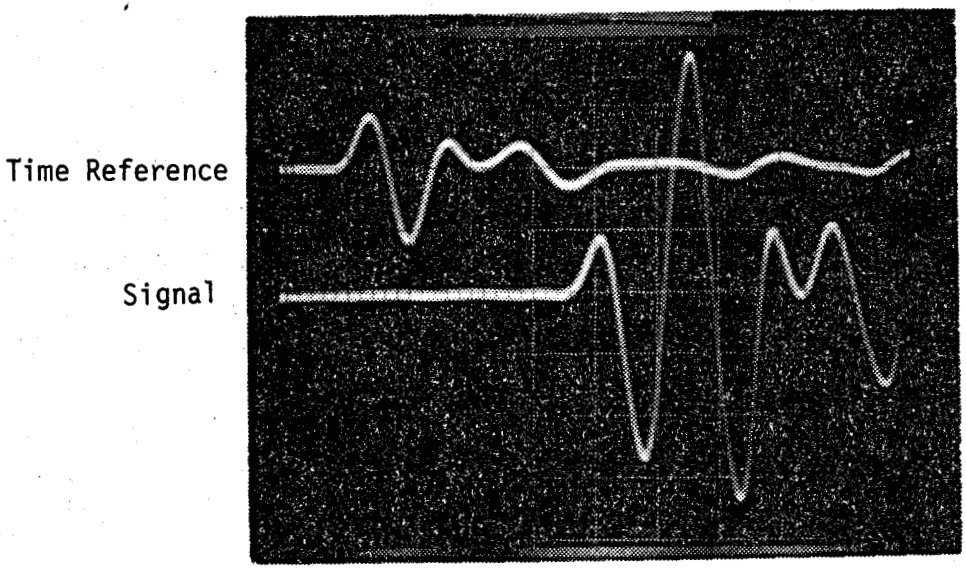

Figure 3.1. Typical field waveform with time reference. (2 ns/div)

water and that no air bubbles were trapped under the antenna rotating carriage. Also, care was taken to insure that the ground screen was in intimate contact with the sand at all locations, especially near the borehole and the receiving probe. In all cases the pulser was operated at voltages of 50 volts or less in a repetitive mode.

3.3.2 Leakage Tests

Tests were performed to insure that no leakage signals were contaminating the desired data by replacing either the transmitting or receiving antennas individually with 50 Ohm dummy loads while maintaining normal cable routing and connection for the remaining antenna.

3.3.3 Maximum Bandwidth

All oscilloscope sensitivity settings were maintained at 5 milli-volts or greater to achieve the greatest bandwidth. The scope was triggered on the time reference signal, where the reference cable length was selected to have the time reference pulse arrive a few nano-seconds before the received signal. In addition, the scope inputs were operated in the internal 50 Ohm termination mode.

3.3.4 Identifying Chamber Wall Reflections

Test chamber wall reflections were observed by looking at greater times while superimposing, by double exposure, the reflections off the normal sand/air interface and a sand/metal interface formed by placing aluminum foil on the wall surface. As seen in Figure 3.2, the wall reflection is measurably beyond the primary ring down response of the system.

3.3.5 Other Reflections

Other possible reflections consist of chamber floor, intra-borehole and, signal cables. As mentioned in Section 2.1 on the experiment design, all of the reflection sources were considered and either cable lengths, matched terminations, critical distances were selected to either eliminate or provide clear time for uncontaminated time domain measurements.

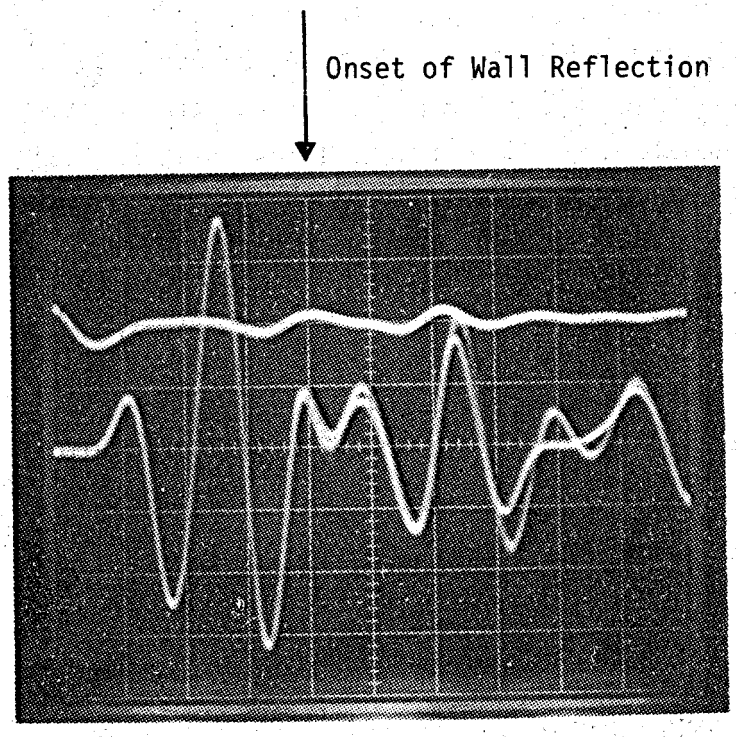

Figure 3.2. Wall reflection identification. (2 ns/div)

SECTION 4
RESULTS

In this section we discuss the results of the various antenna configuration measured responses as well as the determination of the test media electrical properties. Each antenna type that was measured will have its field patterns displayed and the collected data summarized in tabular form. Also, for the most promising configuration of each antenna type, the Fourier transform is shown along with the transfer function formed by dividing the received signal by the transmitter pulse.

4.1 Monopole in Simulated Borehole

The eccentrically positioned monopole in the water filled borehole represents the simplest antenna configuration to be tested and is also the simplest to implement. It is also of significance because from the data collected, certain multi-element array responses can be synthesized by simple computational techniques. These techniques will be discussed in Section 4.3 along with a sample problem.

4.1.1 Excitation

Data was collected for the monopole excited by an impulse having an amplitude of 50 volts or less and a pulse width of about 1.3 ns at half amplitude with a rise-time of about 0.7 ns (see Fig. 4.1).

4.1.2 Field Patterns

A polar scan of 360 degrees was made in 22.5 degree increments for each possible monopole location provided for in the experiment design. These locations are tabulated in Table 4.1.

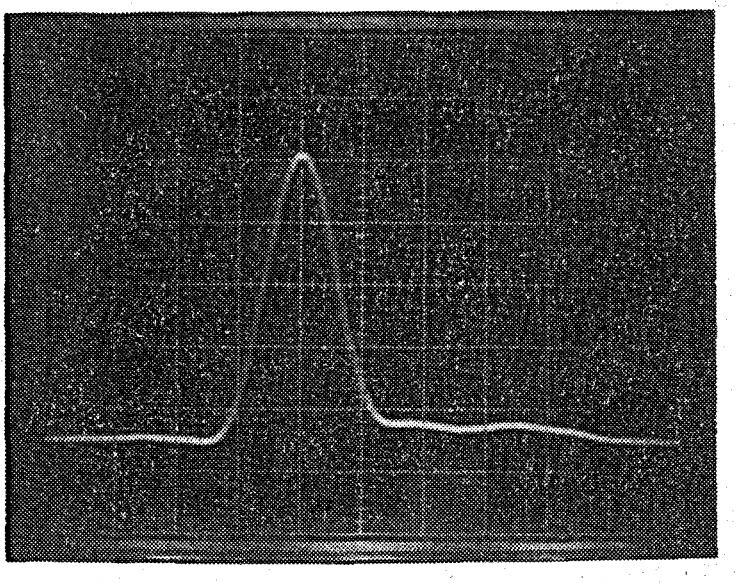

Figure 4.1. Pulser output used to drive antennas (Scale = 1 ns/div).

TABLE 4.1. MONOPOLE LOCATIONS BY NUMBER ON BOREHOLE RADIUS

Location ID	Radius
1	0.00 cm
2	2.37 cm
3	3.19 cm
4	4.85 cm
5	6.35 cm

In anticipation that in future applications, radar signal processing will permit use of the first and possibly the second pulses seen by the target (i.e., positive or negative), we have determined the resulting field patterns and front-to-back ratios for each of these pulses. Figure 4.2 illustrates the field patterns derived in this manner for one of the eccentrically positioned monopoles.

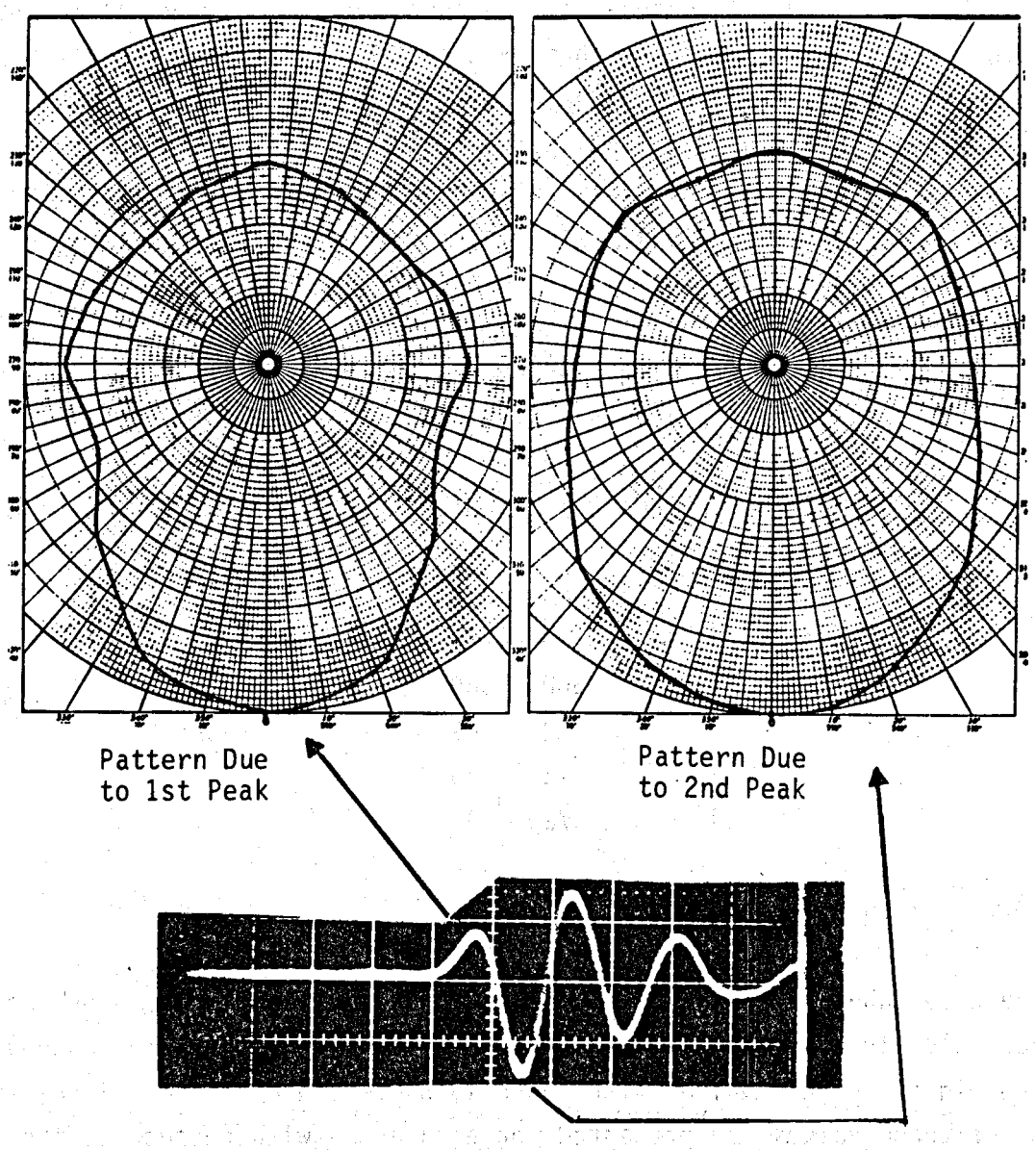

Figure 4.2. Field pattern for the eccentric monopole placed at 3.19 cm off center.

Since location #1 is centered in the borehole, it was used as an omni-directional reference and as such has no directional pattern. Location #5 proved to be too close to the borehole wall to be practical and had a poorly behaved pattern. Hence, its pattern and summary data are not included in this report. The field patterns related to the first positive and first negative arriving pulses for locations #2, #3,and #4 are shown in Figures 4.3a,b; 4.4a,b; and 4.5a,b respectively.

It is from these figures that we derive the beam width angles for the positive (+) and negative (-) pulses tabulated below:

TABLE 4.2. BEAM WIDTHS FOR THE ECCENTRICALLY POSITIONED MONOPOLE

Radius	Beam Width +	-
1	360	360
2	84	109
3	78	78
4	n/a	48

4.1.3 Tabulated Results

We have tabulated below, the measured peak received signals for the eccentrically located monopole for each of the four radii mentioned above. The raw digitized peak values with photo ID numbers are listed. Then, the ratios of these values are presented for each angle with respect to the forward direction, or zero angle. Then, these ratios are turned into decibels for convenient evaluation of performance.

4.2 Corner Reflector Antenna

The corner reflector in the water filled borehole represents another simple antenna configuration that was tested and is also easy to

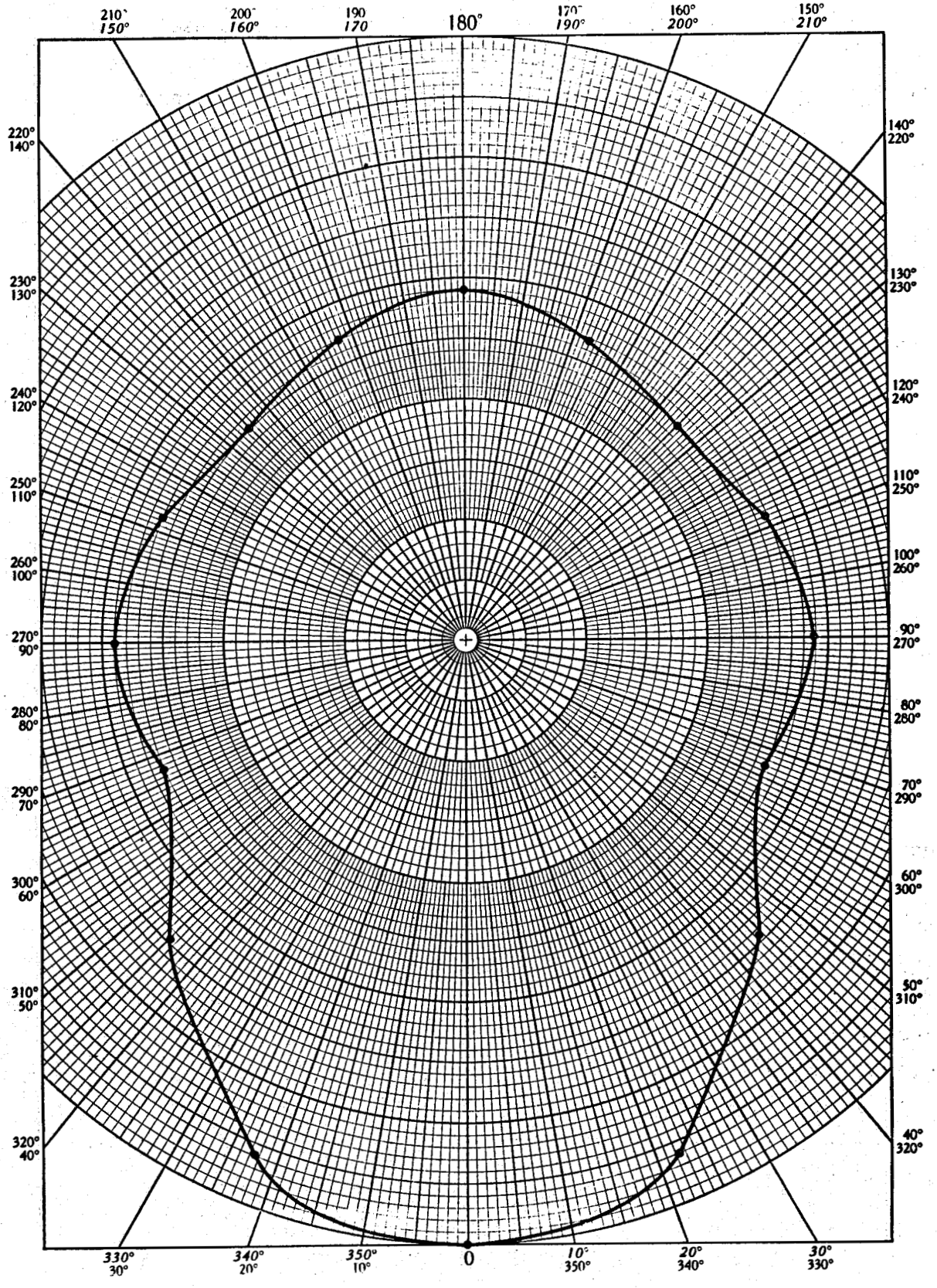

Figure 4.3a. Field pattern using first pulse for monopole. (radius = 2.37 cm)

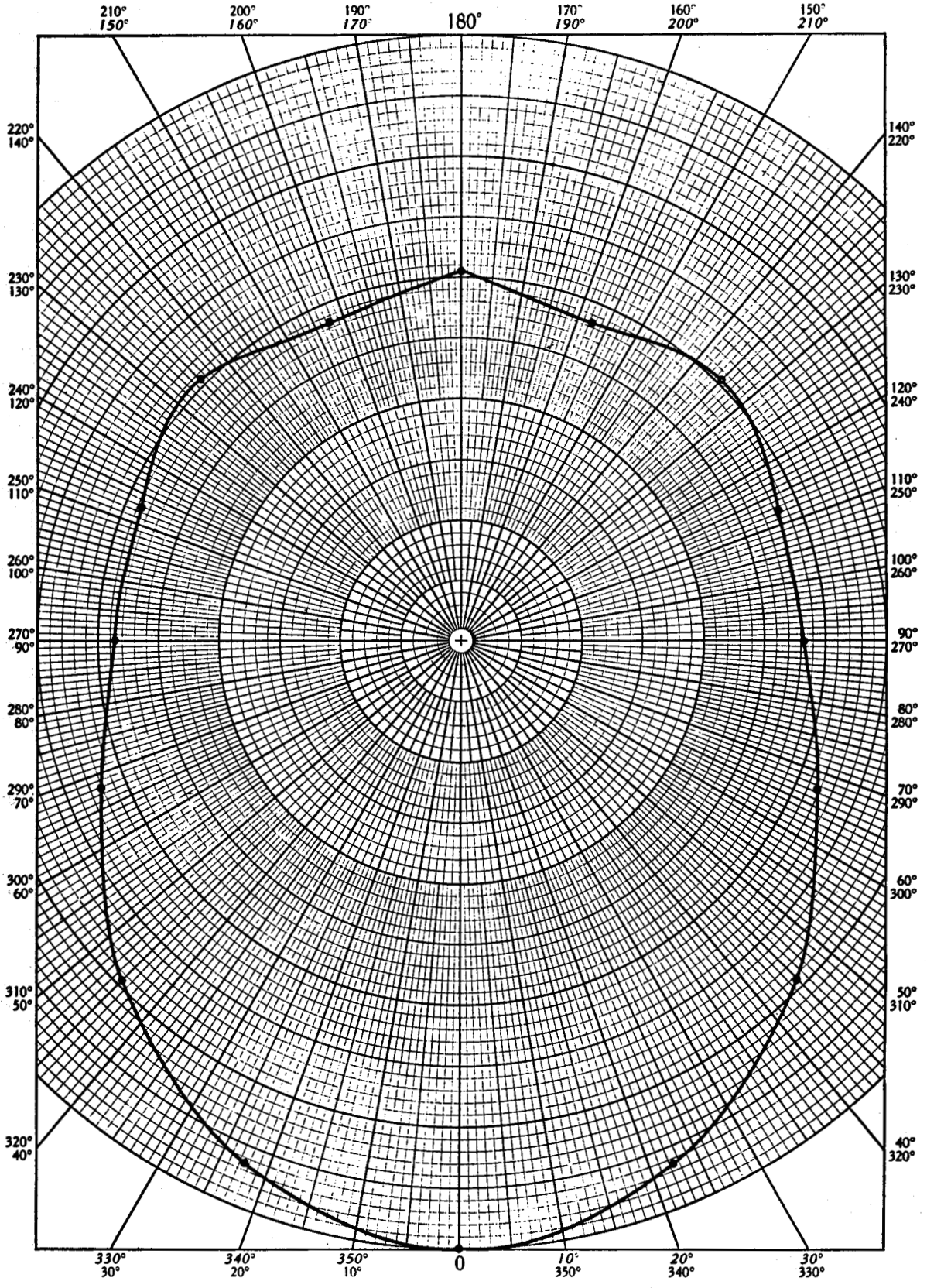

Figure 4.3b. Field pattern using second pulse for monopole. (radius = 2.37 cm)

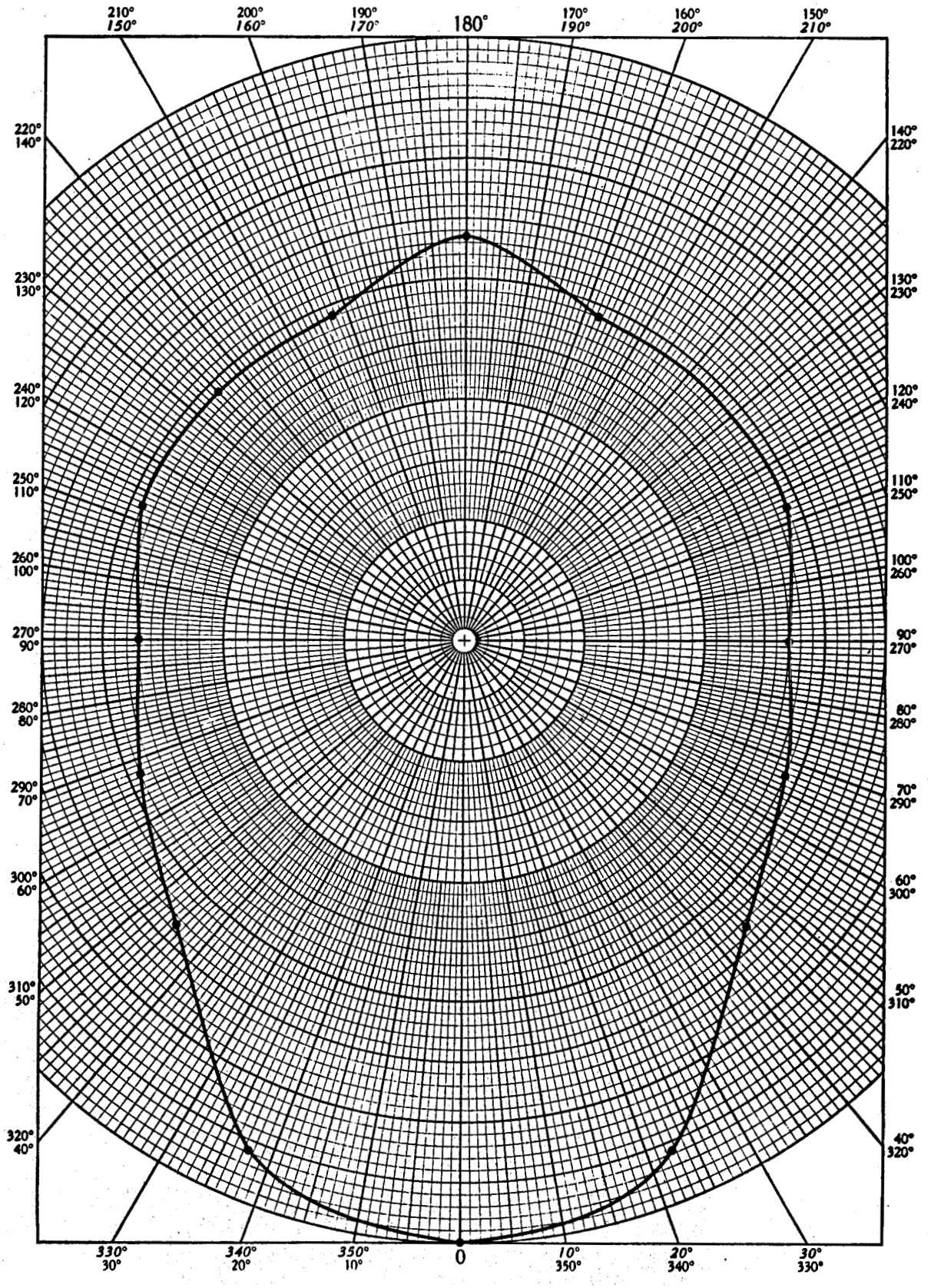

Figure 4.4a. Field pattern using first pulse for monopole. (radius = 3.19 cm)

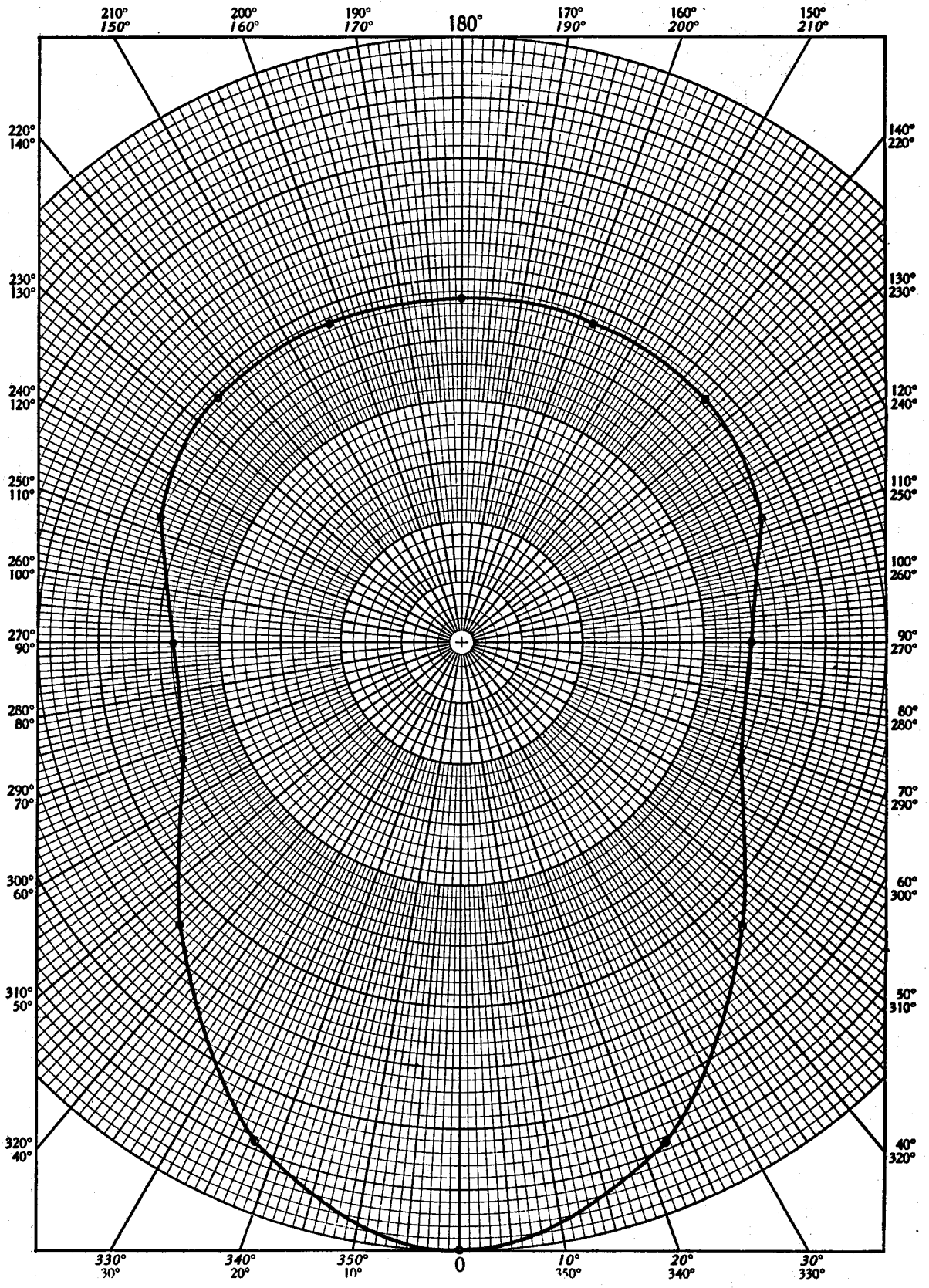

Figure 4.4b. Field pattern using second pulse for monopole. (radius = 3.19 cm)

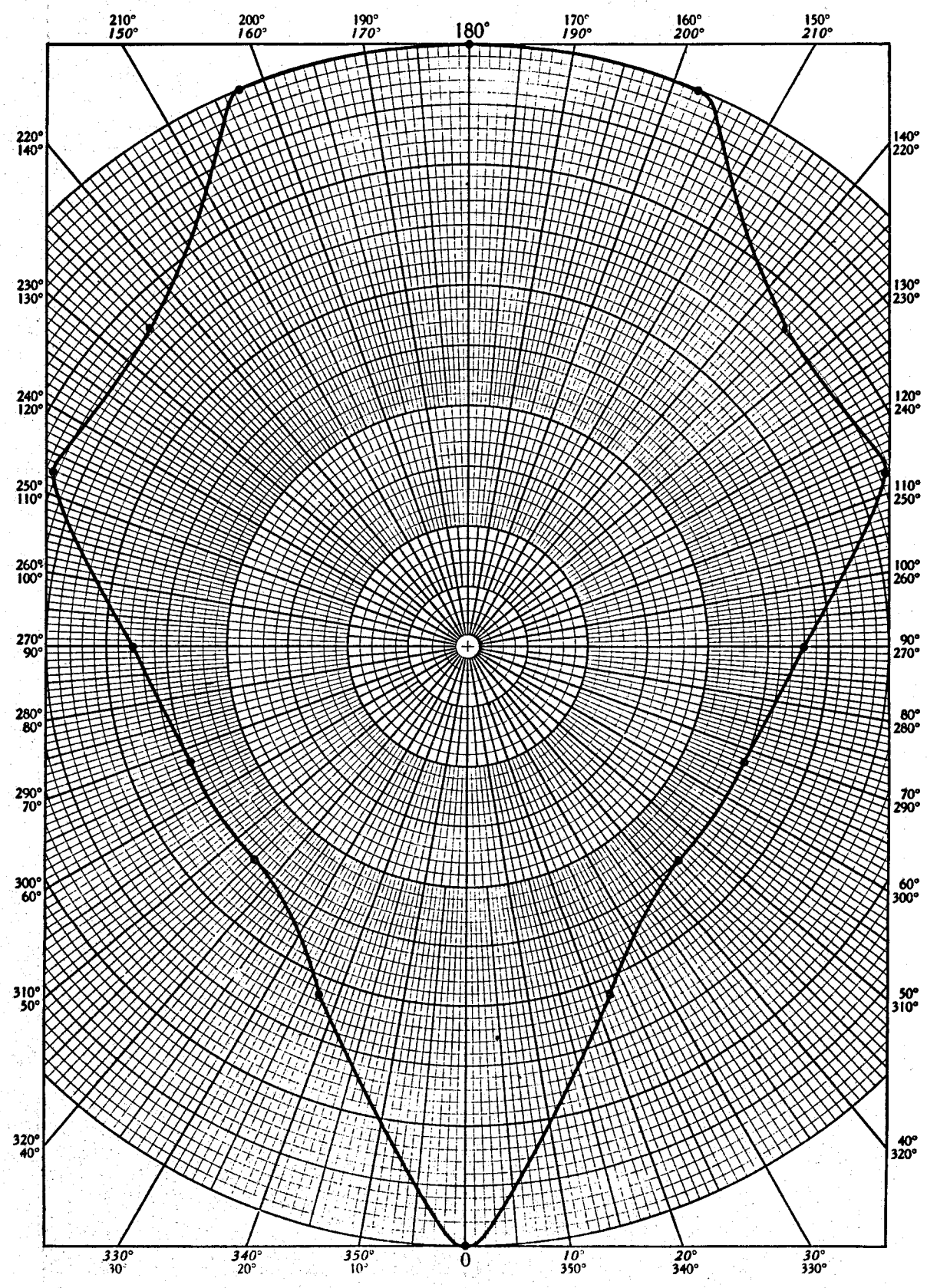

Figure 4.5a. Field pattern using first pulse for monopole. (radius = 4.85 cm)

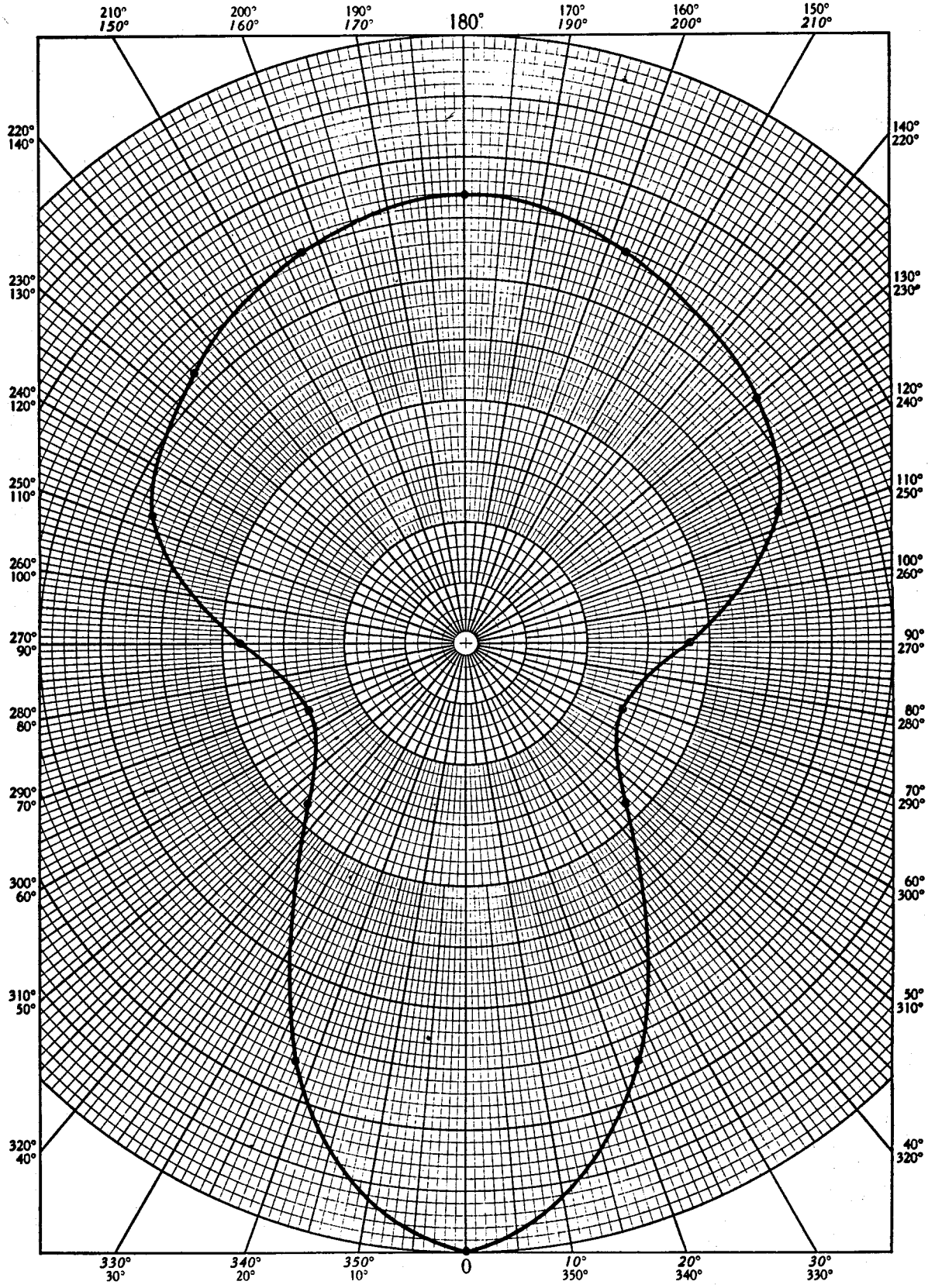

Figure 4.5b. Field pattern using second pulse for monopole. (radius = 4.85 cm)

TABLE 4.3. MONOPOLE IN RADIUS #1 (CENTERED)

MONOPOLE IN RADIUS 1

	RATIOS WRT 0		LOG OF RATIOS		RAW DATA		
ANGLE	POS	NEG	POS	NEG	POS	NEG	ID #
ALL	1.00	1.00	.00	.00	.90	2.30	2460

TABLE 4.4. MONOPOLE IN RADIUS #2 (2.37 cm)

MONOPOLE IN RADIUS 2

	RATIOS WRT 0		LOG OF RATIOS		RAW DATA		
ANGLE	POS	NEG	POS	NEG	POS	NEG	ID #
.00	1.00	1.00	.00	.00	1.30	2.80	2428
22.50	.92	.93	-.70	-.64	1.20	2.60	2429
45.00	.69	.79	-3.19	-2.09	.90	2.20	2430
67.50	.54	.64	-5.38	-3.84	.70	1.80	2431
90.00	.58	.57	-4.78	-4.86	.75	1.60	2432
112.50	.54	.57	-5.38	-4.86	.70	1.60	2433
135.00	.50	.61	-6.02	-4.33	.65	1.70	2434
157.50	.54	.57	-5.38	-4.86	.70	1.60	2435
180.00	.58	.61	-4.78	-4.33	.75	1.70	2436

TABLE 4.5. MONOPOLE IN RADIUS #3 (3.19 cm)

MONOPOLE IN RADIUS 3

	RATIOS WRT 0		LOG OF RATIOS		RAW DATA		
ANGLE	POS	NEG	POS	NEG	POS	NEG	ID #
.00	1.00	1.00	.00	.00	1.20	2.80	2418
22.50	.92	.89	-.76	-.98	1.10	2.50	2417
45.00	.67	.66	-3.52	-3.60	.80	1.85	2416
67.50	.58	.50	-4.68	-6.02	.70	1.40	2415
90.00	.54	.48	-5.33	-6.34	.65	1.35	2414
112.50	.58	.54	-4.68	-5.42	.70	1.50	2413
135.00	.58	.57	-4.68	-4.86	.70	1.60	2412
157.50	.58	.57	-4.68	-4.86	.70	1.60	2411
180.00	.67	.57	-3.52	-4.86	.80	1.60	2410

TABLE 4.6. MONOPOLE IN RADIUS #4 (4.85 cm)

MONOPOLE IN RADIUS 4

	RATIOS WRT 0		LOG OF RATIOS		RAW DATA		
ANGLE	POS	NEG	POS	NEG	POS	NEG	ID #
.00	1.00	1.00	.00	.00	.80	2.15	2444
22.50	.63	.74	-4.08	-2.57	.50	1.60	2445
45.00	.50	.37	-6.02	-8.59	.40	.80	2446
67.50	.50	.28	-6.02	-11.09	.40	.60	2447
90.00	.56	.37	-5.00	-8.59	.45	.80	2448
112.50	.75	.56	-2.50	-5.07	.60	1.20	2449
135.00	.75	.63	-2.50	-4.04	.60	1.35	2450
157.50	1.00	.70	.00	-3.13	.80	1.50	2451
180.00	1.00	.74	.00	-2.57	.80	1.60	2452

*** NOTE ***

FOR ALL DATA, THE FOLLOWING VALUES REMAIN THE SAME:

SIGNAL SENSITIVITY = 5E-3 VOLTS
REFERENCE SENSITIVITY = 1E-2 VOLTS
SWEEP SPEED = 2E-9 SECONDS
PULSER LEVEL = 12.5 VOLTS
RADIUS 1 = 0.00 CM
RADIUS 2 = 2.37 CM
RADIUS 3 = 3.19 CM
RADIUS 4 = 4.85 CM

implement. It is interesting because it is directly related to a four element array through imaging as implemented for this study. The relation to four elements is because of the 90 degree angle used at the apex.

4.2.1 Excitation

Data was collected for the monopole in front of the corner reflector excited by an impulse having an amplitude of 50 volts or less and a pulse width of about 1.3 ns at half amplitude with a rise-time of about 0.7 ns (the same as for the eccentric monopole, see Fig. 4.1).

4.2.2 Field Patterns

A polar scan of 360 degrees was made in 22.5 degree increments for each possible monopole location provided for in the experiment design with the corner reflector in place. These locations have already been tabulated in Table 4.1 in the previous section.

As discussed in Section 4.1.2, we anticipate that in future applications, radar signal processing will permit use of the first and possibly the second pulses seen by the target (i.e., positive or negative), we have determined the resulting field patterns and front-to-back ratios for each of these pulses.

In this case, the monopole located at radius #1 is of interest even though it is located at the center of the borehole. In fact, this is of special interest because a radar could be implemented with the monopole fixed and the reflector rotating about it. The field patterns related to the first positive and first negative arriving pulses for locations #1,#2, #3,and #4 are shown in Figures 4.6a,b; 4.7a,b; 4.8a,b and 4.9a,b respectively.

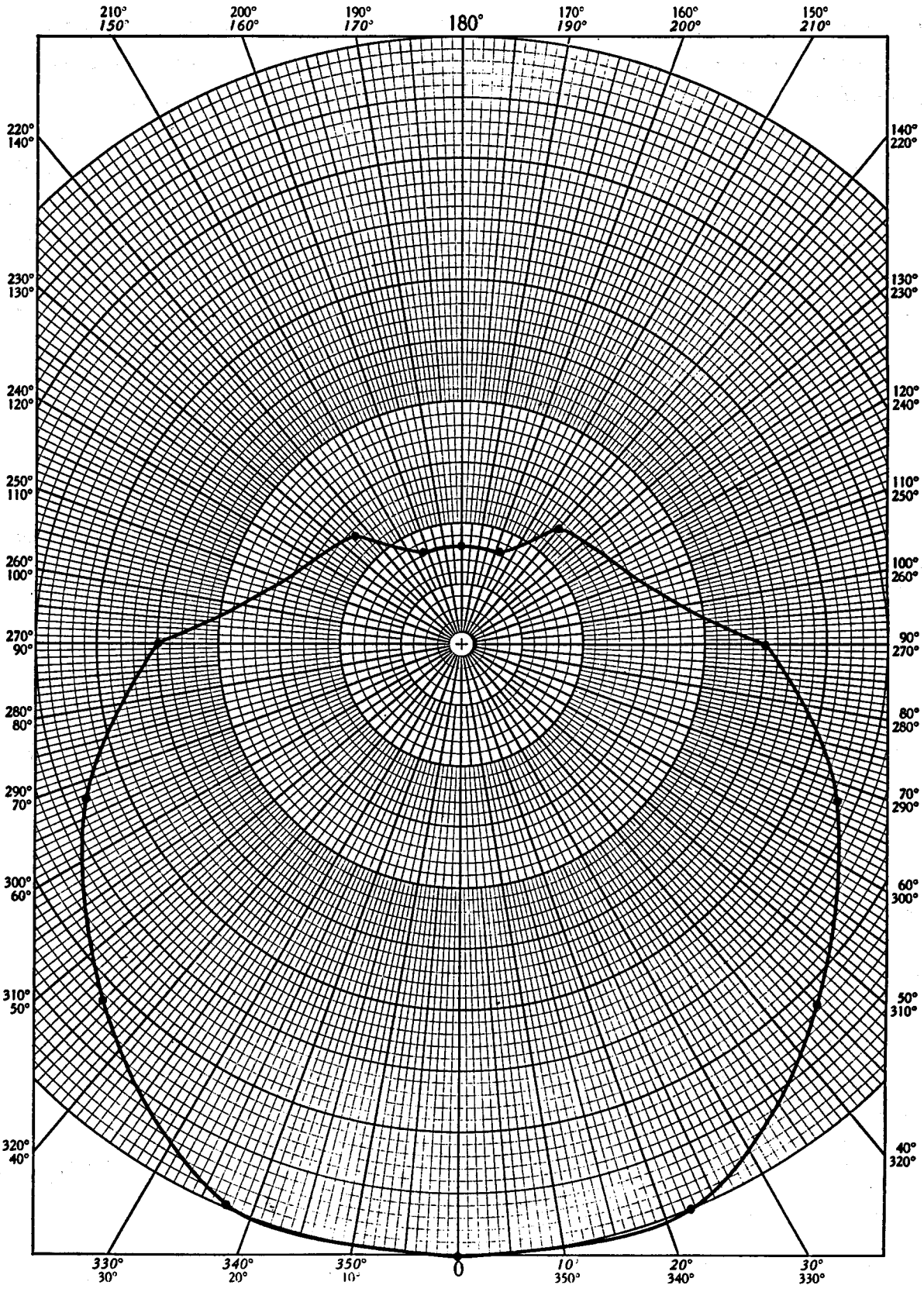

Figure 4.6a. Field pattern using first pulse for corner reflector. (monopole at radius = 0.00 cm)

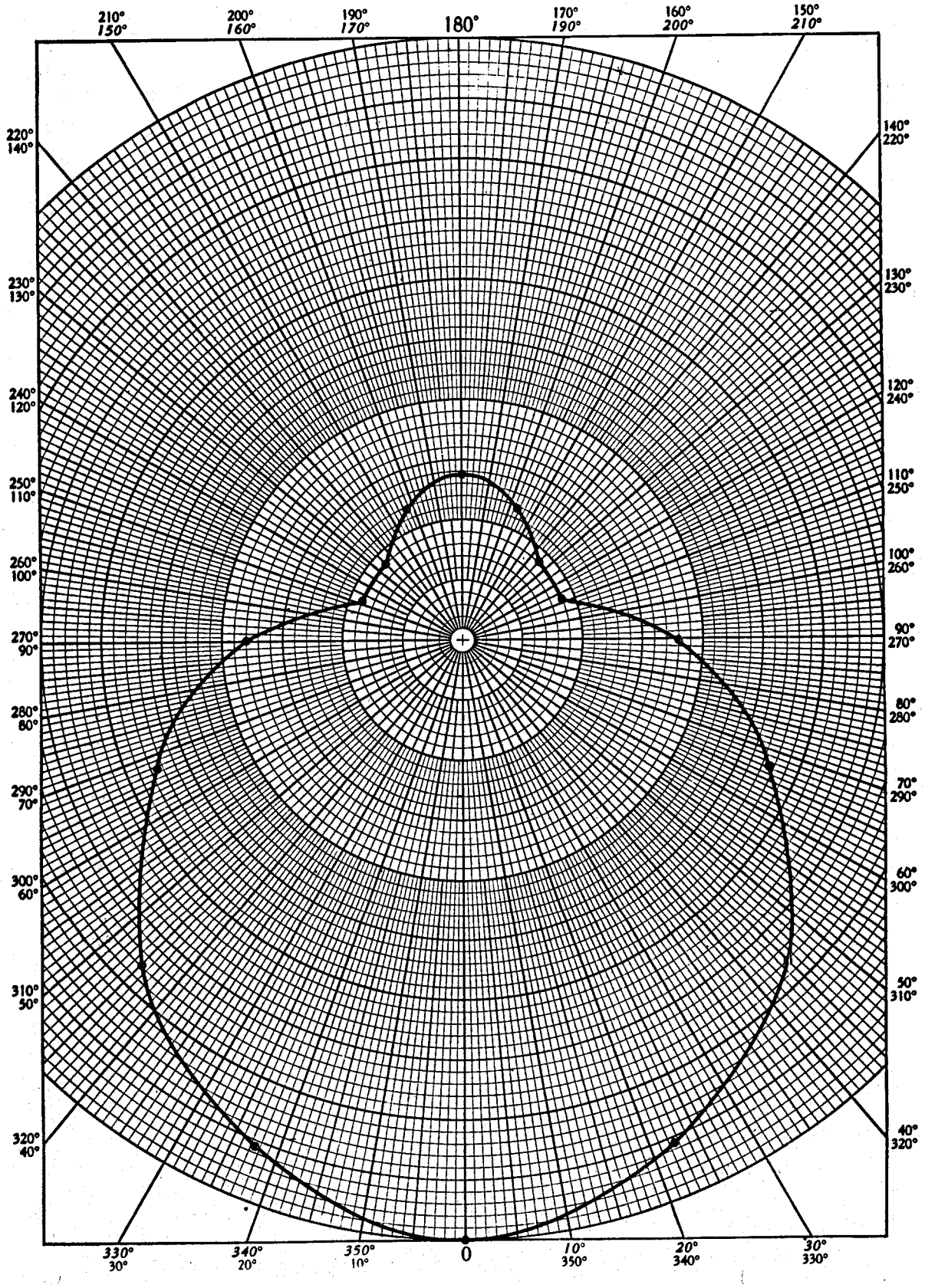

Figure 4.6b. Field pattern using second pulse for corner reflector. (monopole at radius = 0.00 cm)

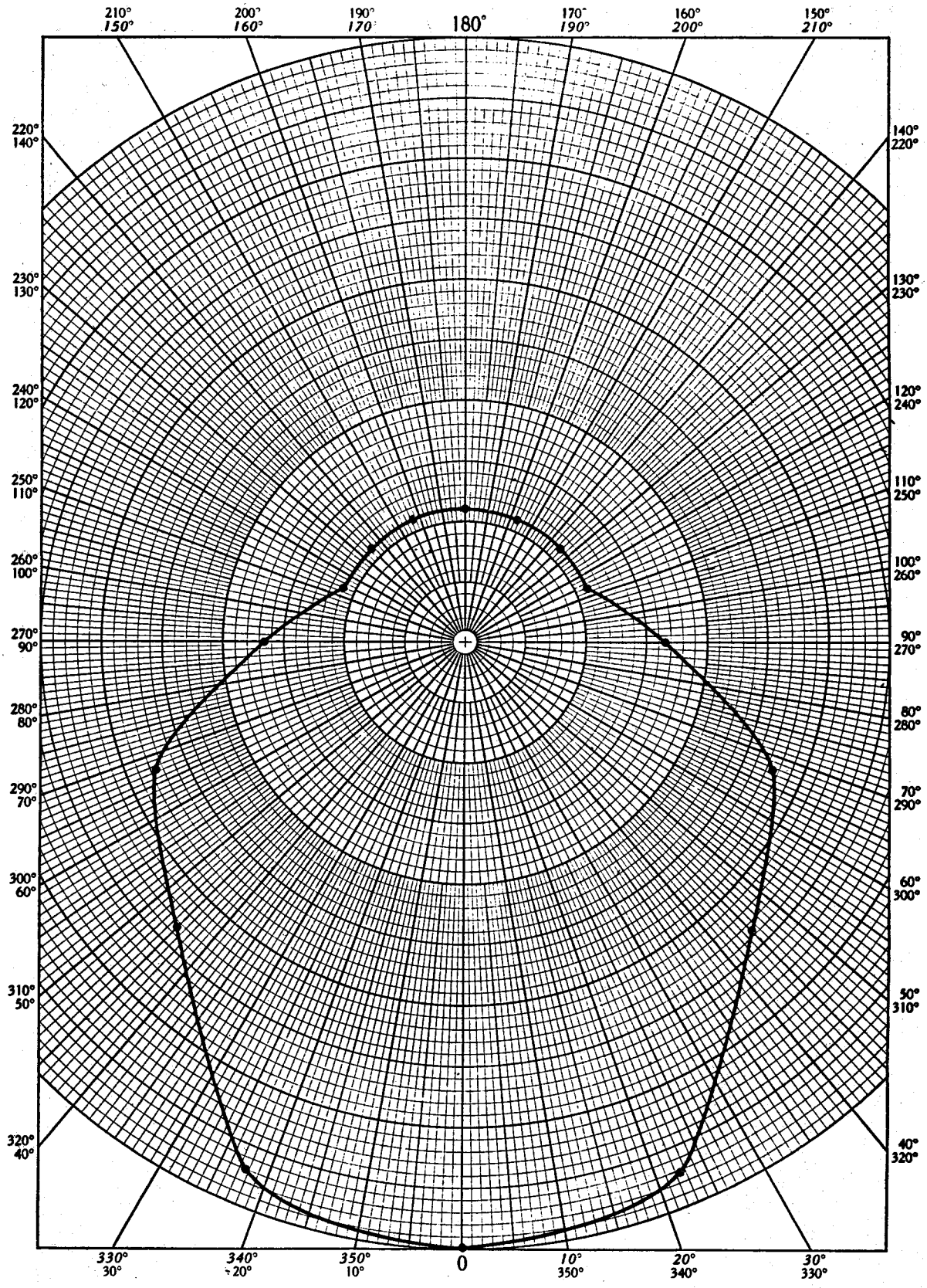

Figure 4.7a. Field pattern using first pulse for corner reflector. (monopole at radius = 2.37 cm)

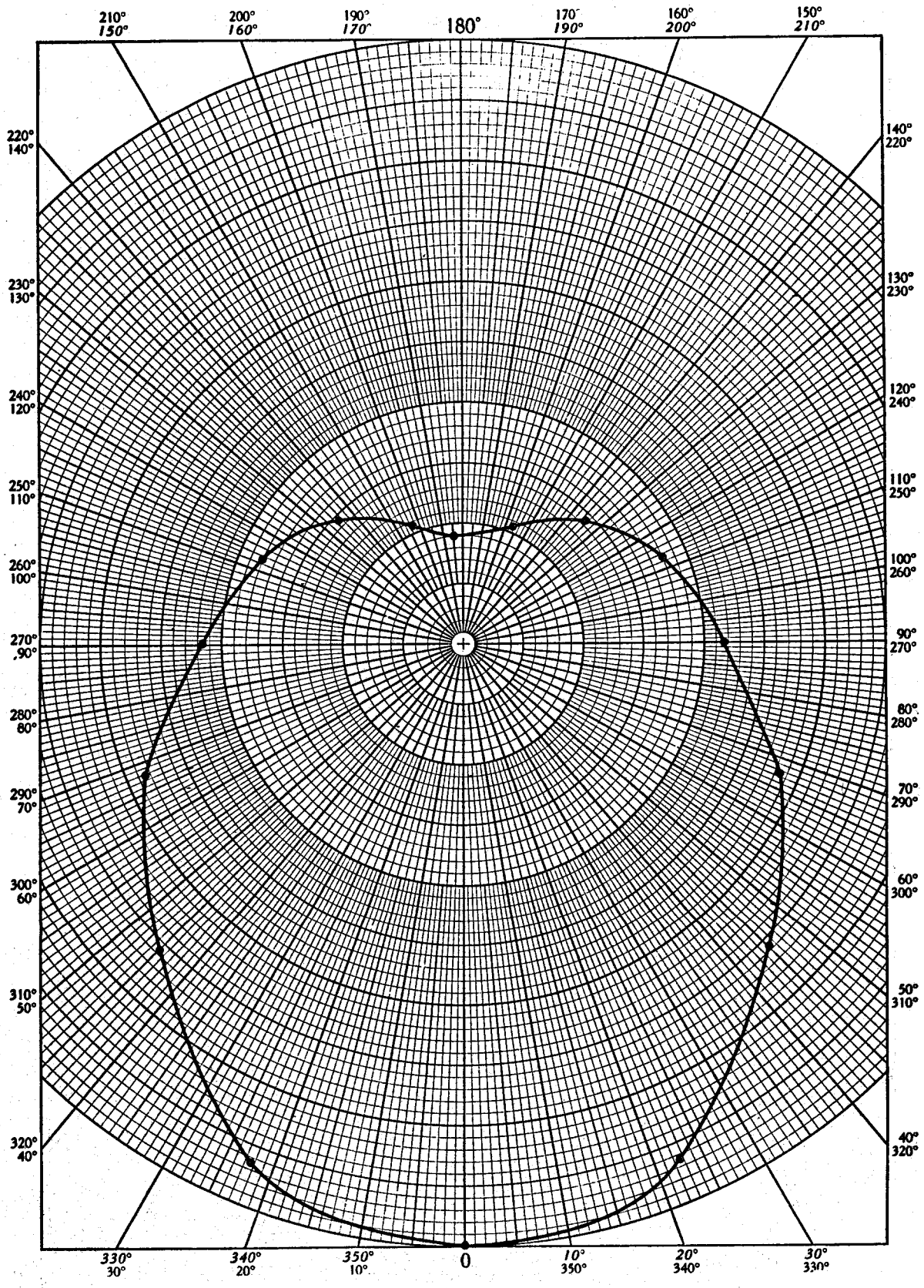

Figure 4.7b. Field pattern using second pulse for corner reflector. (monopole at radius = 2.37 cm)

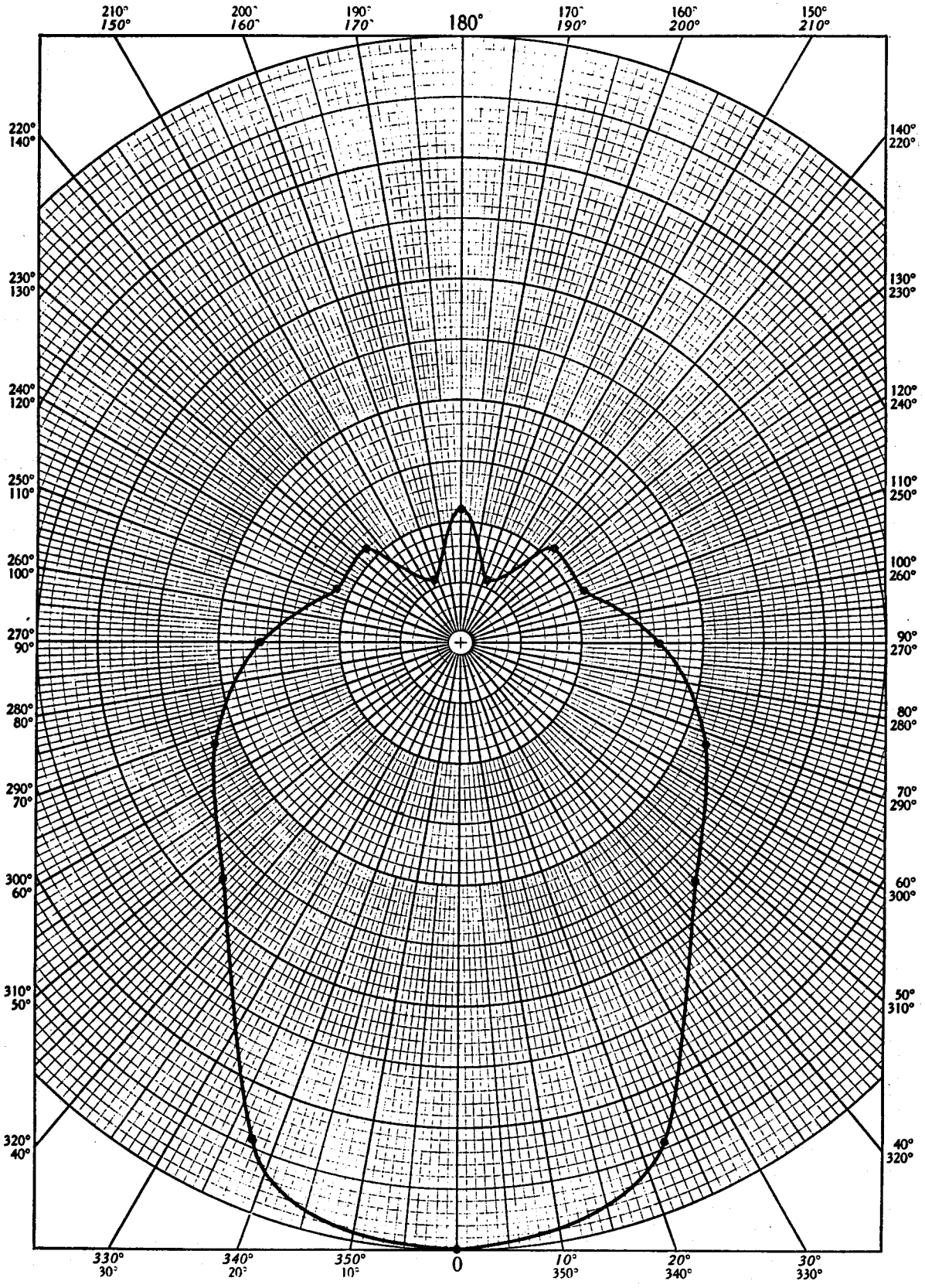

Figure 4.8a. Field pattern using first pulse for corner reflector. (monopole at radius = 3.19 cm)

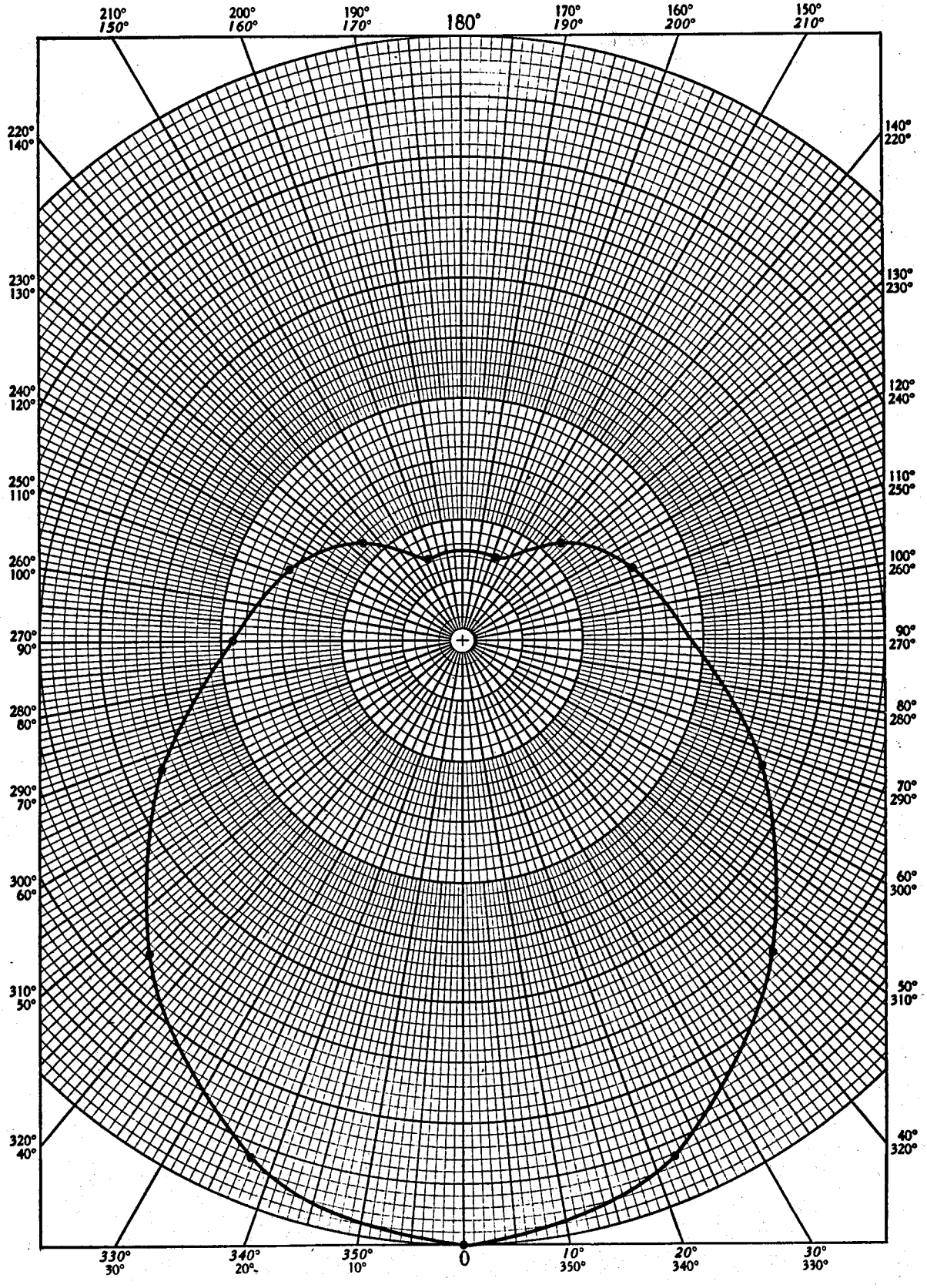

Figure 4.8b. Field pattern using second pulse for corner reflector. (monopole at radius = 3.19 cm)

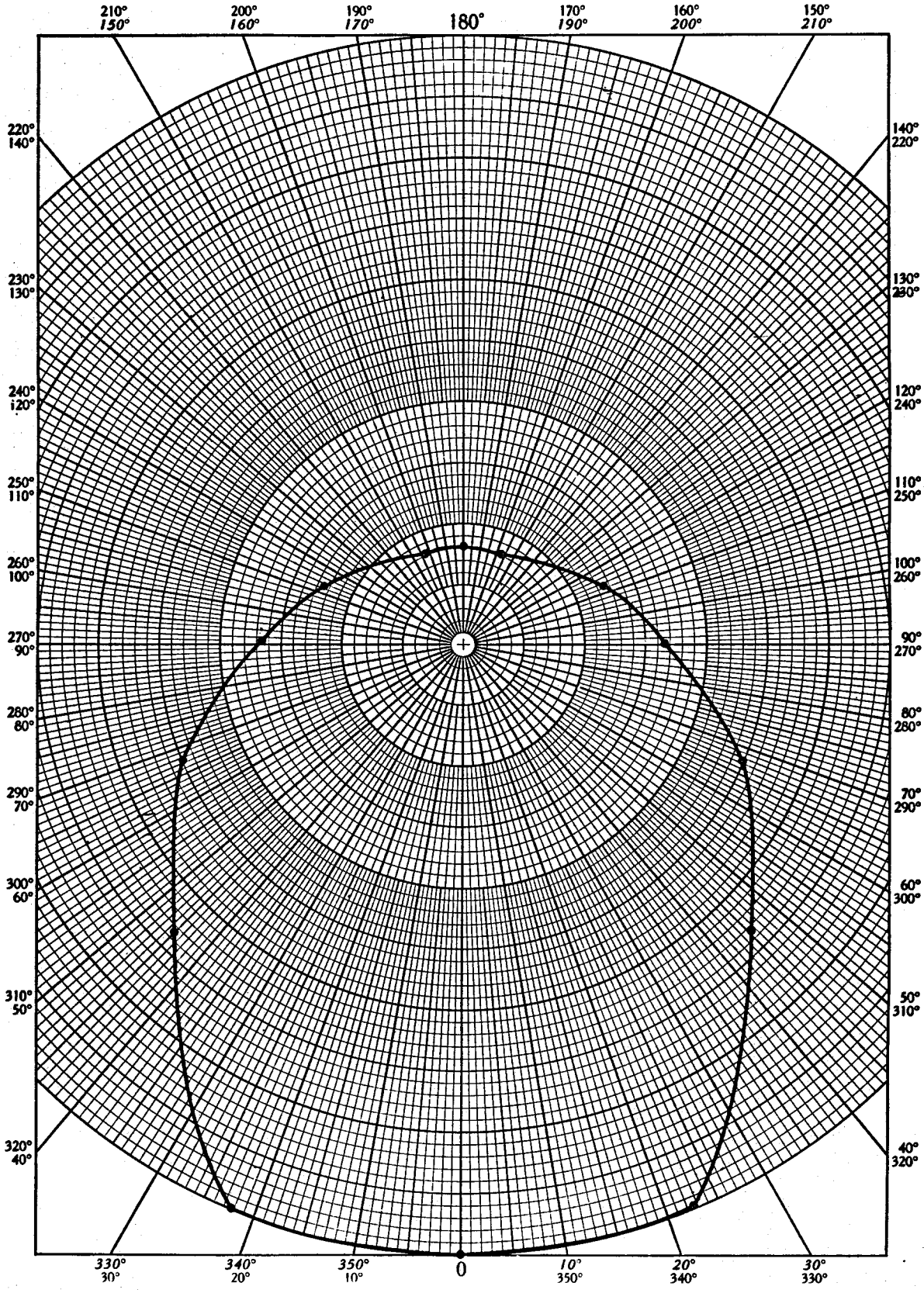

Figure 4.9a. Field pattern using first pulse for corner reflector. (monopole at radius = 4.85 cm)

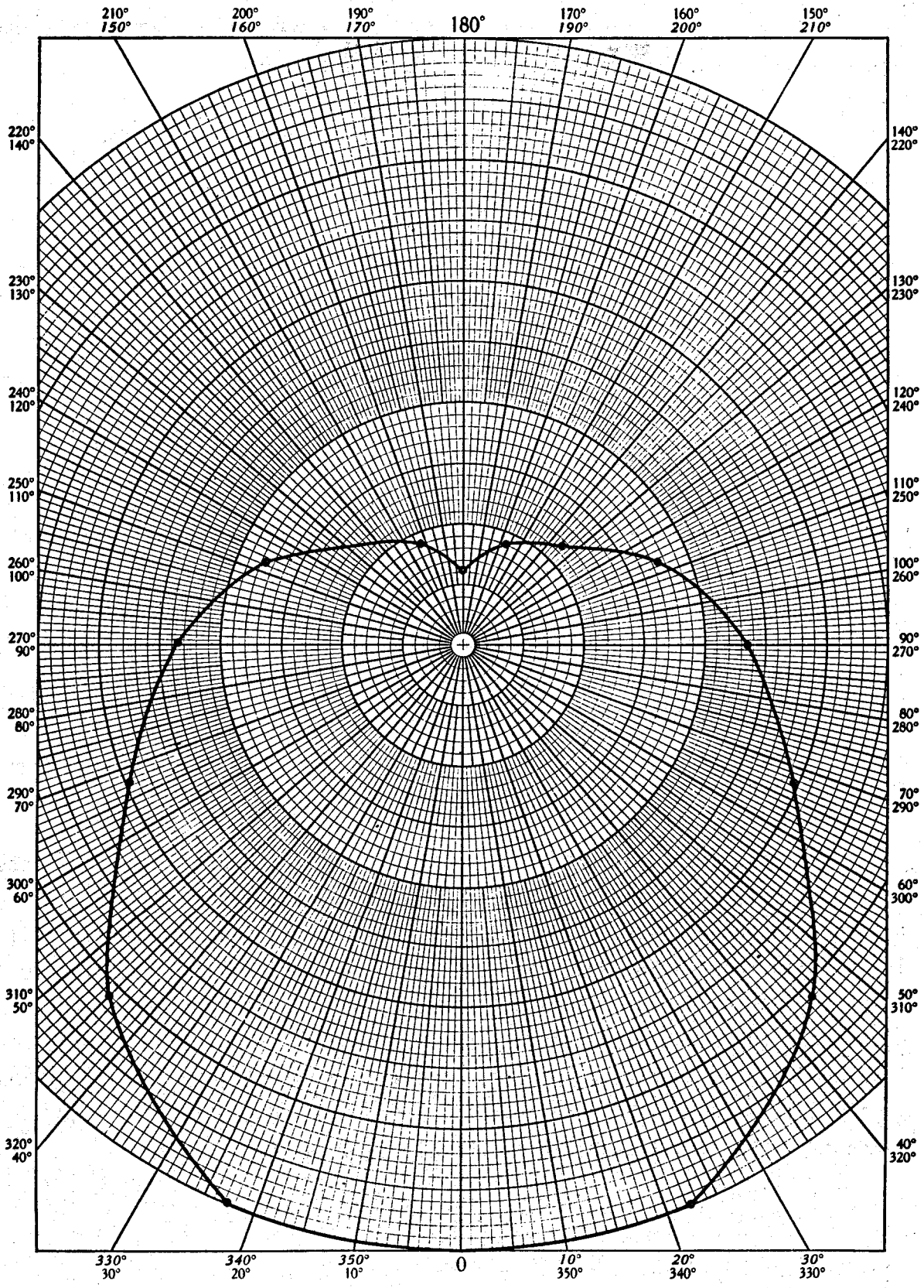

Figure 4.9b. Field pattern using second pulse for corner reflector. (monopole at radius = 4.85 cm)

It is from these figures that we derive the beam width angles for the positive (+) and negative (-) pulses tabulated below:

TABLE 4.7. BEAM WIDTHS FOR THE CORNER REFLECTOR ANTENNA

Radius	Beam Width	
	+	-
1	124	97
2	80	90
3	62	93
4	84	108

4.2.3 Tabulated Results

We have tabulated below, the measured peak received signals for the corner reflector antenna for each of the four radii mentioned above. The raw digitized peak values with photo ID numbers are listed. Then, the ratios of these values are presented for each angle with respect to the forward direction, or zero angle. Then, these ratios are turned into decibels for convenient evaluation of performance.

4.3 Synthesized Two-element Array

The two-element antenna array in the water filled borehole represents another simple antenna configuration that was synthesized from the data obtained on the eccentrically positioned monopole reviewed in Section 4.1. It was also constructed and measured for comparison. That discussion is found in Section 4.3.2. It is of interest because the synthesis method, when shown to be usefully accurate, permits computer simulation of other more complicated multi-element arrays utilizing the measured data from that family collected for the eccentrically positioned monopole. This is evident if the mutual coupling of the elements in the array to be

TABLE 4.8. MONOPOLE IN RADIUS #1 (CENTERED)

MONOPOLE IN RADIUS 1

SIGNAL SENSITIVITY = .01 VOLTS
REFERENCE SENSITIVITY = .01 VOLTS
SWEEP SPEED = 2E-9 SECONDS
PULSER LEVEL = 30.0 VOLTS

	RATIOS WRT 0		LOG OF RATIOS		RAW DATA		
ANGLE	POS	NEG	POS	NEG	POS	NEG	ID #
.00	1.00	1.00	.00	.00	1.20	3.30	3171
22.50	1.00	.91	.00	-.83	1.20	3.00	3172
45.00	.83	.76	-1.58	-2.41	1.00	2.50	3173
67.50	.67	.55	-3.52	-5.26	.80	1.80	3174
90.00	.50	.36	-6.02	-8.79	.60	1.20	3175
112.50	.33	.18	-9.54	-14.81	.40	.60	3176
135.00	.25	.18	-12.04	-14.81	.30	.60	3177
157.50	.17	.24	-15.56	-12.31	.20	.80	3178
180.00	.17	.27	-15.56	-11.29	.20	.90	3179

TABLE 4.9. MONOPOLE IN RADIUS #2 (2.37 cm)

MONOPOLE IN RADIUS 2

SIGNAL SENSITIVITY = .01 VOLTS
REFERENCE SENSITIVITY = .01 VOLTS
SWEEP SPEED = 2E-9 SECONDS
PULSER LEVEL = 30.0 VOLTS

	RATIOS WRT 0		LOG OF RATIOS		RAW DATA		
ANGLE	POS	NEG	POS	NEG	POS	NEG	ID #
.00	1.00	1.00	.00	.00	.90	2.80	3139
22.50	.94	.93	-.50	-.64	.85	2.60	3140
45.00	.67	.71	-3.52	-2.92	.60	2.00	3141
67.50	.56	.57	-5.11	-4.86	.50	1.60	3142
90.00	.33	.43	-9.54	-7.36	.30	1.20	3143
112.50	.22	.36	-13.06	-8.94	.20	1.00	3144
135.00	.22	.29	-13.06	-10.88	.20	.80	3145
157.50	.22	.21	-13.06	-13.38	.20	.60	3146
180.00	.22	.18	-13.06	-14.96	.20	.50	3147

TABLE 4.10. MONOPOLE IN RADIUS #3 (3.19 cm)

MONOPOLE IN RADIUS 3

SIGNAL SENSITIVITY = .01 VOLTS
REFERENCE SENSITIVITY = .01 VOLTS
SWEEP SPEED = 2E-9 SECONDS
PULSER LEVEL = 30.0 VOLTS

	RATIOS WRT 0		LOG OF RATIOS		RAW DATA		
ANGLE	POS	NEG	POS	NEG	POS	NEG	ID #
.00	1.00	1.00	.00	.00	.90	2.60	3155
22.50	.89	.92	-1.02	-.70	.80	2.40	3156
45.00	.56	.73	-5.11	-2.72	.50	1.90	3157
67.50	.44	.54	-7.04	-5.38	.40	1.40	3158
90.00	.33	.38	-9.54	-8.30	.30	1.00	3159
112.50	.22	.31	-13.06	-10.24	.20	.80	3160
135.00	.22	.23	-13.06	-12.74	.20	.60	3161
157.50	.11	.15	-19.08	-16.26	.10	.40	3162
180.00	.22	.15	-13.06	-16.26	.20	.40	3163

TABLE 4.11. MONOPOLE IN RADIUS #4 (4.85 cm)

MONOPOLE IN RADIUS 4

SIGNAL SENSITIVITY = .01 VOLTS
REFERENCE SENSITIVITY = .01 VOLTS
SWEEP SPEED = 2E-9 SECONDS
PULSER LEVEL = 40.0 VOLTS

	RATIOS WRT 0		LOG OF RATIOS		RAW DATA		
ANGLE	POS	NEG	POS	NEG	POS	NEG	ID #
.00	1.00	1.00	.00	.00	.60	1.70	3123
22.50	1.00	1.00	.00	.00	.60	1.70	3124
45.00	.67	.82	-3.52	-1.69	.40	1.40	3125
67.50	.50	.59	-6.02	-4.61	.30	1.00	3126
90.00	.33	.47	-9.54	-6.55	.20	.80	3127
112.50	.25	.35	-12.04	-9.05	.15	.60	3128
135.00	.17	.24	-15.56	-12.57	.10	.40	3129
157.50	.17	.18	-15.56	-15.07	.10	.30	3130
180.00	.17	.12	-15.56	-18.59	.10	.20	3131

synthesized is negligible and the location of each element within the confines of the borehole was measured in the monopole study.

4.3.1 Excitation

The excitation used for the synthesized array was simply that recorded for the monopole when located in hole #3 (3.19 cm) with a delay added (1.68 ns) to the forward element sufficient to cause the first pulses from each driven element to arrive at the same time at the target receive probe.

To create the resulting data set, we added the delayed monopole responses to the un-delayed for the appropriate angles shown in Table 4.12.

TABLE 4.12. SYNTHESIS TABLE FOR TWO-ELEMENT ARRAY PATTERN

Element 1 (no delay)	Element 2 (1.68 ns delay)	Result
0 degrees	180 degrees	0 degrees
22.5	157.5	22.5
45	135	45
67.5	112.5	67.5
90	90	90
112.5	67.5	112.5
135	45	135
157.5	22.5	157.5
180	0	180

This procedure involved the digitization in detail (approximately 200 data points per photo) of nine photos. Followed by standardization of the time increments by interpolating to a standard of 200 evenly spaced time steps for the 8 division records. This allowed a 0.08 ns resolution to be

used in the delay and addition of wave forms (i.e., data was recorded at 2 ns per division).

4.3.2 Field Patterns

The resulting synthesized field response for the two-element array was digitized for peak values at each 22.5 degree increment calculated. Again as discussed in Section 4.1.2, we anticipate that in future applications, radar signal processing will permit use of the first and possibly the second pulses seen by the target (i.e. positive or negative), we have determined the resulting field patterns and front-to-back ratios for each of these pulses. Figures 4.10a,b show the resulting field patterns for the first and second (positive and negative) pulses seen at the receiver.

It is from these figures that we derive the beam width angle for the positive pulse of 70 degrees and negative pulse of 80 degrees.

4.3.3 Tabulated Results

We have tabulated below, the predicted peak received signals for the two-element array antenna. The digitized peak values with ID numbers are listed. These numbers are formed from the combination of original monopole ID numbers (i.e., 241810 is derived from 2418 added to a delayed 2410). Then, the ratios of these values are presented for each angle with respect to the forward direction, or zero angle. Then, these ratios are turned into decibels for convenient evaluation of performance.

4.4 Measured Two-element Array

After looking at the two-element array as synthesized from the eccentric monopole data, we constructed the same and fed the two elements with the prescribed delay of 1.68 ns. The main interest here was to test the accuracy of the synthesis procedure and the practical implementation of a

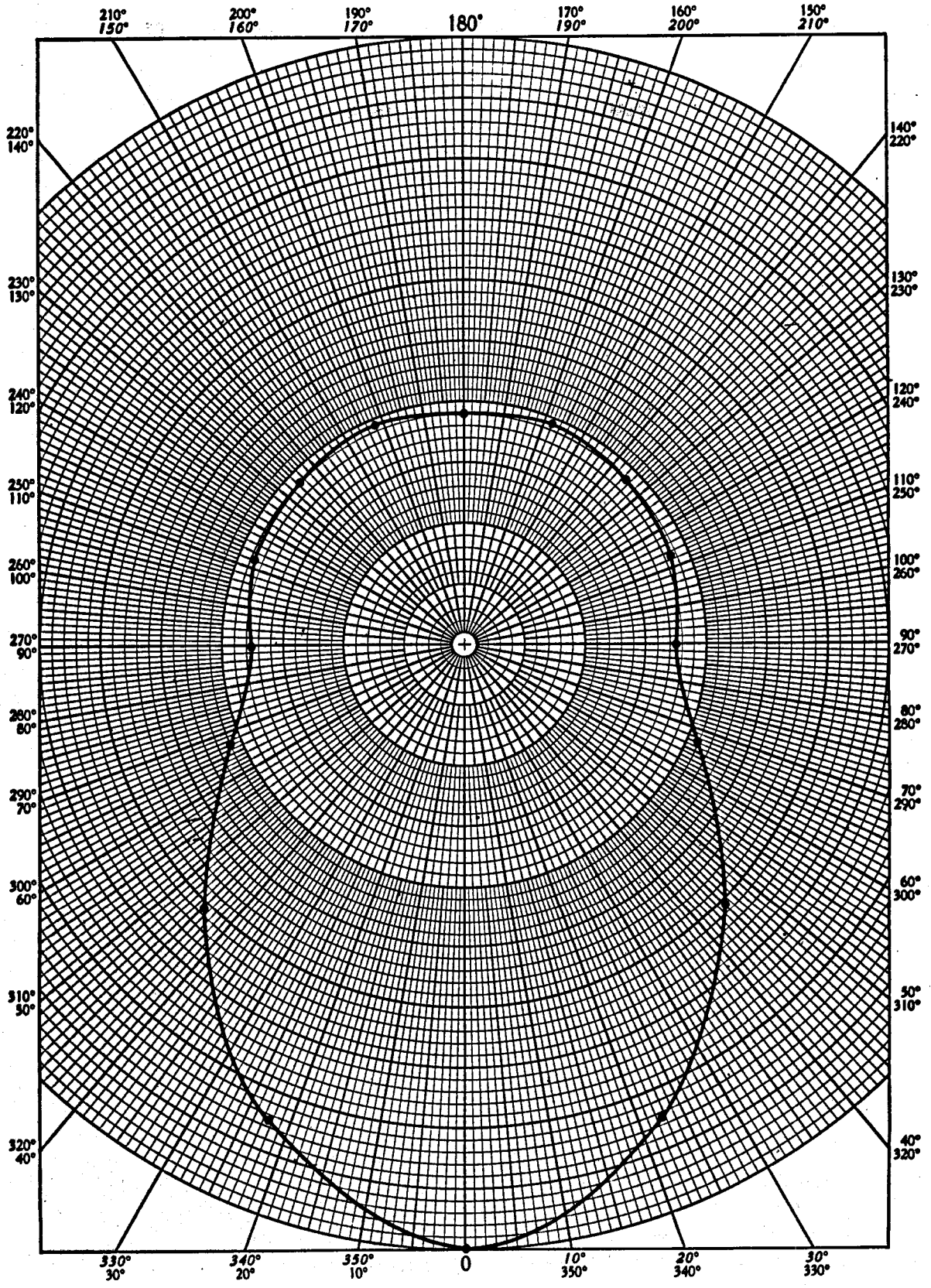

Figure 4.10a. Field pattern using first pulse for synthesized two-element array. (elements at radius = 3.19 cm)

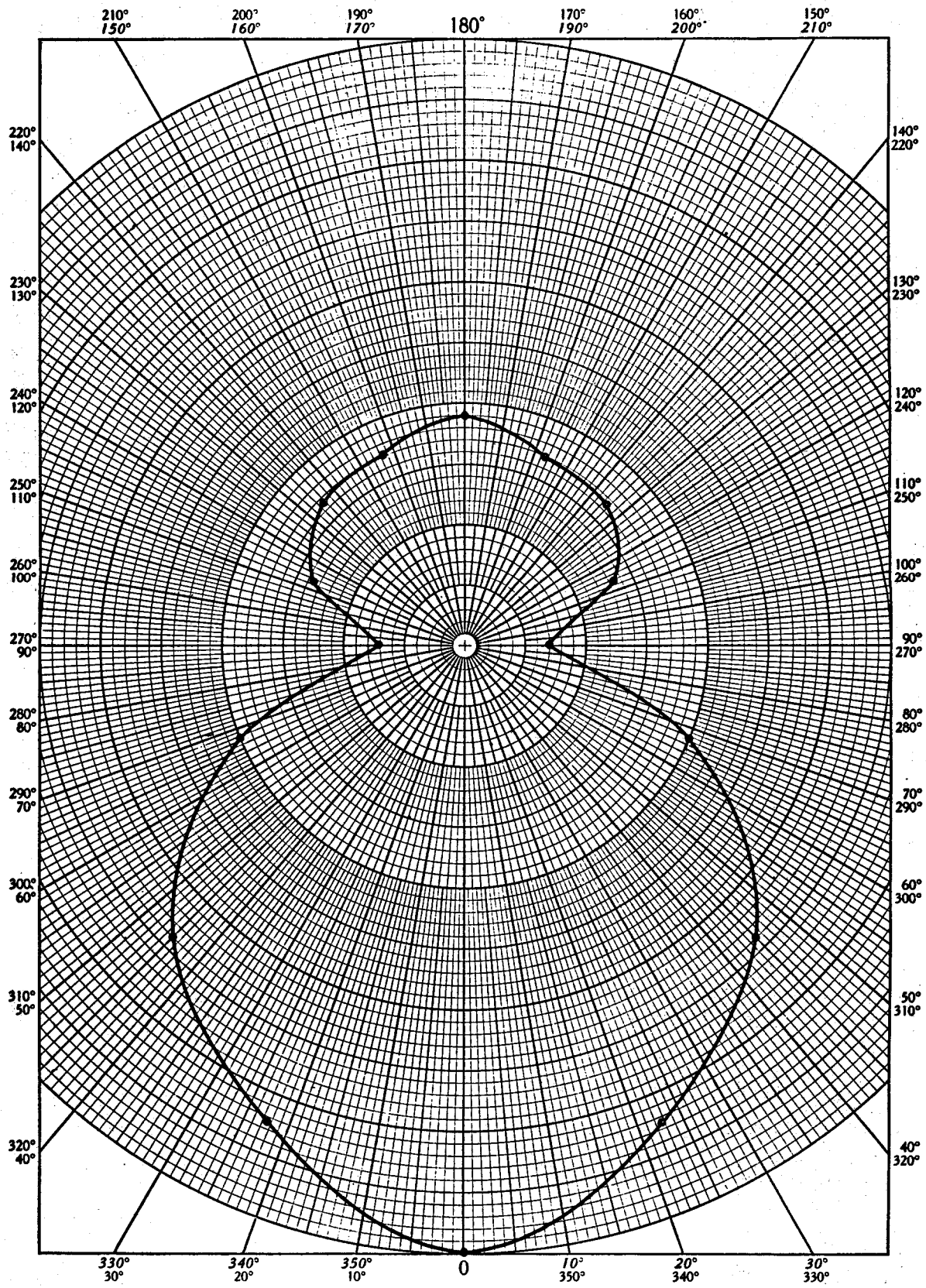

Figure 4.10b. Field pattern using second pulse for synthesized two-element array. (elements at radius = 3.19 cm)

TABLE 4.13. SYNTHESIZED TWO-ELEMENT ARRAY
(ELEMENTS PLACED AT RADIUS = 3.19 cm)

MONOPOLE IN RADIUS 3

SIGNAL SENSITIVITY = .005 VOLTS
REFERENCE SENSITIVITY = .01 VOLTS
SWEEP SPEED = 2E-9 SECONDS
PULSER LEVEL = 12.5 VOLTS

	RATIOS WRT 0		LOG OF RATIOS		RAW DATA		
ANGLE	POS	NEG	POS	NEG	POS	NEG	ID #
.00	1.00	1.00	.00	.00	2.06	4.50	241810
22.50	.85	.85	-1.43	-1.43	1.74	3.82	241711
45.00	.61	.68	-4.27	-3.32	1.26	3.08	241612
67.50	.42	.40	-7.48	-7.92	.87	1.81	241513
90.00	.35	.14	-9.09	-16.80	.72	.65	241414
112.50	.37	.27	-8.73	-11.32	.75	1.22	241315
135.00	.38	.33	-8.33	-9.53	.79	1.50	241216
157.50	.39	.34	-8.18	-9.32	.80	1.54	241117
180.00	.38	.38	-8.40	-8.42	.78	1.71	241018

multi-element array although it was only two elements. Section 5 makes a comparison between the actual and synthesized array response for this configuration.

4.4.1 Excitation

Each element of the array was excited with the fast rise time (0.7ns) short duration (1.3 ns) pulse with one element delayed with respect to the other by 1.68 ns. For all measurements, the pulser voltage was set at 50 volts or less. Since the pulser has a 50 Ohm source impedance, and the two elements feed lines were connected to the same pulser by a "T" connector, each received about one half the voltage as set on the pulser dial.

4.4.2 Field Patterns

The measured field response for the two-element array was digitized for peak values at each 22.5 degree increment. Again, as discussed in Section 4.1.2, we anticipate that in future applications, radar signal

processing will permit use of the first and possibly the second pulses seen by the target (i.e., positive or negative) and we have determined the resulting field patterns and front-to-back ratios for each of these pulses. Figures 4.11a,b show the resulting field patterns for the first and second (positive and negative) pulses seen at the receiver.

It is from these figures that we derive the beam width angle for the positive (+) and negative (-) pulses tabulated below:

TABLE 4.14. BEAM WIDTHS FOR THE SYNTHESIZED TWO-ELEMENT ARRAY

Radius	Beam Width +	-
3	86	90 degrees

4.4.3 Tabulated Results

We have tabulated below, the measured peak received signals for the two-element array antenna. The digitized peak values with photo ID numbers are listed. The ratios of these values are presented for each angle with respect to the forward direction, or zero angle. Finally, these ratios are turned into decibels for convenient evaluation of performance.

4.5 Media Electrical Properties

Sand blasting sand, specified as medium grade was used to simulate the downhole granite. This sand was used in order to have a uniform mixture of particles and because of its availability in a controlled dry state.

Electrical properties for the sand used in the test chamber was measured for two cases, that of dry and wet. By dry, we mean the sand as it was delivered from the gravel company after being kiln dried as specified for sand blasting. Wet, means saturated with tap water found in the

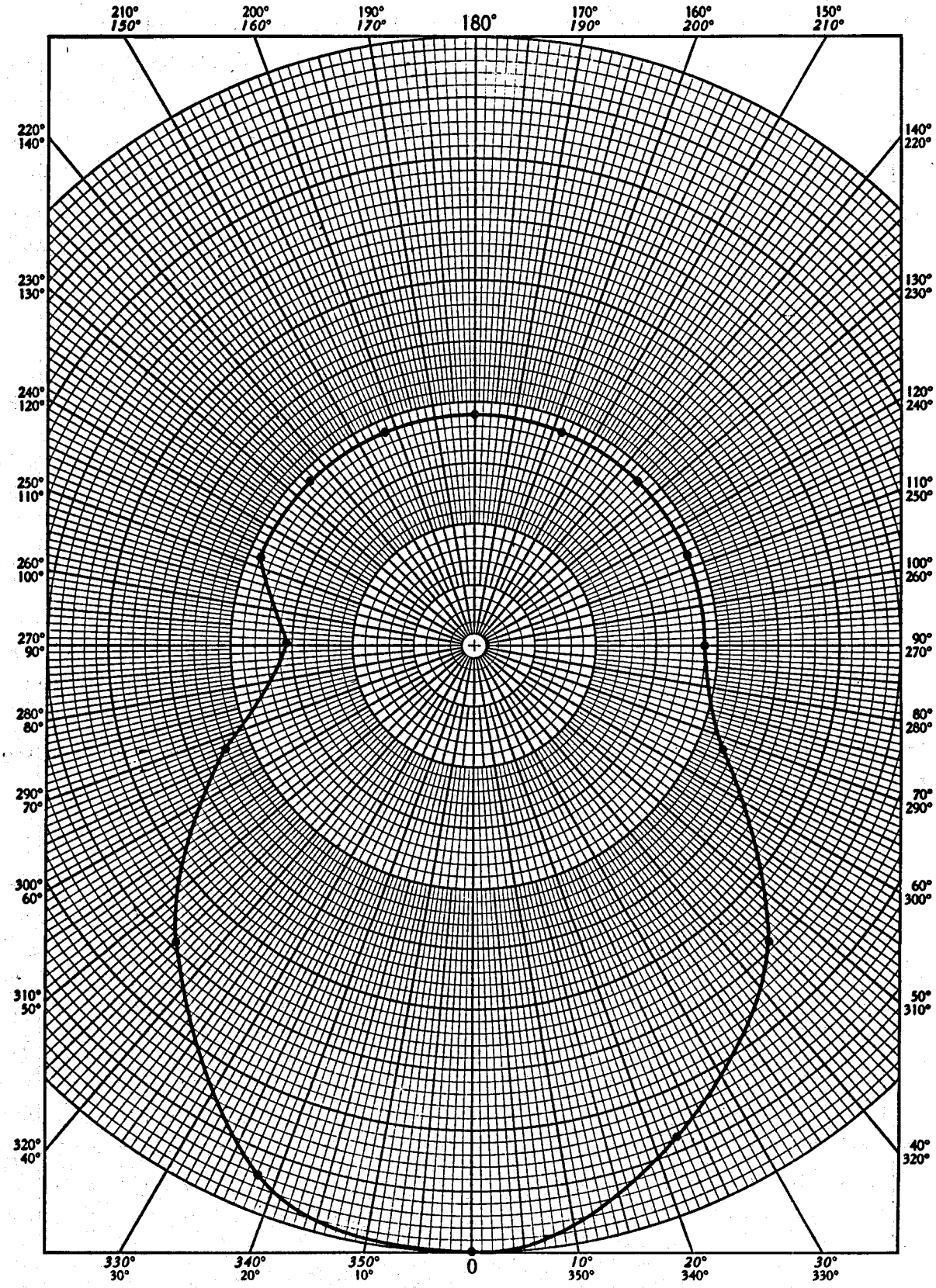

Figure 4.11a. Field pattern using first pulse for measured two-element arrays. (elements at radius = 3.19 cm)

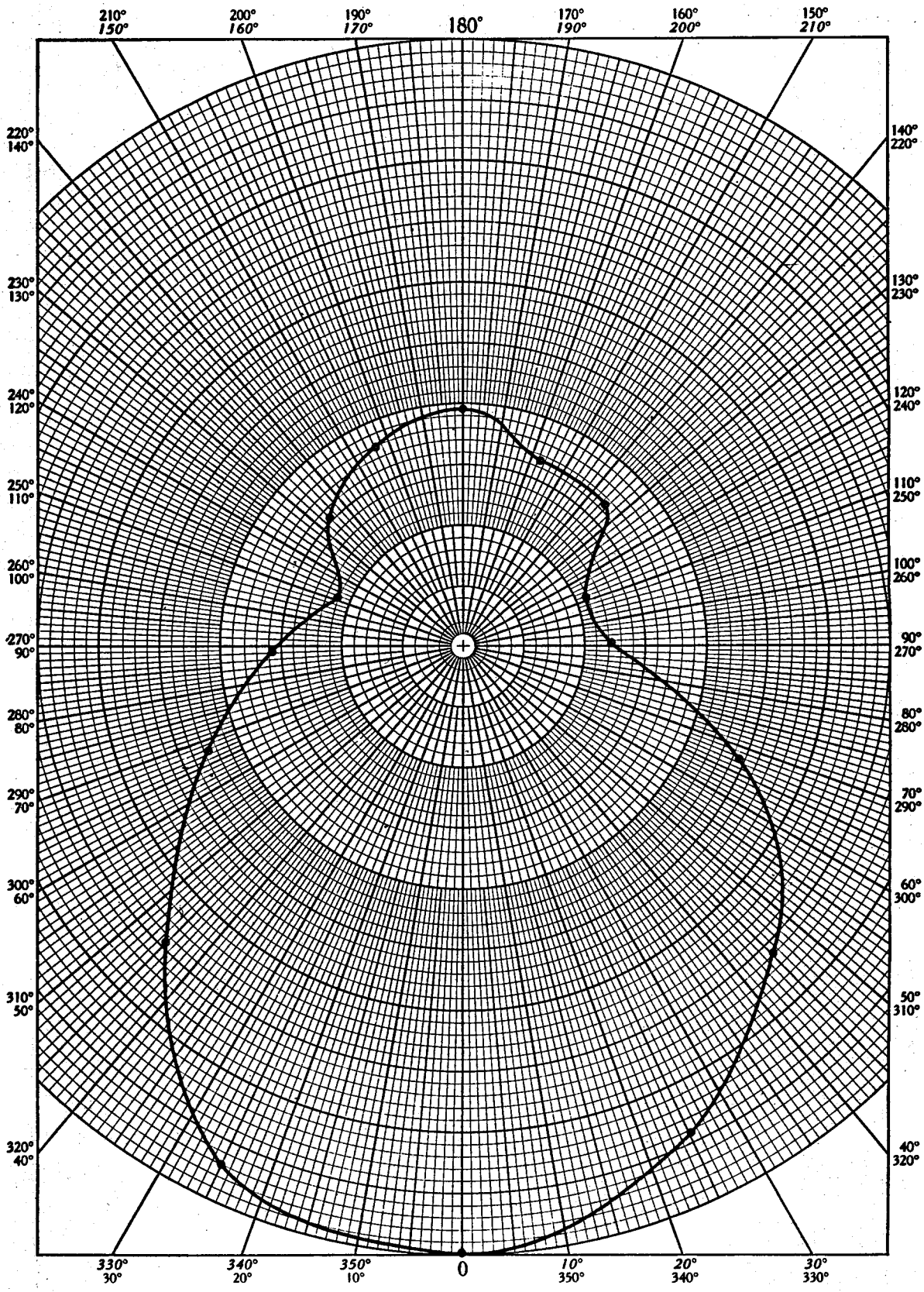

Figure 4.11b. Field pattern using second pulse for measured two-element array. (elements at radius = 3.19 cm)

TABLE 4.15. MEASURED TWO-ELEMENT ARRAY
(ELEMENTS AT RADIUS = 3.19 cm)

SIGNAL SENSITIVITY = .05 VOLTS
REFERENCE SENSITIVITY = .05 VOLTS
SWEEP SPEED = 2E-9 SECONDS
PULSER LEVEL = 15.0 VOLTS

	RATIOS WRT 0		LOG OF RATIOS		RAW DATA		
ANGLE	POS	NEG	POS	NEG	POS	NEG	ID #
.00	1.00	1.00	.00	.00	1.60	3.60	419
22.50	.88	.89	-1.16	-1.02	1.40	3.20	420
45.00	.69	.72	-3.25	-2.83	1.10	2.60	421
67.50	.44	.50	-7.18	-6.02	.70	1.80	422
90.00	.38	.25	-8.52	-12.04	.60	.90	423
112.50	.38	.22	-8.52	-13.06	.60	.80	436
135.00	.38	.33	-8.52	-9.54	.60	1.20	425
157.50	.38	.33	-8.52	-9.54	.60	1.20	426
180.00	.38	.39	-8.52	-8.20	.60	1.40	427
202.50	.38	.36	-8.52	-8.85	.60	1.30	428
225.00	.38	.31	-8.52	-10.30	.60	1.10	429
247.50	.38	.22	-8.52	-13.06	.60	.80	430
270.00	.31	.22	-10.10	-13.06	.50	.80	431
292.50	.44	.50	-7.18	-6.02	.70	1.80	432
315.00	.69	.75	-3.25	-2.50	1.10	2.70	433
337.50	.94	.92	-.56	-.76	1.50	3.30	434

laboratory area. The dry density was measured to be 1.63 g/cc and the saturated was 1.95 g/cc. Thus the saturated sand had 19.33% water by weight. It is believed that this is the only practical moisture level to try to maintain in a uniform fashion through out the test chamber. This is done by uniformly sprinkling the surface until water starts to percolate through into the drip pan beneath the chamber.

4.5.1 Dry Sand

Electrical measurements of the sand's dielectric constant and conductivity were made using the V-I Impedance Probe as described in Section 2.1.10 in the VHF band. This was done over a period of about 30 days. Over this time little variation was observed in the dielectric constant while greater variation was observed for the conductivity. The reason for these results is that by using the same probe as that used for the radar

receiver and operating in the VHF band, the data reduction is more accurate for the dielectric constant than for the conductivity. That is, the probe appears highly reactive for the VHF band while immersed in dry sand. Table 4.16 details these results.

TABLE 4.16. DRY MEDIA ELECTRICAL PROPERTIES

Date	Frequency (MHz)	Relative Dielectric	Conductivity (mho/meter)
09-29-83	100	3.93	n/a
"	150	3.14	5.77E-3
"	200	2.98	1.26E-3
"	250	3.32	4.85E-3
"	300	3.13	8.39E-3
10-03-83	150	3.08	2.27E-3
10-18-83	300	3.92	9.40E-3
10-24-83	50	3.49	n/a
"	100	3.17	1.36E-3
"	150	3.95	2.30E-3
"	200	3.31	3.77E-3
	average value -->	3.40	--> 4.374E-3

Using these average values are not strictly rigorous since we know the the electrical properties of moist earth is some what frequency dependent (Ref. 4.1). Since our system response is seen to have a principal component around 300 MHz that is, much of the energy is in a modest band centered about that frequency, it is reasonable to use these averages for engineering approximations.

4.5.2 Wet Sand

Electrical measurements of the wet sand's dielectric constant and conductivity were made using the V-I Impedance Probe as described in Section 2.1.10 in the VHF band. This was done after the sand had remained in the saturated condition over a period of 24 hours. The same probe as that used for the radar receiver and operating in the VHF band was used for the data collection but the reduction is more accurate for both the dielectric constant and for the conductivity. This was because the probe appears less reactive for the VHF band than while it was immersed in dry sand. Table 4.17 details these results.

TABLE 4.17. WET MEDIA ELECTRICAL PROPERTIES

Date	Frequency (MHz)	Relative Dielectric	Conductivity (mho/meter)
10-28-83	50	10.20	1.40E-2
"	150	9.74	1.17E-2
	average value -->	9.97	--> 1.29E-2

Again, using these average values are not strictly rigorous as stated above but, in this case, since the measurement is so much more stable and the values are so close to each other at 50 and 150 MHz, little error is introduced by using these average values for VHF band engineering calculations.

SECTION 5
DISCUSSION

A promising technique for detection and location of fractures in geothermally active granite matrix is that of an electromagnetic radar type downhole probe. Range is determined by time delay of the return echo while direction is determined by rotation of the directional transmitting antenna while observing the signal strength. To improve both detection range and directional resolution, the transmitting antenna should have maximum forward gain perpendicular to the borehole. That is, the narrowest beam width and the lowest side lobes, that can be designed to physically fit within the confines dictated by the borehole diameter.

Until now, no measurements have been reported of the field patterns for the eccentrically located dipole of monopole antenna within a high dielectric constant media surrounded by a lower dielectric constant media. However, theoretical predictions have been reported (Ref. 5-1).

The reasons for selecting a high dielectric constant media within the confines of the borehole are twofold. First, the borehole is likely to be filled, at depths of primary interest, with water (high relative dielectric constant, ~80), hence to minimize the number of discontinuities traversed by the radar pulse the antenna should be immersed in a similar dielectric constant media. Secondly, a directional antenna design is enhanced by the electrical length shortening factor afforded by the antenna immersed in the media. To effectively control an antenna array pattern, separation distances of the order of element lengths are needed. The presence of water then, as the dielectric in which the array elements are immersed, permits a relatively higher gain (improved directional) antenna to be designed within the confines of a water or brine filled borehole with minimal electrical discontinuities to scatter the radar energy.

5.1 Utility of Three Designs

The measurements made in this study have shown that reasonable beam widths and front-to-back ratios can be achieved by proper selection of driven element positioning within a water filled cylinder. An eccentrically positioned monopole, a corner reflector and a two-element array were measured for a number of possible configurations. The summary table (Table 5.1) was prepared from the data in Section 4 for ease of comparison. From this table we selected in some sense optimal configurations for the narrowest beam width together with the larger front-to-back ratios and summarized them in Table 5.2.

In anticipation that future radar signal processing will permit use of the first and possibly the second pulses seen by the target (i.e., positive or negative), we have determined the resulting field patterns and front-to-back ratios for each pulse.

5.1.1 Eccentrically Positioned Monopole

The eccentrically positioned monopole is of special interest for several reasons. One, it is the simplest to construct and implement. Two, the data derived from its performance in this environment can be used to synthesize more complex arrays through simple computational procedures. That is, one can synthesize a number of symmetric arrays such as 2,4,8 and 16 element circular arrays. And finally, having one element makes it easier to understand the physics of its performance. Figures 5.1a and 5.1b illustrates the field patterns derived from the first and second pulse received from the monopole positioned at the location found to be optimum for the size borehole and antenna height used.

TABLE 5.1. SUMMARY OF BEAM WIDTHS AND FRONT-TO-BACK RATIOS FOR THE ECCENTRIC MONOPOLE, CORNER REFLECTOR AND TWO-ELEMENT ARRAY

Radius	Beam Width Degrees (+)	Beam Width Degrees (-)	Front-to-Back Ratio dB (+)	Front-to-Back Ratio dB (-)
ECCENTRIC MONOPOLE				
1	360	360	0	0
2	84	109	4.78	4.33
3	78	78	3.52	4.86
4	N/A	48	N/A	2.57
CORNER REFLECTOR				
1	124	97	15.56	11.29
2	80	90	13.06	14.96
3	62	93	13.06	16.26
4	84	108	15.56	18.59
TWO-ELEMENT ARRAY (Synthesized)				
3	70	80	8.40	8.42
(Measured)				
3	86	90	8.52	8.20

TABLE 5.2. SUMMARY OF OPTIMAL CONFIGURATIONS FOR THREE ANTENNAS

ANTENNA (monopole location)	BEAM WIDTH (degrees) (+)	(-)	FRONT-TO-BACK (ratio in dB) (+)	(-)
eccentric monopole (located at r = 3.19 cm)	78	78	3.52	4.86
corner reflector (located at r = 3.19 cm)	62	93	13.06	16.26
two-element (computed) (both at r = 3.19 cm)	70	80	8.40	8.42
two-element (measured (both at r = 3.19 cm)	86	90	8.52	8.20
Note: (+) and (-) denote the first positive and negative pulses to arrive at the target.				

Note that the first pulse field pattern is omnidirectional for about 180 degrees with forward energy developing a beam width of 78 degrees, but the omnidirectional portion is so large the front-to-back ratio is only 3.52 dB. The second pulse (negative) however, is a bit better formed with the beginning of nulls at 90 and 270 degrees. The rearward radiation is still high, yielding a front-to-back ratio of 4.86 dB.

5.1.2 Corner Reflector Antenna

The corner reflector is another interesting antenna implementation because it is directly related to the 4-element circular array with each neighboring element being a negative image. Also, it is simple to construct and if the monopole were to be centrally located, a directional system can be constructed where the reflector rotates about the monopole. This location, although not excessively poor in performance, was not optimum. The optimum location was found to be with the monopole at a

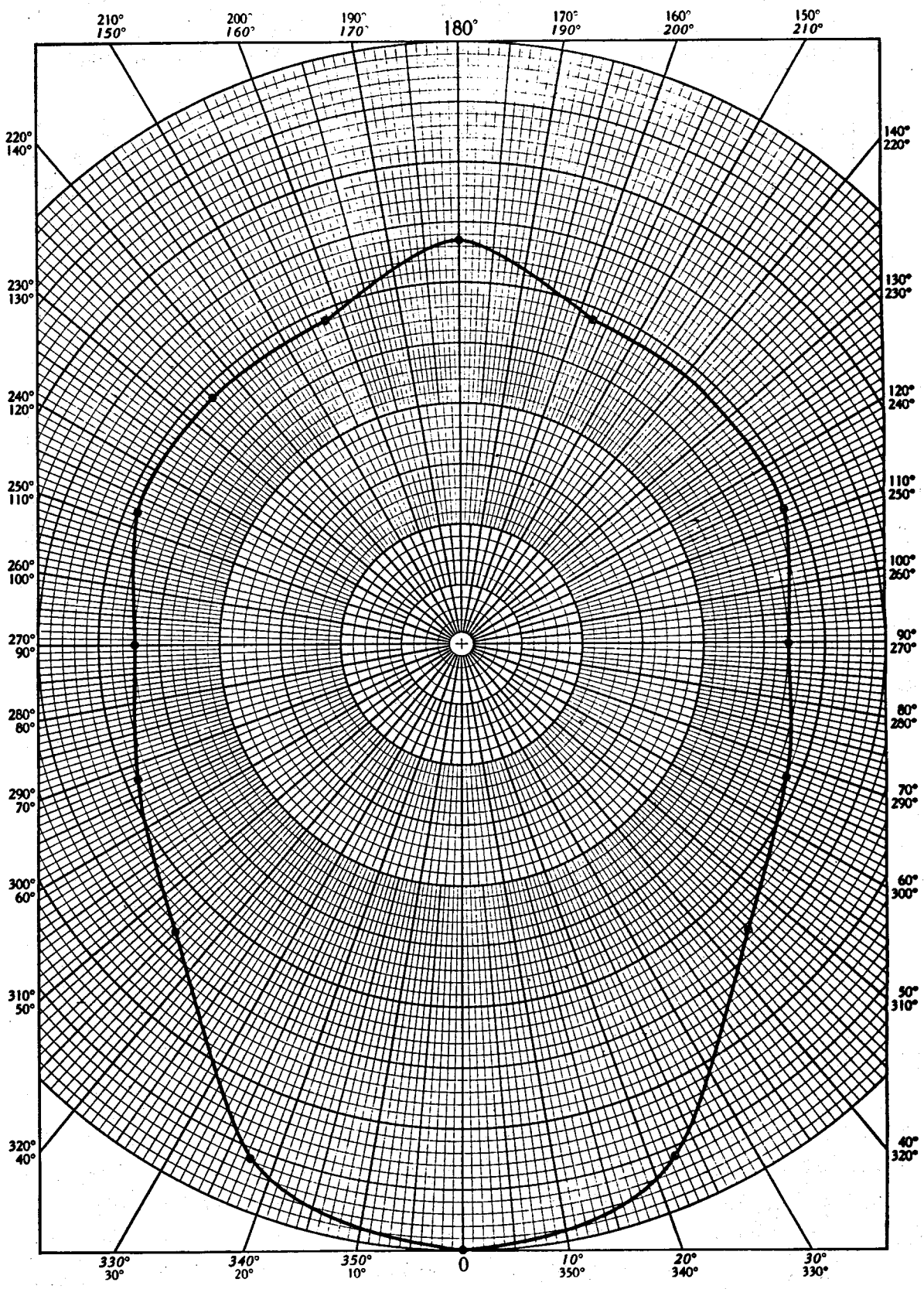

Figure 5.1a. Field pattern for the eccentric monopole. (First pulse with radius = 3.19 cm)

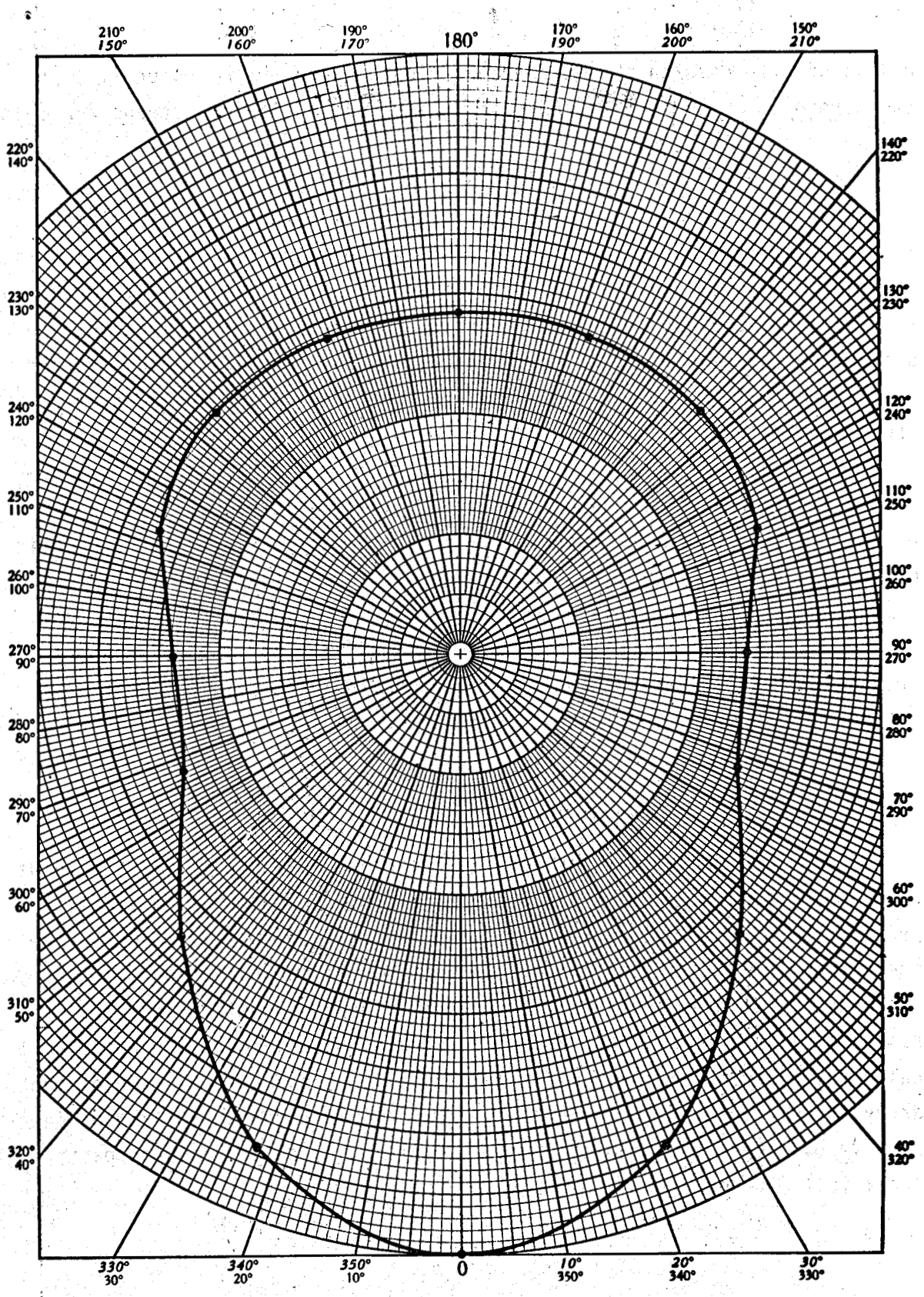

Figure 5.1b. Field pattern for the eccentric monopole. (Second pulse with radius = 3.19 cm)

radius of 3.19 cm with the 90 degree reflector apex at the outer limit of the borehole. Figures 5.2a and b are the resulting field patterns for this antenna.

We note the the pattern for the first pulse is quite nicely formed with a relatively narrow beam width of 63 degrees and a front-to-back ratio of 13 dB. Since these patterns were measured only a meter away from the radiating antenna, it is possible that the pattern is being filled out to some degree by near field energy. That is to say that if we had a larger simulation chamber, it is likely that the pattern would have a better front-to-back ratio.

The pattern for the second arriving pulse (negative) is some what broader in beam width but improved in front-to-back ratio. Although it is certain that chamber wall reflections were abundant (at late time), for the time window from which this data is derived, we could observe no contamination due to reflections. This was tested by placing large pieces of conducting material at each wall while recording with multiple exposures the primary (early time) antenna response.

5.1.3 Two-element Array Antenna

The two-element array was particularly interesting because it gave us a chance to test our ability to predict array performance using simple procedures working on measured data from the family of data collected for the eccentrically positioned monopole. As described in Section 4, we synthesized a two element array from the measured monopole date for a radius position of 3.19 cm. From this process we determined the optimum delay needed for beam enhancement and actually constructed the two-element array. The resulting field patterns are shown in Figures 5.3a and b where we have overlayed the predicted patterns with the actual measured pattern for a full 360 degrees.

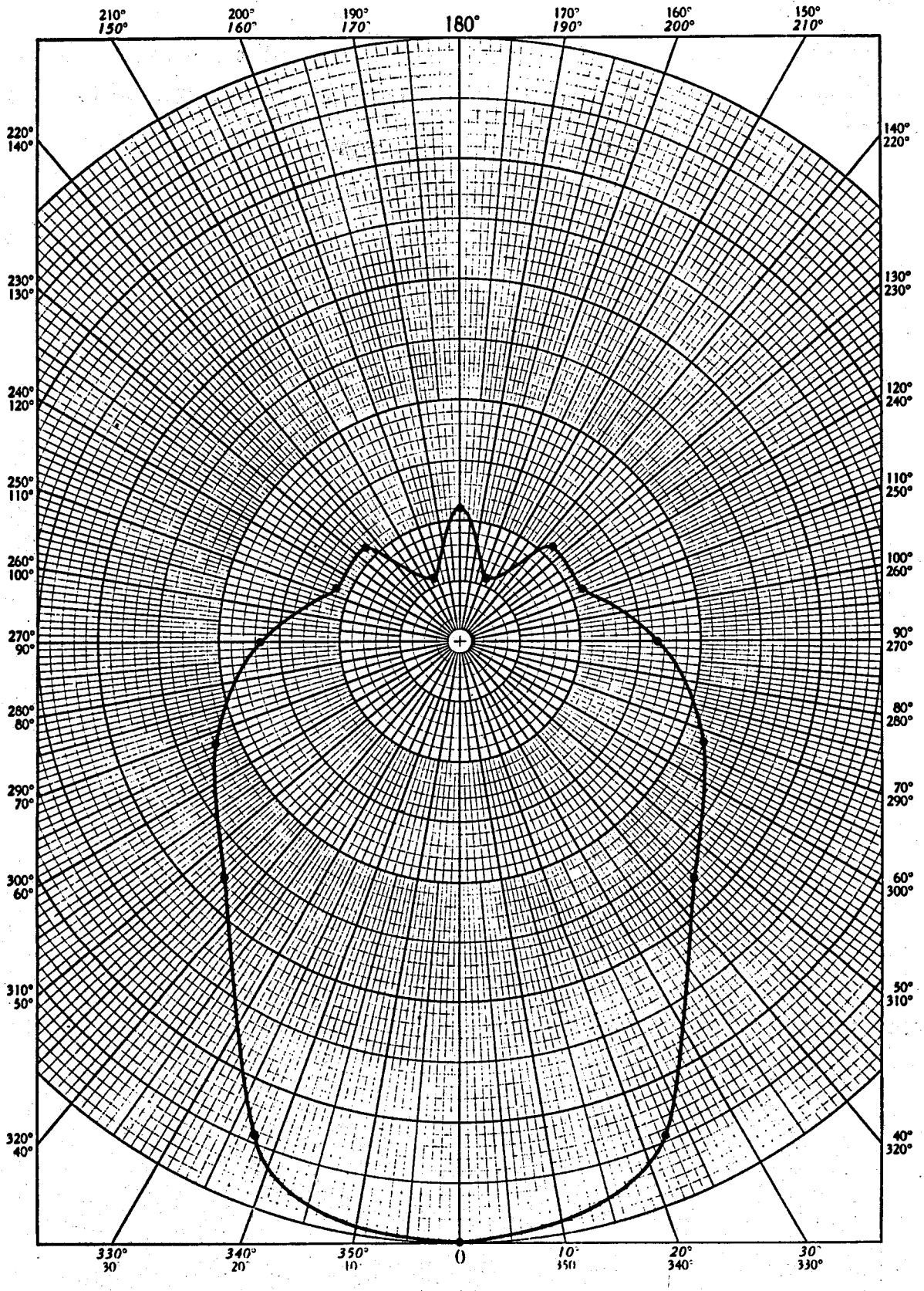

Figure 5.2a. Field pattern for the corner reflector antenna. (First pulse with radius = 3.19 cm)

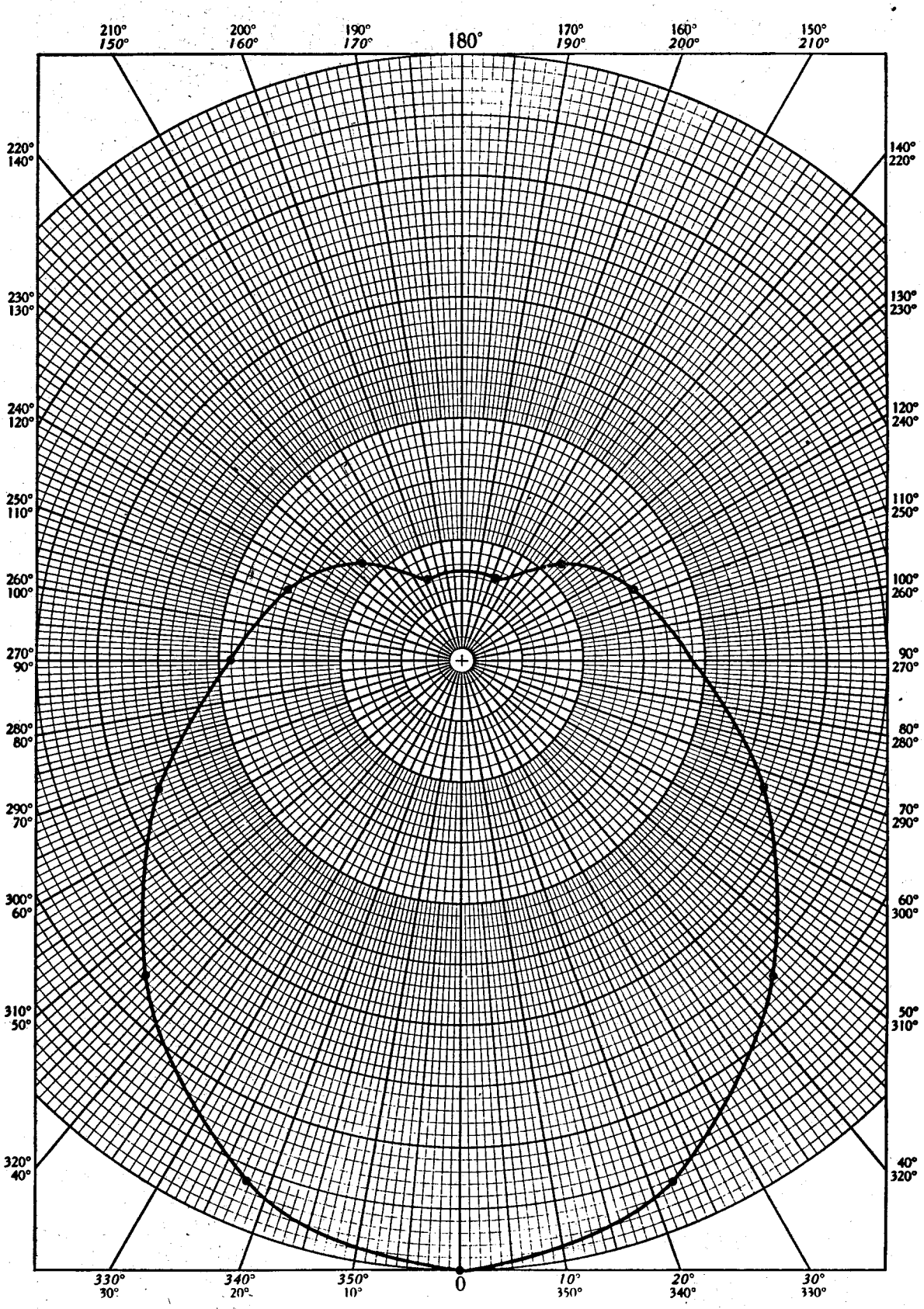

Figure 5.2b. Field pattern for the corner reflector antenna. (Second pulse with radius = 3.19 cm)

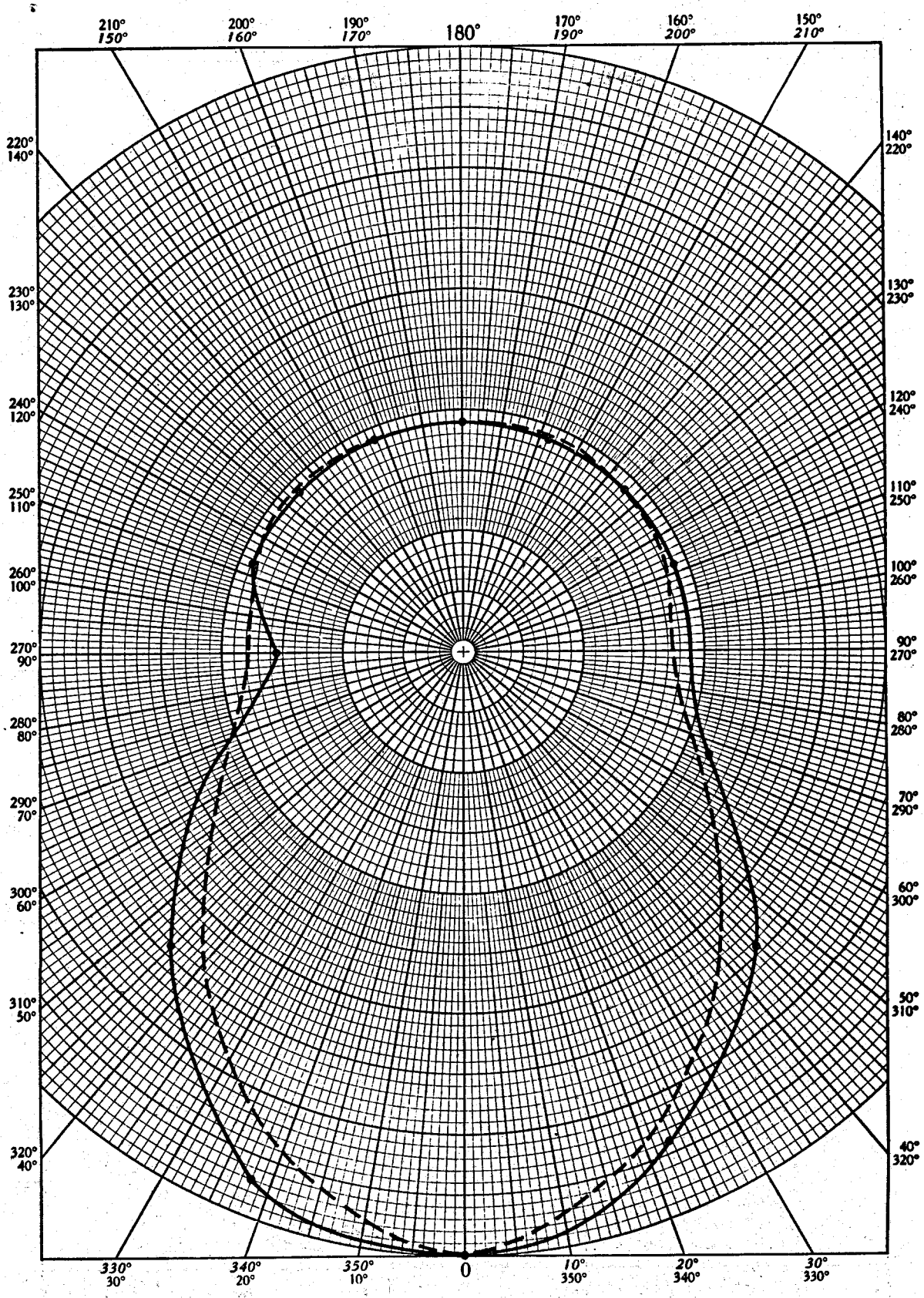

Figure 5.3a. Field patterns for synthesized (dash line) and measured (solid line) two-element array. (First pulse with radius = 3.19 cm)

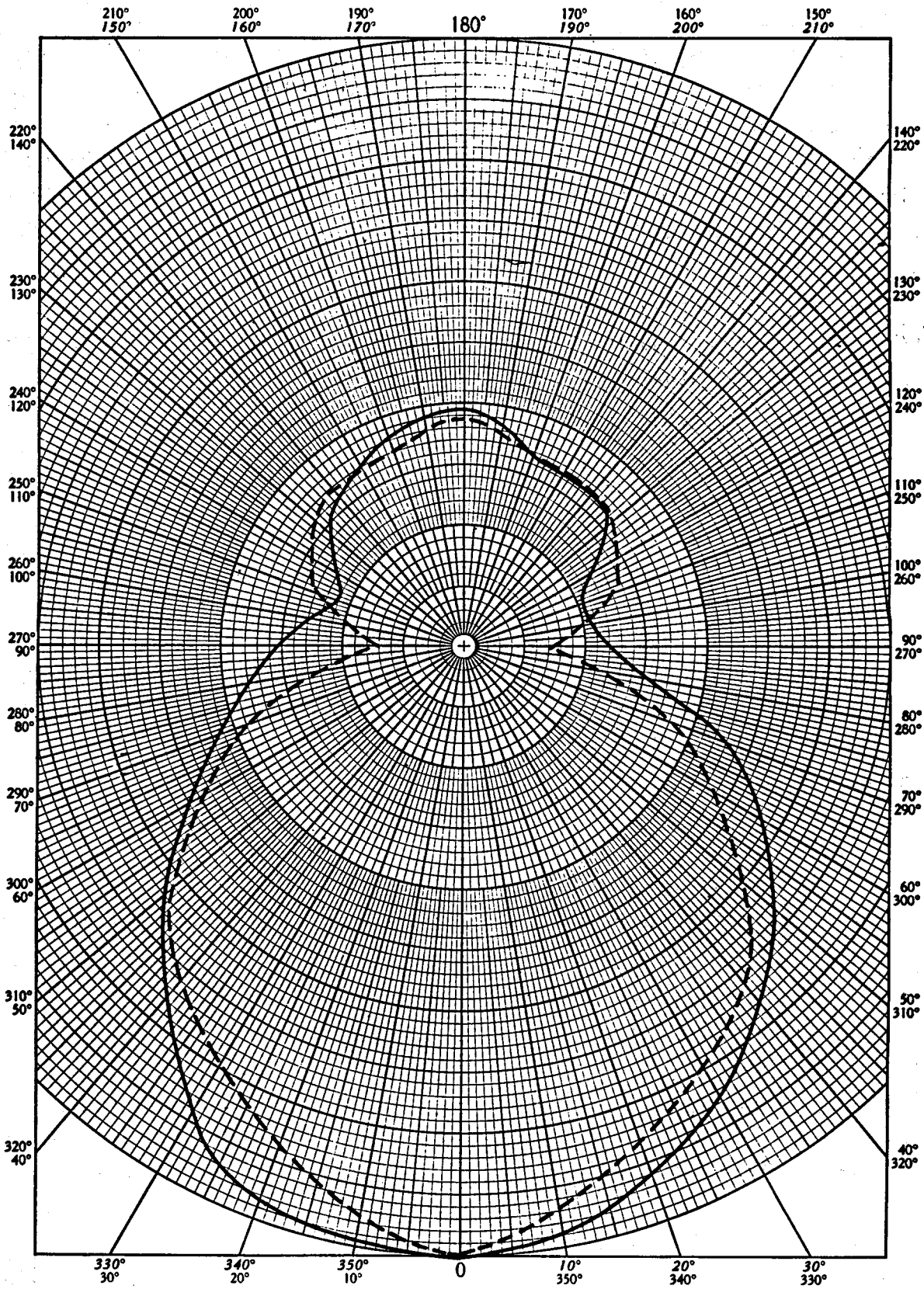

Figure 5.3b. Field patterns for synthesized (dash line) and measured (solid line) two-element array. (Second pulse with radius = 3.19 cm)

For this antenna system, we note a much improved front-to-back ratio but with a slightly broader beam width than afforded by the eccentrically located monopole alone. The front-to-back ratio for the measured and synthesized (predicted) cases are quite close, 8.52 dB and 8.40 dB respectively, while the beam widths were 86 and 70 degrees. Its is likely that a larger test chamber would have yielded better agreement with the absence of a small amount of near field energy. In Figure 5.3b, for the second pulse, we can see a definite null filling in the measured data as compared with the predicted data. Again this suggests either near field contamination or more likely some mutual coupling between the two elements not accounted for in the synthesis procedure.

5.2 Fourier Transforms

To better understand the response and performance of each antenna system and to aid in the engineering design of possible radar systems utilizing these antennas, we have digitized the wave forms recorded for each antenna type measured in preparation for the Fourier integral transform. Limitations in the high frequency validity for these transforms, as stated below, is based on the methods and error determination techniques reported in Reference 5.2 by Scott.

5.2.1 Eccentrically Positioned Monopole

Figure 5.4 is the photo of the oscilloscope trace showing the received signal from the monopole driven by an approximation to an impulse function shown in Figure 5.5. In Figure 5.4 note that the time reference signal is on the lower portion of the photo.

After digitizing the waveform and prior to transforming it to the frequency domain, a truncation point was selected to eliminate the test chamber wall reflections. This is shown in Figure 5.6. The scales shown are

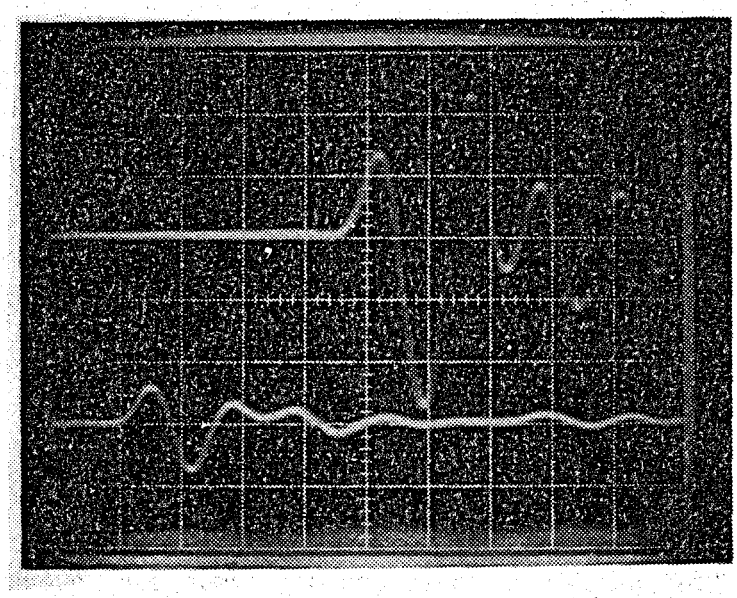

Figure 5.4. Eccentric monopole response (2 ns/div.).

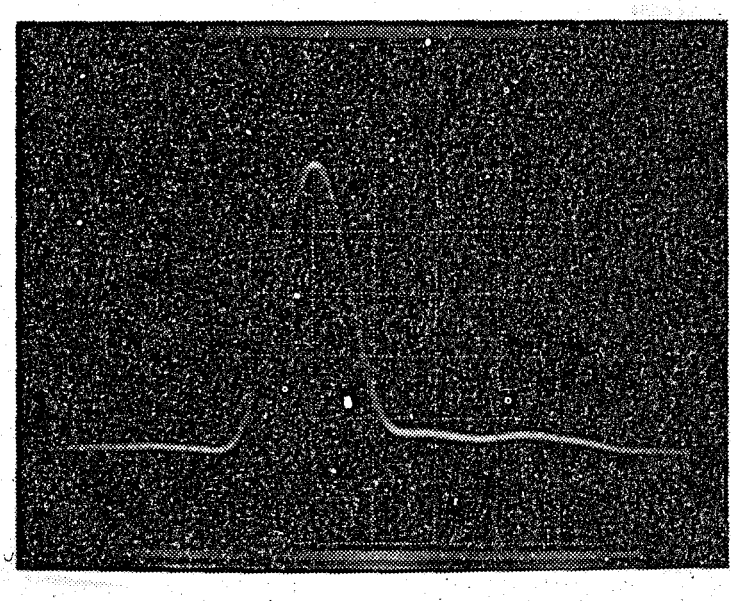

Figure 5.5. Driving pulse (1 ns/div.).

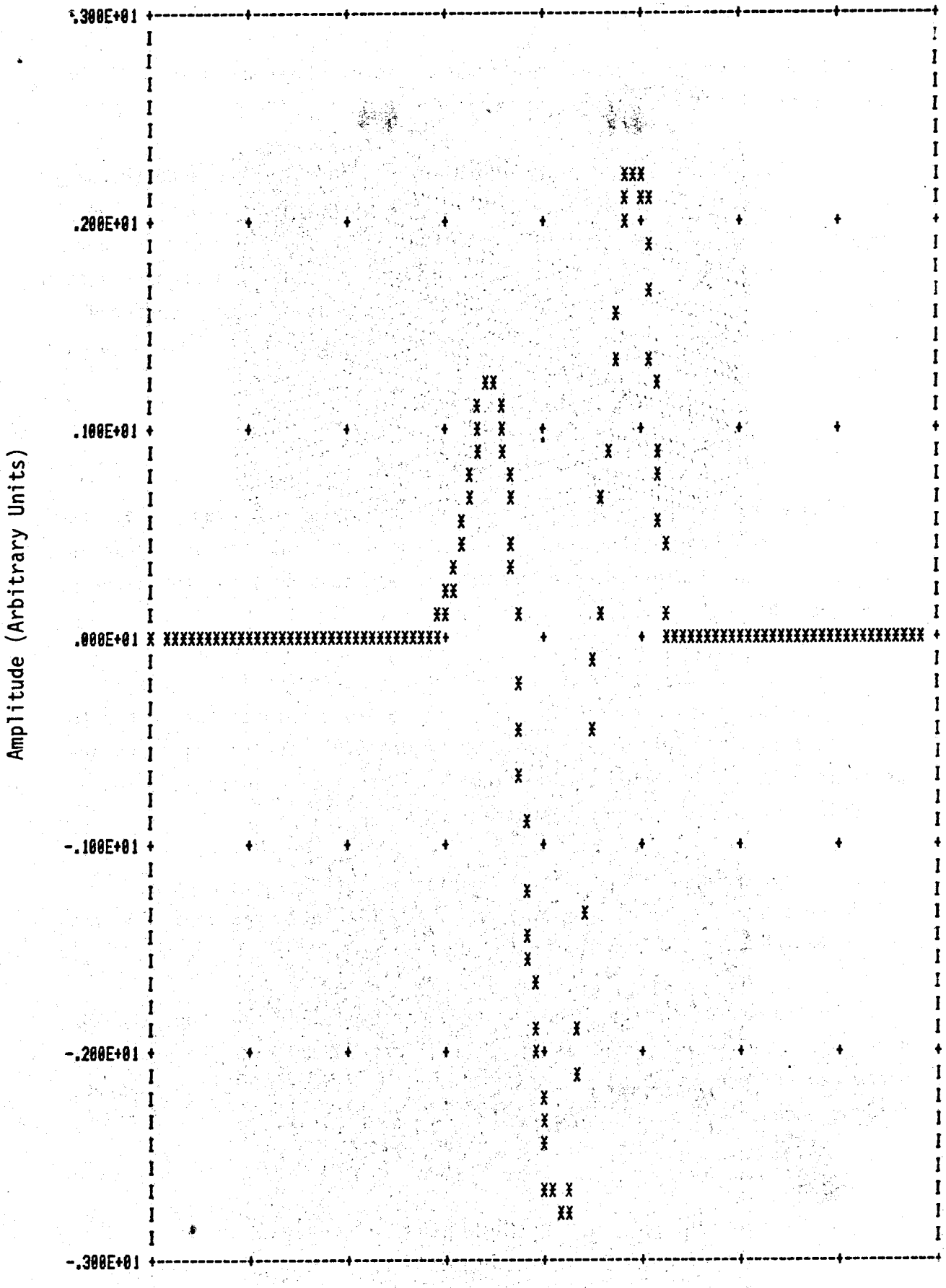

Figure 5.6. Digitized monopole response.

still in units of oscilloscope graticules. Actual time units were introduced in the Fourier transform program.

Finally, Figure 5.7 shows the Fourier transform for the eccentrically positioned monopole for radius = 3.19 cm (i.e., the optimum case). The frequency range shown is from 10 MHz to 1000 MHz. The transform is only valid for frequencies lower than about 500 MHz since the measurement system starts to roll off at 300 MHz. We note a broad peak of energy centered around 288 MHz which is not too surprising after looking at the time domain response in Figure 5.4.

5.2.2 Corner Reflector

Figure 5.8 is the oscilloscope photo showing the received signal from the corner reflector antenna driven by the near impulse function shown in Figure 5.5. In Figure 5.8 note the time reference signal in now on the upper portion of the photo.

After digitizing the waveform and prior to transforming to the frequency domain, a truncation point was selected to eliminate the test chamber wall reflections. This is shown in Figure 5.9. The scales shown are still in units of oscilloscope graticules. Actual time units were introduced in the Fourier transform program.

Finally, Figure 5.10 shows the Fourier transform for the corner reflector antenna for radius = 3.19 cm (i.e., the optimum case). The frequency range shown is from 10 MHz to 1000 MHz.

The transform is only valid for frequencies lower than about 500 MHz since the measurement system starts to roll off at 300 MHz. We note a broad peak of energy centered around 302 MHz which is similar to that seen for the eccentric monopole.

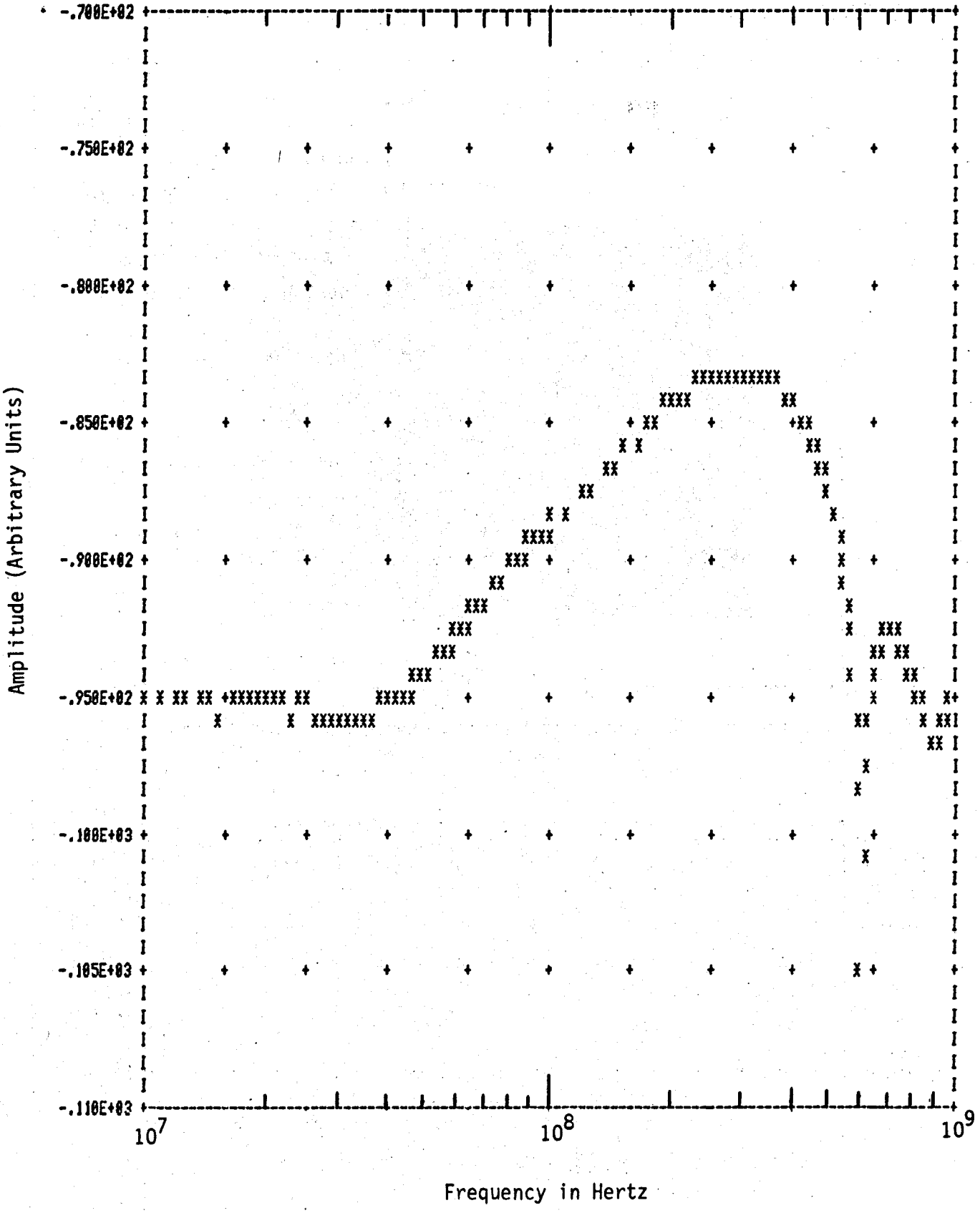

Figure 5.7. Fourier transform of monopole response.

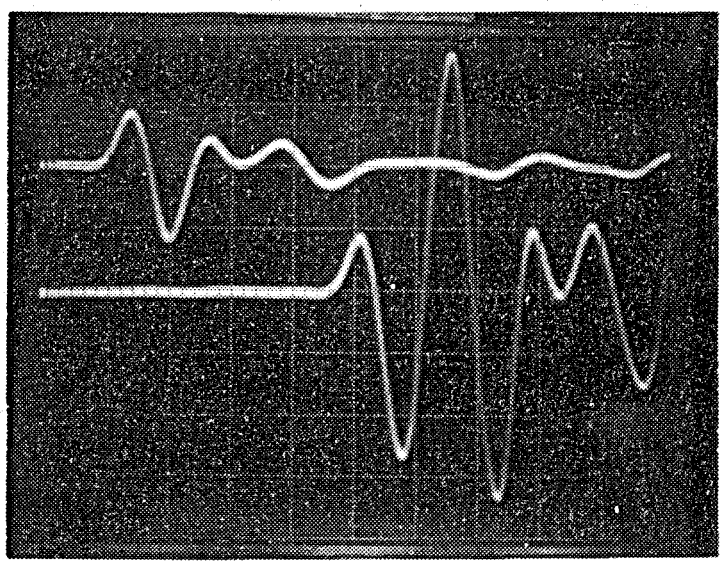

Figure 5.8. Corner reflector response. (2 ns/div)

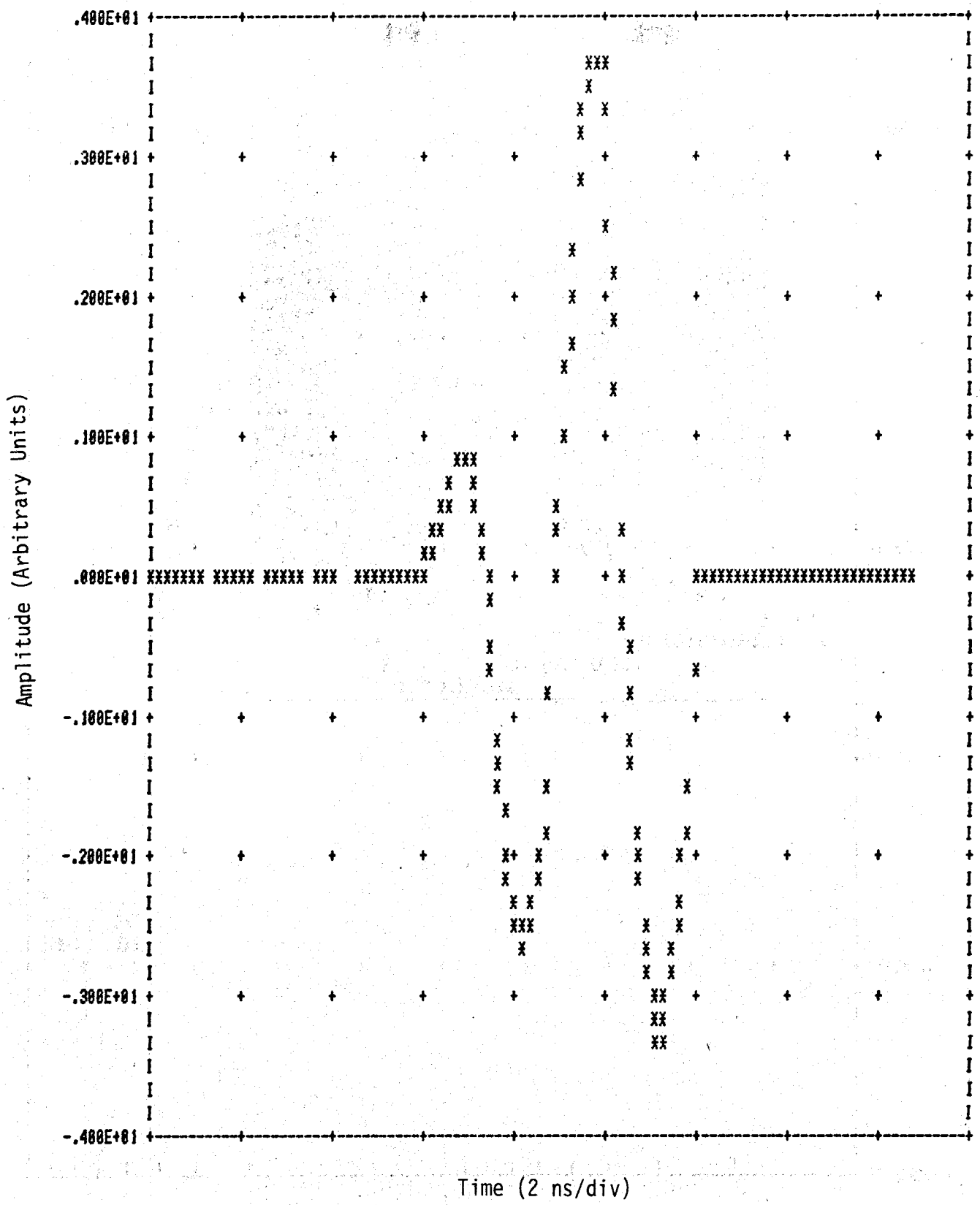

Figure 5.9. Digitized corner reflector response.

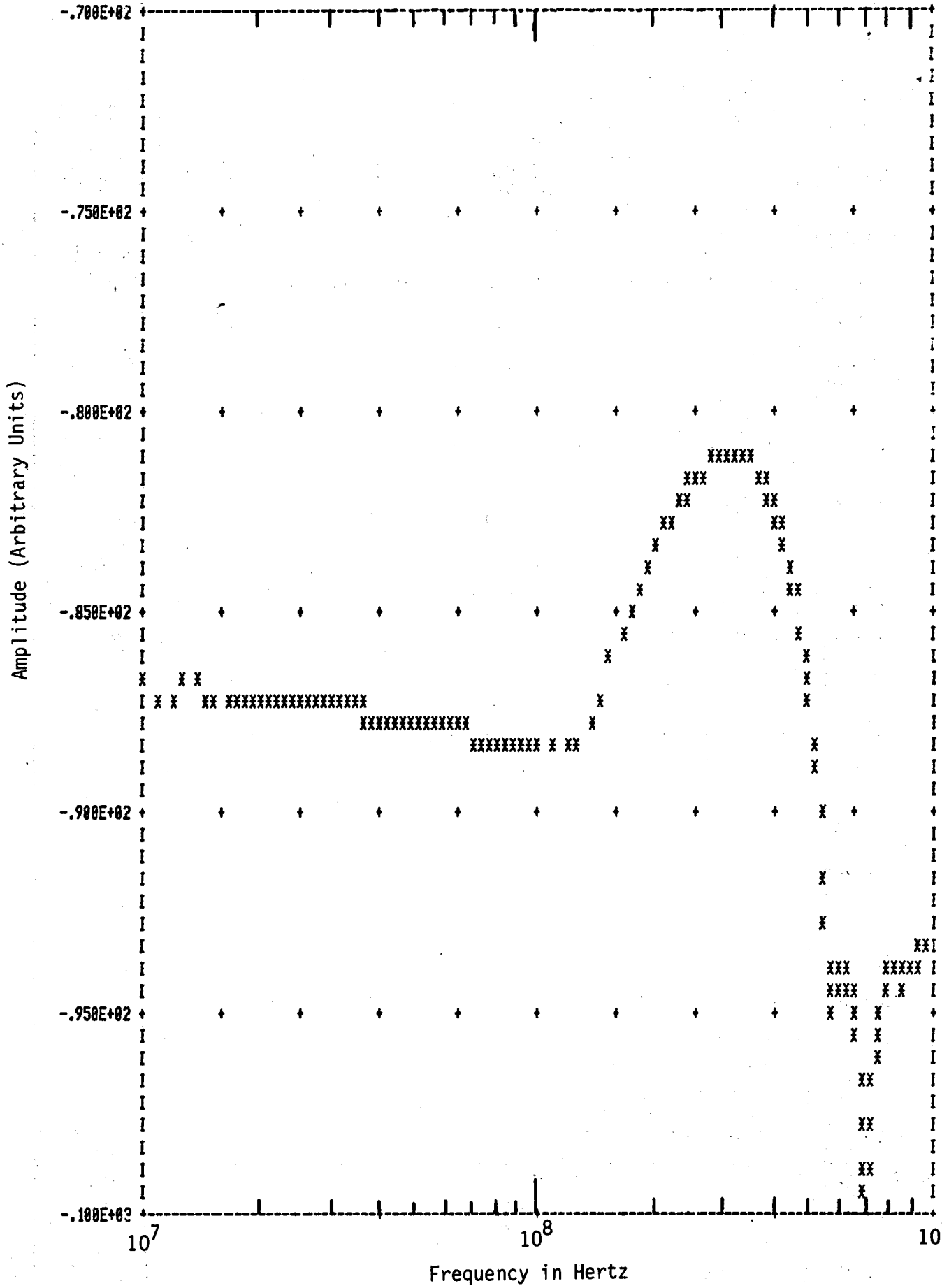

Figure 5.10. Fourier transform of corner reflector antenna response.

5.2.3 Two-element Array

Figure 5.11 is the oscilloscope photo showing the received signal from the two-element array antenna driven by the near impulse function shown in Figure 5.5. In Figure 5.11 the time reference signal is back on the lower portion of the photo. After digitizing the waveform and prior to transforming to the frequency domain, a truncation point was selected to eliminate the test chamber wall reflections. This is shown in Figure 5.12. The scales shown are in units of oscilloscope graticules. Actual time units were introduced in the Fourier transform program.

Finally, Figure 5.13 shows the Fourier transform for the two-element array antenna for radius = 3.19 cm (i.e., the optimum case). The frequency range shown is from 10 MHz to 1000 MHz.

The transform is only valid for frequencies lower than about 500 MHz since the measurement system starts to roll off at 300 MHz. We note a broad peak of energy centered around 263 MHz which is similar to that seen for the other two antennas.

5.2.4 Driving Pulse

The pulse used to drive all of these antennas turned out to be a reasonable approximation to that of an impulse for the limitations of the measurement system (i.e., 300 MHz -3 dB point). The pulse is pictured in Figure 5.5 and was recorded at a faster sweep speed (1 ns/div) than the other photos (2 ns/div).

The Fourier transform of this pulse, shown in Figure 5.14 is probably more representative of the overall measurement system response than of the true energy content of the pulse. We note a smooth roll off above 300 MHz as specified for the oscilloscope. The pulser specifications call for a rise time of 0.25 ns while our system was only able to resolve 0.7 ns.

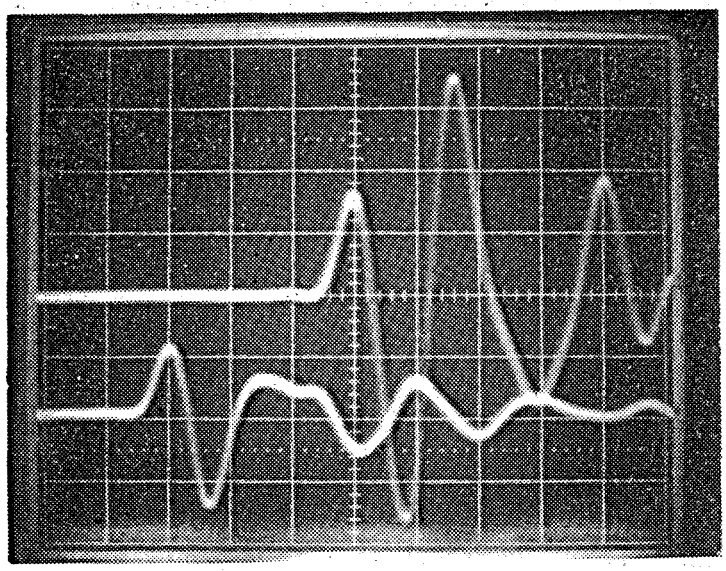

Figure 5.11. Two-element array antenna response. (2 ns/div)

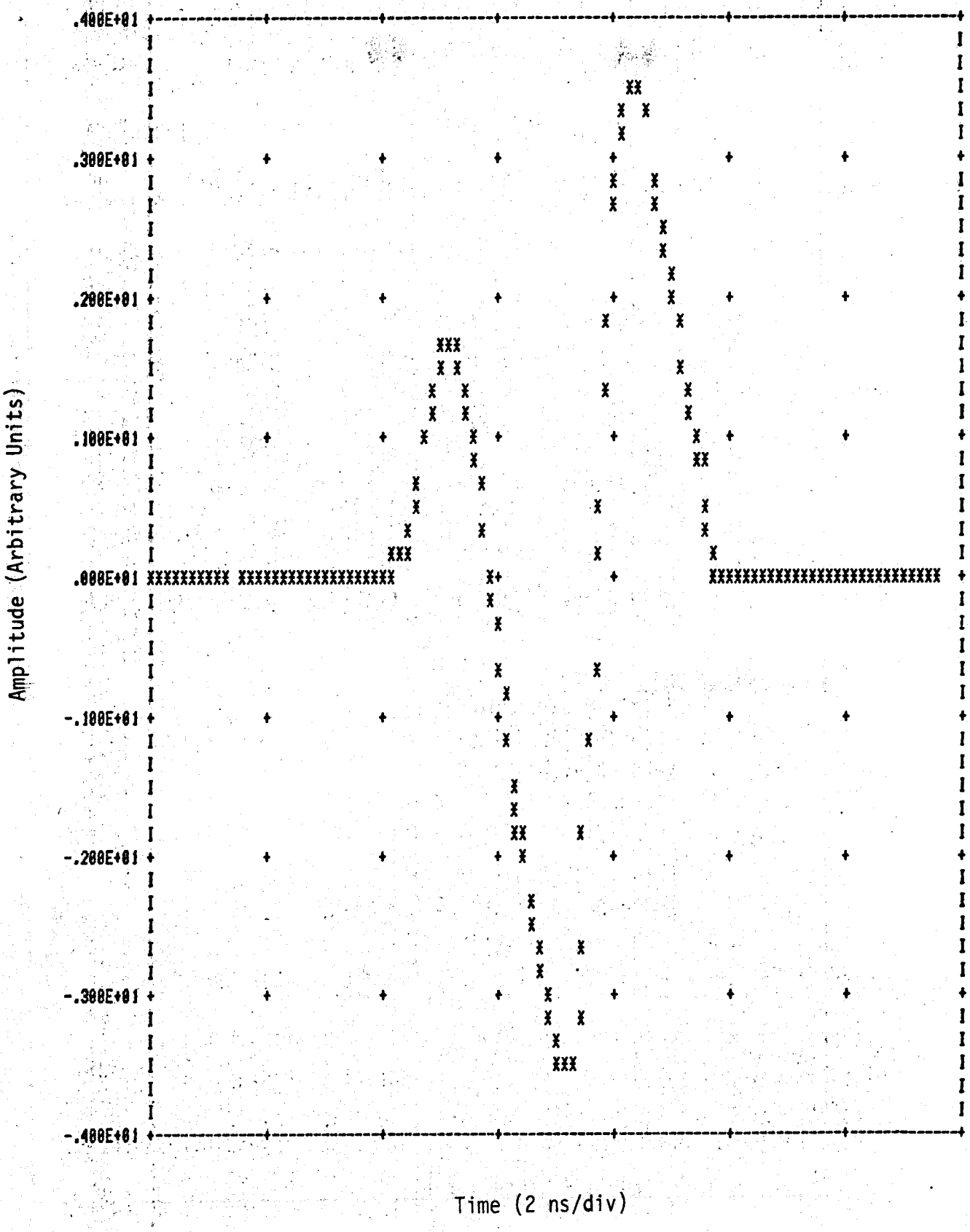

Figure 5.12. Digitized two-element array response.

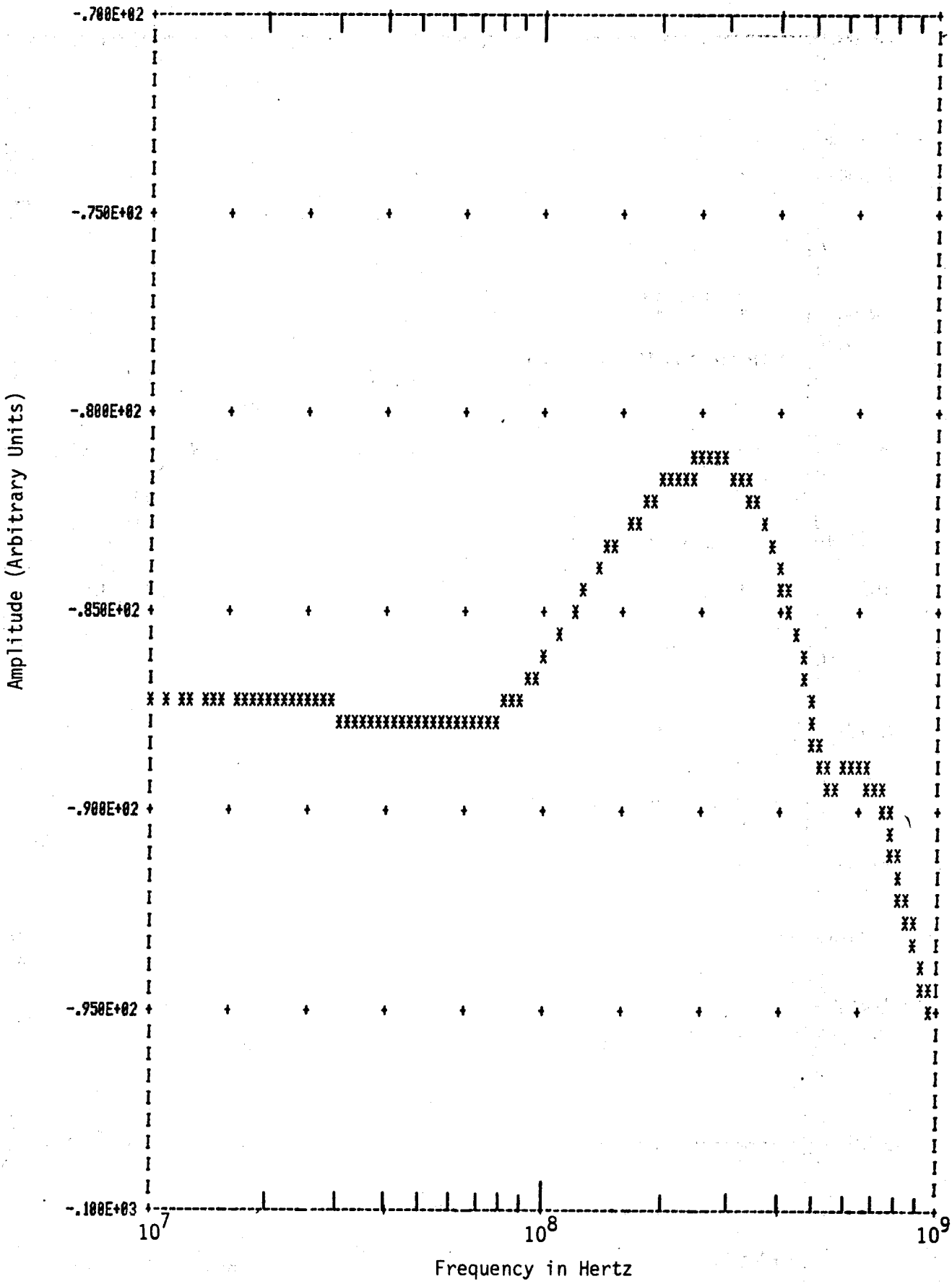

Figure 5.13. Fourier transform of two-element array antenna response.

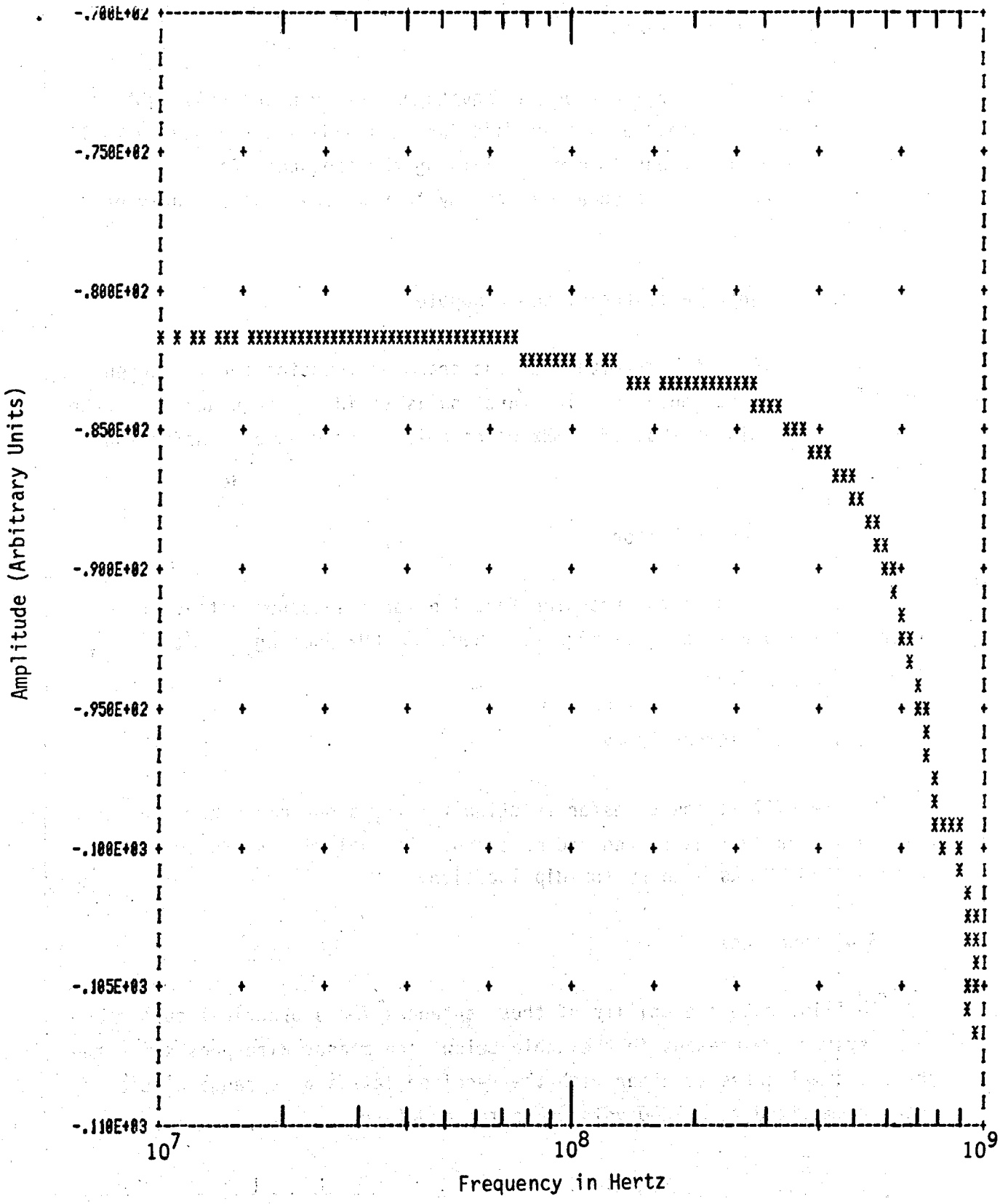

Figure 5.14. Fourier transform of driving pulse.

5.3 Transfer Functions

Many times transfer functions are quite useful when the driving function is not as well behaved as that used for this experiment. Now we will look at transfer functions formed by dividing the frequency domain responses for each type antenna measured by that of the measured driving pulse.

5.3.1 Eccentrically Positioned Monopole

Figure 5.15 is the magnitude of the transfer function for the eccentrically positioned monopole. The function is valid in frequency up to the high frequency dip at about 575 MHz where noise renders the transfer function invalid.

5.3.2 Corner Reflector

Figure 5.16 shows the transfer function for the corner reflector antenna and appears to be valid up to about 537 MHz judging from the high frequency dip seen.

5.3.3 Two-element Array

Figure 5.17 is the transfer function for the two-element array antenna that was actually constructed and measured. Its validity seems to be up to about 513 MHz as seen by the dip location.

5.4 Path Loss

To illustrate the utility of these antennas for a practical subsurface radar system, we present in the table below, the measured responses for the three optimal cases together with the received levels at a range of one meter normalized to a 1000 volt pulse for a driver.

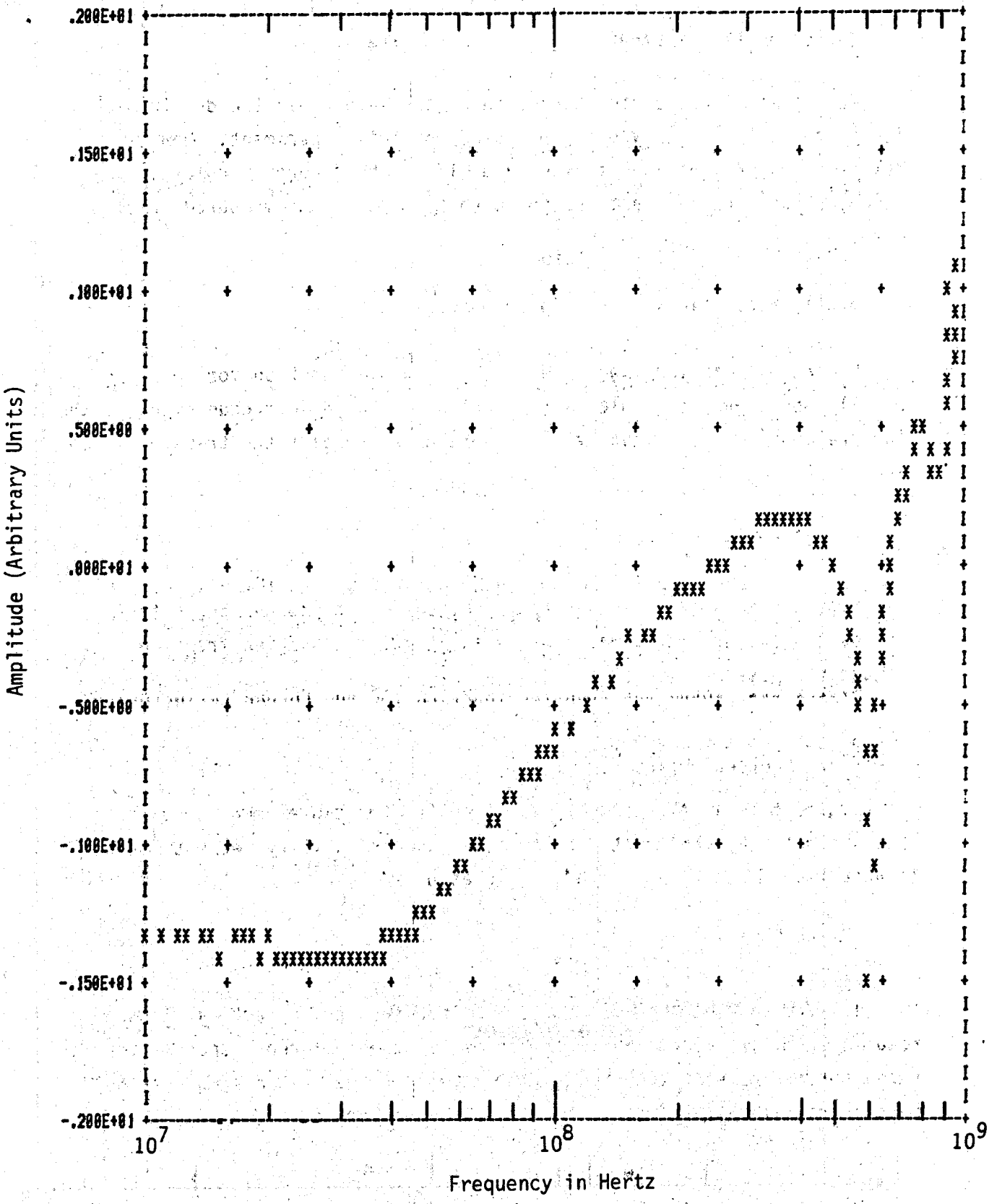

Figure 5.15. Fourier transform for eccentrically positioned monopole.

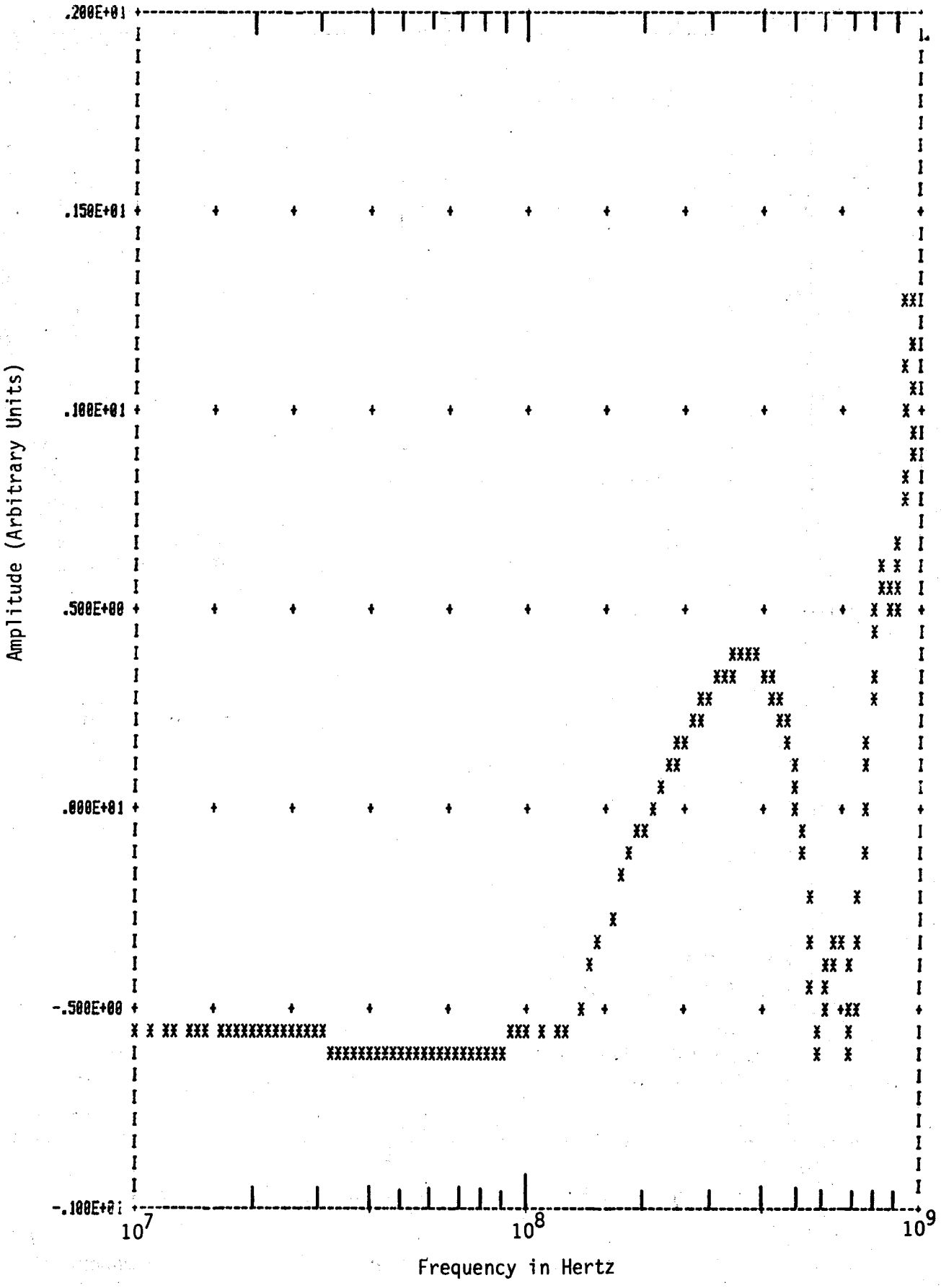

Figure 5.16. Fourier transform for corner reflector antenna.

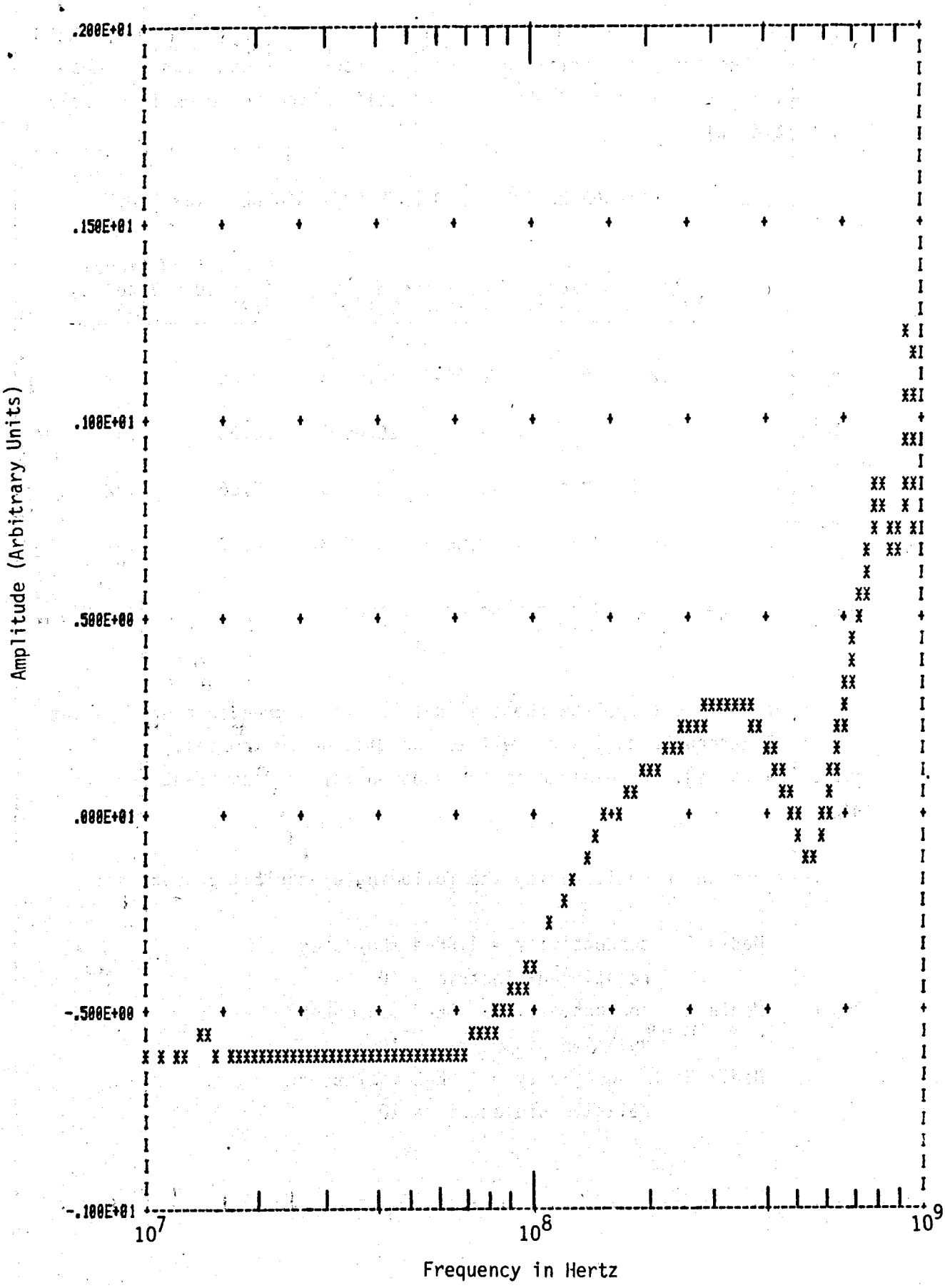

Figure 5.17. Fourier transform for two-element array.

Note that the pulser dial settings are recorded along with the measured pulse output into a 50 Ohm load for calibration purposes (see Table 3.1, Section 3).

TABLE 5.3. ANTENNA RESPONSE AND PATH LOSS AT ONE METER RANGE

Antenna	Pulser Voltage) (dial/measured)	Measured Signal (actual values)		Normalized Signal (for 1000 V pulse) (+)	(-)
Eccentric Monopole	12.5/9.2	6.0E-3	14.0E-3	0.65	1.52
Corner Reflector	30/27	9.0E-3	26.0E-3	0.33	0.95
Two-element Array (syn)	12.5/9.2 *	10.3E-3	22.5E-3	0.56	1.22
Two-element Array (meas)	15/16.8 *	8.0E-3	18.0E-3	0.47	1.07

*Note: voltage delivered to the power splitter

In order to extrapolate these signal levels to greater ranges we let the signal attenuate as 1/R as well as the dissipative losses, exp(-alpha*range), where alpha is the exponential loss constant for the media.

Consider three media having the following electrical properties:

Media 1 conductivity = 1.0E-4 mho/meter
relative dielectric = 10
Media 2 conductivity = 1.0E-3 mho/meter
relative dielectric = 10
Media 3 conductivity = 1.0E-2 mho/meter
relative dielectric = 10

We will use plane wave techniques and assume a center frequency of 300 MHz to obtain the necessary loss constants. Thus the overall attenuation is expressed as

$$A = \frac{1}{R} e^{-\alpha R} \quad \text{(attenuation factor)}$$

where R = range (total path length)

$$\alpha = \omega\sqrt{\varepsilon\mu}\, g(p)$$

where $\omega = 2\pi f$

f = frequency

ε = media dielectric constant

μ = media permittivity

$$g(p) = \left[\frac{1}{2}\left(\sqrt{1 + p^2} - 1\right)\right]^{1/2}$$

and $$p = \frac{\sigma}{\omega\varepsilon}$$

where σ = media conductivity. Table 5.4 lists these values for several ranges.

TABLE 5.4. ATTENUATION FOR VARIOUS CONDUCTIVITIES AND RANGES

Range	Media 1	Media 2	Media 3
10 m	9.42E-2	5.50E-2	2.58E-4
30 m	2.78E-2	5.78E-3	5.72E-10
100 m	5.50E-3	2.58E-5	1.31E-28

Now by applying these attenuation factors to our normalized 1000 volt responses we predict the results shown in Tables 5.5, 6 and 7.

TABLE 5.5. MEDIA 1: RADAR RETURN SIGNAL LEVELS FOR A 1 kV PULSE DRIVER

	Radar Range in Media 1		
Antenna	5 m	15 m	50 m
Eccentric (+)	6.12E-2 volts	1.81E-2	3.58E-3
Monopole (-)	1.43E-1	4.23E-2	8.36E-3
Corner (+)	3.11E-2	9.17E-3	1.82E-3
Reflector (-)	8.95E-2	2.64E-2	5.23E-3
2-element (+)	4.43E-2	1.31E-2	2.29E-3
Array (-)	1.01E-1	2.98E-2	5.89E-3
Reflector (-)	8.95E-2	2.64E-2	5.23E-3
2-element (+)	4.43E-2	1.31E-2	2.29E-3
Array (-)	1.01E-1	2.98E-2	5.89E-3

TABLE 5.6. MEDIA 2: RADAR RETURN SIGNAL LEVELS FOR A 1 kV PULSE DRIVER

	Radar Range in Media 2		
Antenna	5 m	15 m	50 m
Eccentric (+)	3.57E-2 volts	3.76E-3	1.68E-5
Monopole (-)	8.36E-2	8.79E-3	3.92E-5
Corner (+)	1.82E-2	1.91E-3	8.51E-6
Reflector (-)	5.23E-2	5.49E-3	2.45E-5
2-element (+)	2.59E-2	2.72E-3	1.21E-5
Array (-)	5.89E-2	6.18E-3	2.76E-5

TABLE 5.7. MEDIA 3: RADAR RETURN SIGNAL LEVELS FOR A 1 kV PULSE DRIVER

Antenna	Radar Range in Media 3		
	5 m	15 m	50 m
Eccentric (+)	1.68E-4 volts	3.72E-10	8.52E-29
Monopole (-)	3.92E-4	8.69E-10	1.99E-28
Corner (+)	8.51E-5	1.89E-10	4.32E-29
Reflector (-)	2.45E-4	5.43E-10	1.25E-28
2-element (+)	1.21E-4	2.69E-10	6.16E-29
Array (-)	2.76E-4	6.12E-10	1.40E-28

From these tables we can see that if the radar receiver can detect and process signals as low as 1 micro-volt then, even these simple antennas will provide useful radar returns from good reflectors (large media discontinuities) at ranges on the order of 50 meters for conductivities of 1E-3 mho/meter and to ranges of a little over 5 meters for conductivities of 1E-2 mho/meter.

SECTION 6
CONCLUSIONS

This study concluded that it is possible to design a directional antenna to fit into a 15 cm diameter borehole to be operated at around 300 MH_z. Because of the constraints of our experimental space, the field patterns were measured at the near zone and the antenna was operated at the high end of the desired frequency bands.

We will investigate in our next project whether similar designs as described in this report can still lead to sufficient directivity and beamwidth as the antenna's mid-frequency is reduced to about 100 MH_z. Such an experiment will be carried out in an outdoor open space so that the far field patterns can be measured.

In this report, the main emphasis on the antenna's directivity has been in the horizontal plane since this is the most difficult area to obtain good directivity due to the small radius of a borehole. However, the directivity in the axial plane is also desirable in some applications. In such cases, phased-array in the axial direction may be required to accomplish this objective.

REFERENCES

1.1 Lytle and Laine, Design of a Miniature Directional Antenna for Geophysical Probing from Boreholes, IEEE Trans. on Geoscience Electronics, Vol. GE-16, No. 4, October, 1978.

2.1 King, R.W.P., Fundamental Electromagnetic Theory, Dover Publications, Inc., NY, 1963, p.267.

2.2 Reference Data for Radio Engineers, IT&T Corp., NY, 1964, p.689.

2.3 King and Smith, Antennas in Matter, The MIT Press, Cambridge MA, 1981, p.198.

2.4 Scott, L.D. and G.S. Smith, Measurement Techniques for Antennas in Dissipative Media, Special issue on Antenna Measurement, IEEE Trans. G-AP, July, 1973.

3.1 Tektronix Model 2465 Oscilloscope User's Manual.

3.2 Tektronix Model C-30B Camera User's Manual.

3.3 Hewlett Packard Model 8405A Vector Voltmeter User's Manual.

3.4 Tektronix Model 109 Pulse Generator User's Manual.

3.5 TSC Model Z-DAP V-I Impedance Probe User's Data Sheet.

4.1 Longmire, C.L., and K.S. Smith, A Universal Impedance for Soils, MRC-N-214, Mission Research Corporation, Santa Barbara, CA, October, 1975.

5.1 Ibid., Lytle and Laine.

5.2 Scott, L.D., Deterministic Error Analysis, Jun, 1977, AFWL Measurement Note #24.

VIII DISTRIBUTION:
TID-4500-R66-UC-66c (474)

Tom Anderson
Drilling Fluid Consultants
17726 S.W. Overlook Ln
Lake Oswego, OR 97034

Ed Bingman
Shell Oil Company
Two Shell Plaza
P.O. Box 2099
Houston, TX 77001

Larry Diamond
Dyna-Drill
P.O. Box C-19576
Irvine, CA 92713

Tom Turner
Phillips Petroleum Company
Geothermal Operations
655 East 4500 South
Salt Lake City, UT 84107

Jim Kingsolver
Geothermal Operations
Smith Tool
P.O. Box C-19511
Irvine, CA 92713

John C. Rowley
Los Alamos National Labs
Mail Stop D-461
Los Alamos, NM 87545

Ed Martin
Superior Oil
Eastern Division
P.O. Box 51108 OCS
Lafayette, LA 70505

B. J. Livesay
2616 Angell Ave.
San Diego, CA 92122

Ben Bradford
Dowell
P.O. Box 2710
Tulsa, OK 74102

Gene Polk
NL Baroid
P.O. Box 280
Sandia Park, NM 87047

James W. Langford
Security Division
Dresser Industries, Inc.
P.O. Box 24647
Dallas, TX 75224

John E. Fontenot
NL, MWD
P.O. Box 60070
Houston, TX 77205

Del E. Pyle
Union Geothermal Division
Union Oil Co. of California
Union Oil Center
Los Angeles, CA 90017

William D. Rumbaugh
Research & Development
Otis
P.O. Box 34380
Dallas, TX 75234

Dwight Smith
Halliburton
Drawer 1431
Duncan, OK 73533

Tom Warren
Amoco Production Company
Research Center
P.O. Box 591
Tulsa, OK 74102

H. E. Mallory
P.O. Box 54696
Tulsa, OK 74144

Jim Combs
Geothermal Resources Int'l Inc.
545 Middlefield Rd., Suite 200
Menlo Park, CA 94025

DISTRIBUTION cont'd

Dr. Melvin Friedman
Center for Tectonophysics
And Dept. of Geology
Texas A&M University
College Station, TX 77843

EG&G Instruments
6612 Renee Ave. NW
Albuquerque, NM 87109

William (Chris) Allen
Science & Technology Division
Union Oil
P.O. Box 76
Brea, CA 92621

S.A. Suhler
T.E. Owen
Dept. of Geosciences
Southwest Research Institute
San Antonio, TX 78284

U.S. Department of Energy (3)
Geothermal Hydropower
Technologies Division
Forrestal Bldg., CE 324
1000 Independence Ave. S.W.
Washington, D.C. 20585
Attn: J. Bresee
R. Toms
D. Allen

Mr. Ken Granzow
Dikewood Corporation
1613 University Blvd., NE
Albuquerque, NM 87106

Mr. Anthony Veneruso
Gearhart Industries, Inc.
P.O. Box 1936
Fort Worth, TX 76101

Mr. Larry Scott
Mission Research Corporation
1720 Randolph Rd., SE
Albuquerque, NM 87106

A. Aduci
U.S. Department of Energy
San Francisco Operations Office
1333 Broadway
Wells Fargo Building
Oakland, CA 94612

Rama Rau
Gearhart Industries, Inc.
P.O. Box 34456
9190 Telephone Rd.
Houston, TX 77034

W.P. Grace, DOE/ALO
Nuclear & Geosciences Division
1540 W. C. Luth
1541 H. C. Hardee
1541 L. C. Bartel
1542 B. M. Butcher
3141 L. J. Erickson (5)
3151 W. L. Garner (3)
2344 J. T. Cordaro
2345 M. W. Callahan
6200 V. L. Dugan
6220 D. G. Schueler
6240 R. K. Traeger
6241 J. R. Kelsey (10)
6241 H. T. Chang (10)
6241 F. M. Wolfenbarger
6246 B. Granoff
6247 P. J. Hommert
6250 B. W. Marshall
6252 H. M. Dodd
6253 J. F. Anderman
6253 D. A. Northrop
6256 D. Engi
6256 C. M. Hart
6256 J. R. Wayland
6257 J. K. Linn
6257 C. A. Searls
6300 R. W. Lynch
6320 R. M. Jefferson
6330 W. D. Weart
7110 J. D. Plimpton
7116 C. W. Cook
7553 R. L. Parker
7553 G. A. Seely
8214 M. A. Pound

☆U.S. GOVERNMENT PRINTING OFFICE:1984—776-027 / 4288